

LOCKHEED MISSILES & SPACE COMPANY
HUNTSVILLE RESEARCH & ENGINEERING CENTER
HUNTSVILLE RESEARCH PARK
4800 BRADFORD DRIVE, HUNTSVILLE, ALABAMA

FINAL REPORT
LAUNCH & SPACE VEHICLE
CONTROL STUDIES

VOLUME I

Digitized Non-Linear Filter
for Launch Vehicle Application

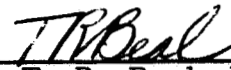
22 September 1967

Contract NAS8-21034

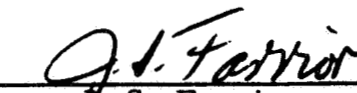
APPROVED BY:



A. J. Besonis, Supervisor
Controls Section



T. R. Beal, Manager
Dynamics & Guidance



J. S. Farrior
Resident Manager

NG8-17653

117 PAGES

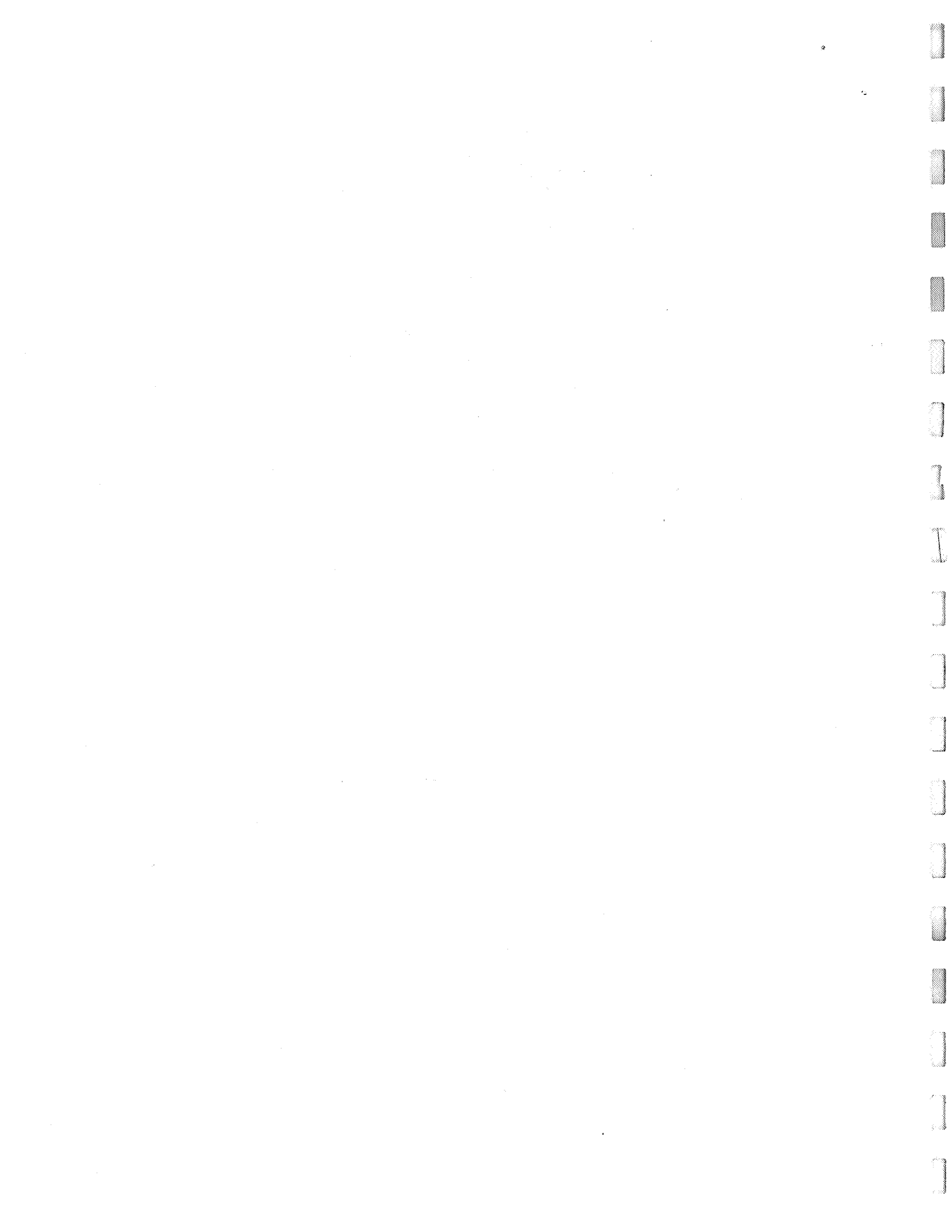


PRECEDING PAGE BLANK NOT FILMED.

FOREWORD

This two-volume document (of which this is Volume I) presents results of all work performed by Lockheed Missiles & Space Company, Huntsville Research & Engineering Center under NASA Contract No. NAS8-21034 under the direction of Mr. Fred W. Swift of the Aero-Astrodynamic Laboratory of Marshall Space Flight Center (MSFC), Dynamics and Flight Mechanics Division, Control Theory Branch.

The main contributors to this study were G. R. Hewitt and J. G. Tuck. Digital computer programming was performed by N. Kovalevsky.



PRECEDING PAGE BLANK NOT FILMED.

CONTENTS

Section		Page
	FOREWORD	iii
	INTRODUCTION AND SUMMARY	1
1	ANALYSIS OF DIGITAL IMPLEMENTATION OF NONLINEAR FILTER	
	1.1 Introduction and Background	1-1
	1.2 Digital Implementation	1-4
	1.3 Digital Filter Performance	1-11
	1.4 Conclusions	1-23
2	SIMULATION AND APPLICATION OF NONLINEAR FILTER TO LAUNCH VEHICLE	2-1
	2.1 Summary	2-1
	2.2 Introduction	2-1
	2.3 Discussion	2-2
	2.4 Results	2-5
	2.5 Conclusions	2-7
	2.6 Illustrations	2-8
Appendix		
A	NONLINEAR FILTER CONCEPT DEVELOPMENT	A-1
B	EQUATIONS OF MOTION FOR LAUNCH VEHICLE WITH BENDING AND SLOSHING	B-1
C	NOMENCLATURE	C-1
D	AS-503 INPUT DATA	D-1
E	REFERENCES	E-1

INTRODUCTION AND SUMMARY

This study covers several topics in control and stabilization of both launch vehicles and space vehicle clusters. The material is presented in two volumes, of which this is Volume I. The first volume is entirely devoted to the study of a digitized version of a nonlinear filter for launch vehicle control and stabilization. This work is a continuation of previous studies in this area at Lockheed Missiles & Space Company, Huntsville Research & Engineering Center. The second volume presents studies in control and stabilization of space vehicles. Considered are topics in passive stabilization, active control of large space vehicle clusters and forms of semi-active control systems.

Because of the numerous topics presented in Volume II, it was found to be most expedient to organize the material into five major study areas; these are:

1. Development of Equations for Orbital Vehicle Attitude Studies.
2. Passive Attitude Stability of Space Vehicle Clusters.
3. Active Control with Control Moment Gyros.
4. Studies of Desaturation for Control Moment Gyros.
5. Semi-Active Systems.

The overall presentation in each of these studies is self-contained so that the reader may examine each topic independently of the material preceding it. To this end each study contains its own list of nomenclature, references and introduction to the particular study area.

Major contributors to each of the major studies are listed on the particular title pages.

Section 1

ANALYSIS OF DIGITAL IMPLEMENTATION
OF NONLINEAR FILTER

- 1.1 Introduction and Background
- 1.2 Digital Implementation
- 1.3 Digital Filter Performance
- 1.4 Conclusions

Section 1
ANALYSIS OF DIGITAL IMPLEMENTATION
OF NONLINEAR FILTER

1.1 INTRODUCTION AND BACKGROUND

A digital implementation of a nonlinear signal filtering concept is presented, the continuous version of which has already been studied extensively. Results of the continuous version study are reported in References 1 and 2, a brief resume of which is presented in Appendix A. However, reference should be made to the above documents for greater detail.

The continuous filter is illustrated by the diagram shown in Figure 1-1. The intent of this mechanization is to provide a sharp cutoff of all frequency components in the incoming signal which are above a certain value, ω_c . Signal components below ω_c are to be passed with a minimum of phase shift. To accomplish this, the filter utilizes a diode bridge in conjunction with the linear networks as illustrated in the figure. The incoming signal is first passed through a second-order lag network then split into two paths. The purpose of this splitting is to develop two signals, e_1 and e_2 , which are in phase at low frequencies (below ω_c) and 180° out of phase at high frequencies (above ω_c). When the high frequencies are passed to the diode bridge, e_2 appears at x_1 when e_1 is positive and at x_2 when e_1 is negative. This prevents passage of the high frequency signals. When low frequency signals occur at the bridge, e_1 appears at both x_1 and x_2 , and the low frequencies are passed.

An example of the response that was obtained with this filter for a multiple sine wave input is shown in Figure 1-2 (Reference 1, page 55). The form of the output indicated in the second strip from the top is characteristic of the operation of the bridge with a multiple frequency input. This

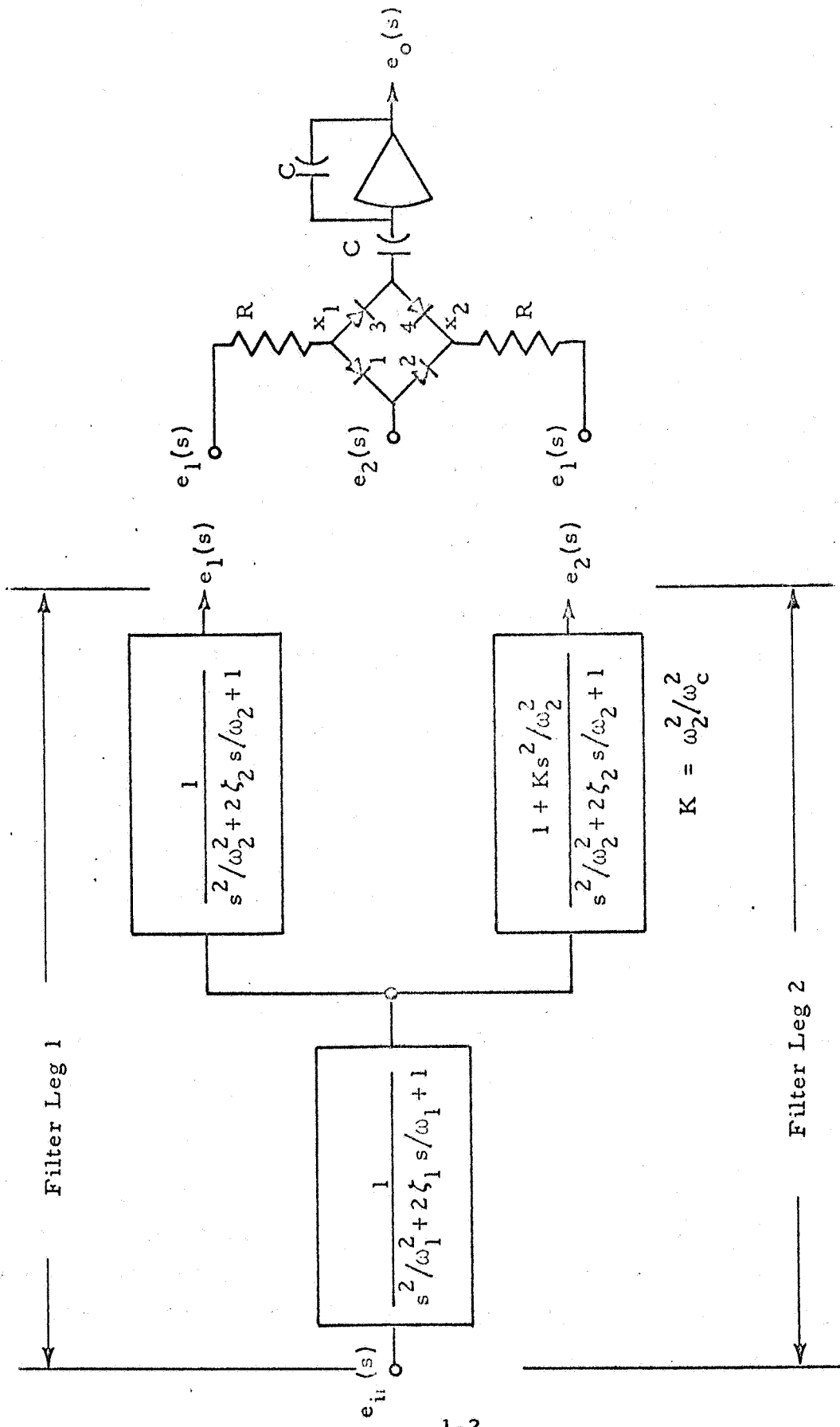


Figure 1-1.- Block Diagram of Revised Nonlinear Filter

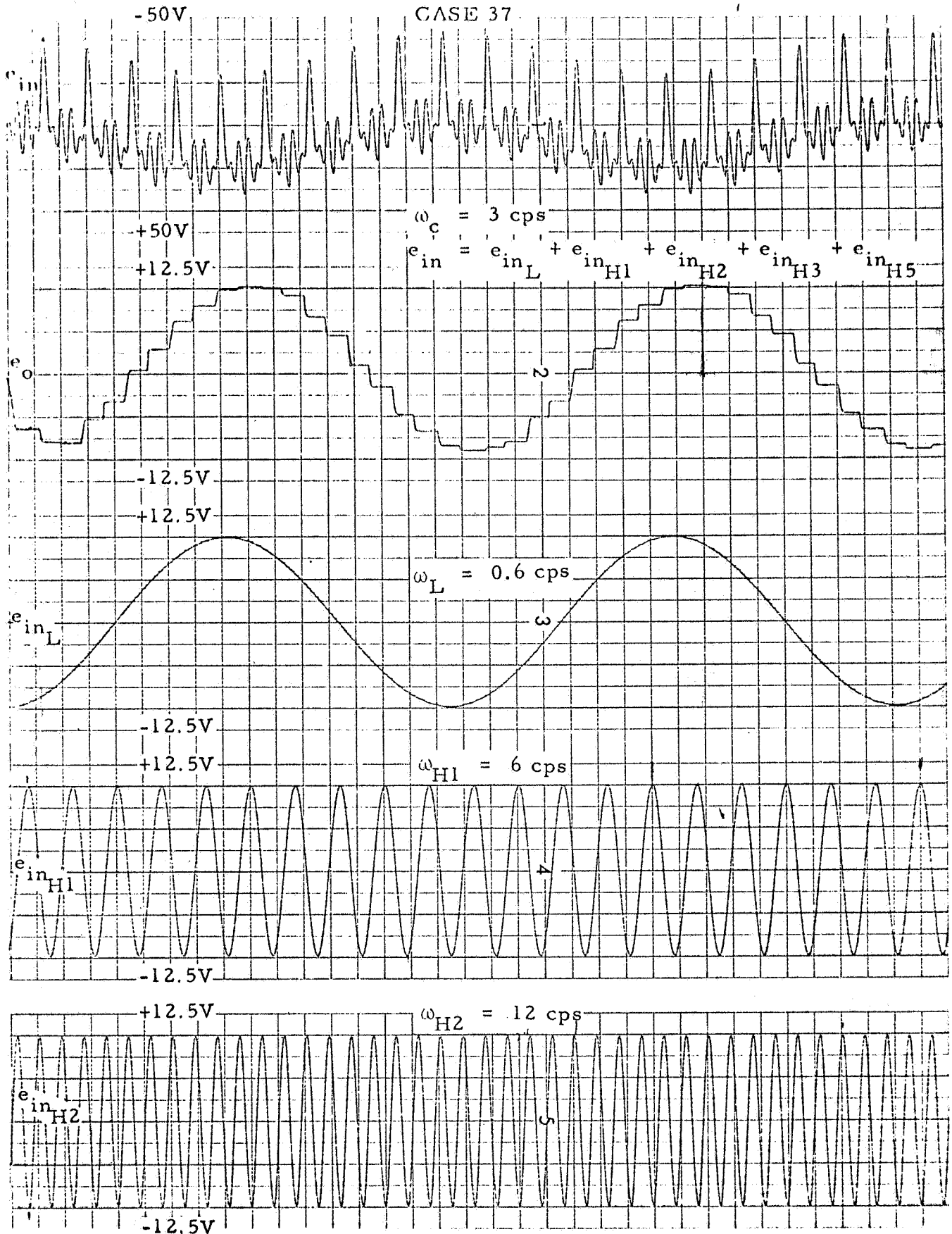


Figure 1-2 - Response of Nonlinear Filter to Low Frequency Signal of 0.6 cps and Multiple High Frequency Inputs

performance was called "quasi-sampling" in Reference 1, and its effects were studied extensively.

The intent of this present study was to determine if similar performance could be obtained using a digital computer.

1.2 DIGITAL IMPLEMENTATION

A straightforward digital implementation would have the configuration shown in Figure 1-3. The incoming continuous signal, $x(t)$, is converted to a sequence of numerical values denoted by $x(n)$. The operators $D_1(z)$ and $D_2(z)$ symbolically represent linear recursion formulas or difference equations that can be programmed in a computer. These formulas perform the same signal-splitting and phase-shifting functions as the linear networks in the analog configuration. The block marked digital logic represents a set of logic statements that will perform the same function as the diode bridge and output amplifier for the analog filter.

No specific consideration was given in this study to the performance of the conversion devices at either the input or output ends of the filter. The conversion from analog to digital signals at the input of the filter is assumed to be simply the ideal conversion of a continuous function of time, $x(t)$, to a sequence of values, $x(n)$. Numerical values of the sequence agree with those of the continuous function at uniformly spaced increments in time. For a sampling interval of T sec,

$$x(n) = x(nT), \quad n = 0, 1, 2, \dots$$

The output conversion is more critical, and the type of conversion and performance requirements will depend on the specific application of the filter.

The development of the logic and the method used to obtain the difference equations are discussed below under individual headings.

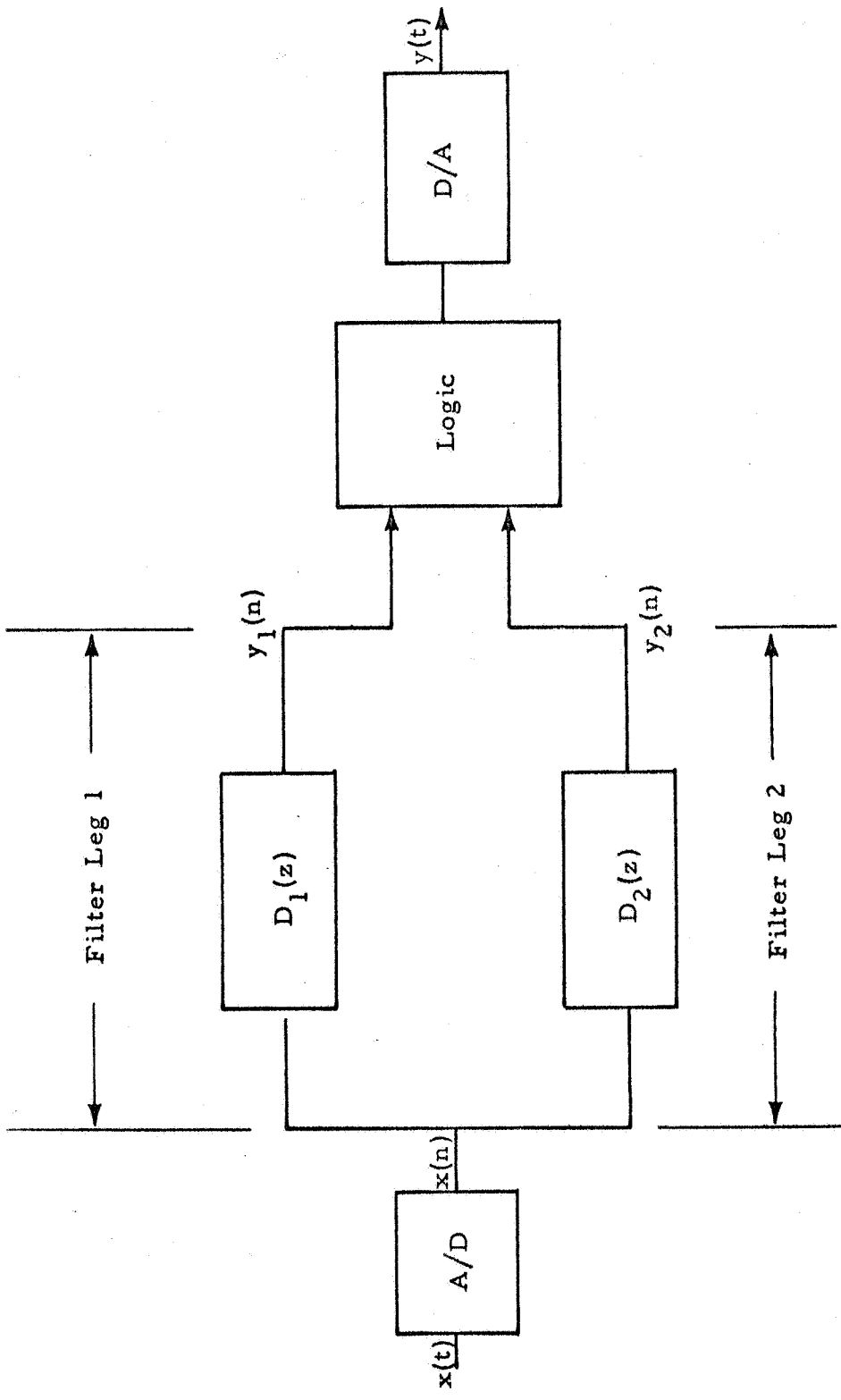


Figure 1-3 - Digital Implementation of Nonlinear Filter

1.2.1 Analytical Description of Diode Bridge Circuit*

The nonlinear circuit consists of a diode bridge and an integrating amplifier with an input capacitance C equal to the feedback capacitance as shown in Figure 1-4.

Amplifier Transfer Function

Let z be the input voltage to the capacitance C of the amplifier with grid voltage e_g and gain factor K then

$$C \frac{d}{dt} (z - e_g) = -C \frac{d}{dt} (e_0 - e_g)$$

and

$$e_0 = -K e_g$$

Substituting yields

$$\frac{d}{dt} \left(z + \frac{e_0}{K} \right) = - \frac{d}{dt} \left(e_0 + \frac{e_0}{K} \right)$$

For K large, we obtain

$$e_0 \approx -z$$

i.e., the amplifier acts like an inverter.

Diode Operation

It is assumed that the bridge diodes have ideal switching characteristics that can be described by

* Acknowledgement is made to Dr. W. Trautwein for the analytical description of the diode bridge.

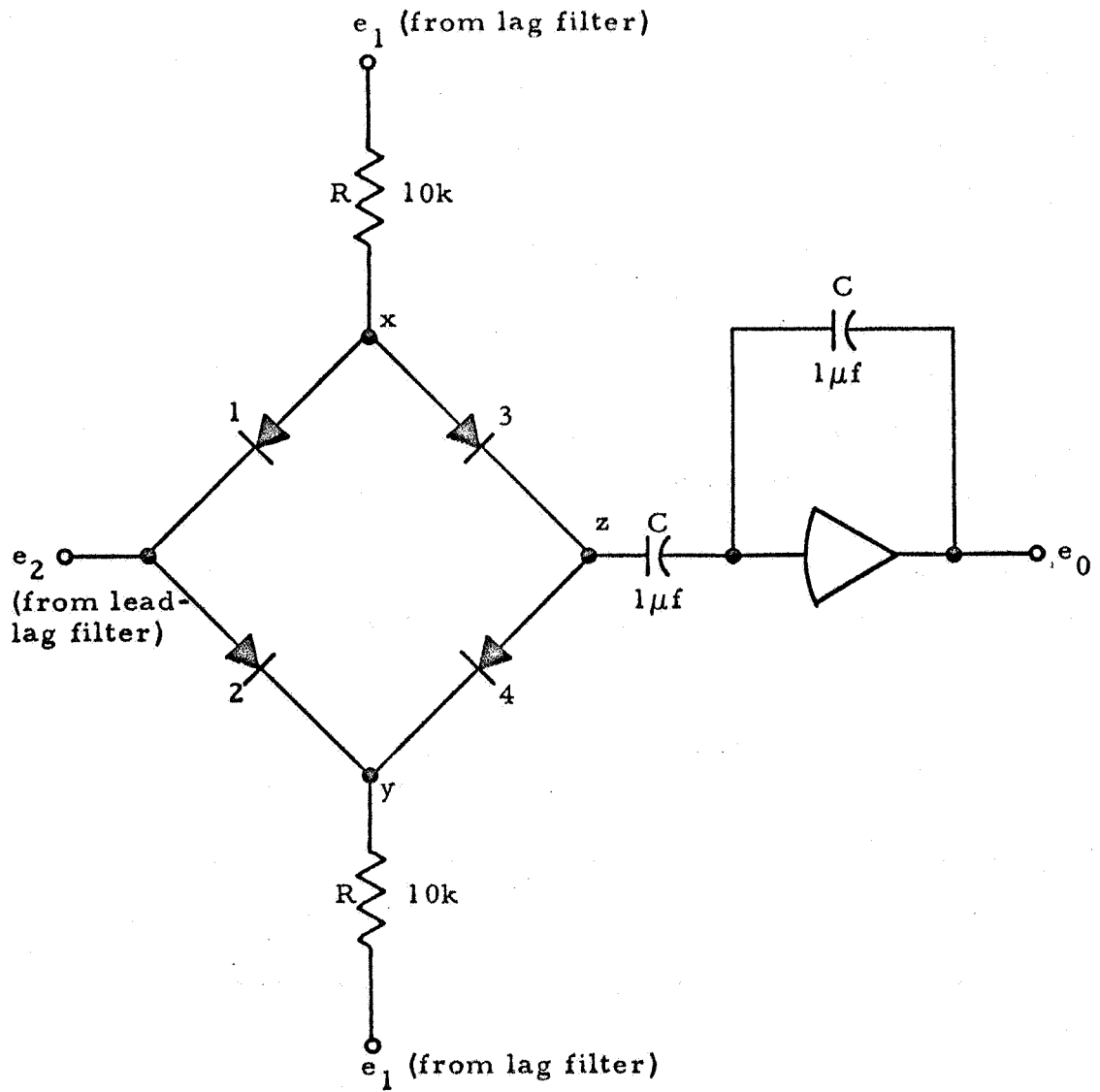
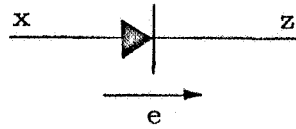


Figure 1-4 - Nonlinear Part of Cutoff Filter



$$R = \begin{cases} \infty & \text{if } e < 0 \\ 0 & \text{if } e \geq 0 \end{cases}$$

where e is the voltage across the diode.

Diode Bridge Switching Logic

The switching logic is governed by the respective values of the input voltage e_1 , e_2 , and the bridge output z .

There exist six different conditions for the diodes which result in three different bridge outputs z as listed in Table 1-1.

Table 1-1
BRIDGE OUTPUT AS A FUNCTION OF RESPECTIVE
INPUT AND OUTPUT VOLTAGES

Case No.	Input-Output Voltage Relation	Resulting Diode States				Resulting Bridge Voltages		Resulting Bridge Output
		Diode No.				x	y	
		1	2	3	4			
1a	$e_2 > e_1 \geq z$	N	C	C	N	e_1	e_2	$z = e_1$
1b	$z \geq e_1 > e_2$	C	N	N	C	e_2	e_1	$z = e_1$
2a	$e_1 > e_2 \geq z$	C	N	C	N	e_2	e_1	$z = e_2$
2b	$z \geq e_2 > e_1$	N	C	N	C	e_1	e_2	$z = e_2$
3a	$e_1 \geq z > e_2$	C	N	N	N	e_2	e_1	$z = z(0)$
3b	$e_2 > z \geq e_1$	N	C	N	N	e_1	e_2	$z = z(0)$

C = conducting
N = nonconducting

Note that both Diodes 3 and 4 are blocked in Case 3 which makes it impossible for the capacitor to discharge. This results in a "hold"-type bridge output in Case 3. The value $z(0)$ in Table 1-1 is to be taken at the most recent switching time of the diodes.

The complete bridge plus capacitor plus amplifier signal transfer can now be described by the relationship:

$$e_0 = -z = \begin{cases} -e_1 & \text{if } e_2 > e_1 \geq -e_0(0) \\ & \text{or } -e_0(0) \geq e_1 > e_2 \\ -e_2 & \text{if } e_1 > e_2 \geq -e_0(0) \\ & \text{or } -e_0(0) \geq e_2 > e_1 \\ e_0(0) & \text{if } e_1 \geq -e_0(0) > e_2 \\ & \text{or } e_2 > -e_0(0) \geq e_1 \end{cases} \quad (1.1)$$

The output $e_0(0)$ is to be taken at the most recent switching time of the diodes. Equation (1.1) can be readily programmed for a digital computer by a number of logical decisions.

1.2.2 Difference Equations

The method used for determining the difference equations represented by $D_1(z)$, $D_2(z)$ in Figure 1-3 is based on a comparison of the classical results of linear differential and difference equations. The exact relationship between transient solutions (for the homogeneous, constant coefficient case) was noted by Shaw (Reference 3). Either equation could be substituted for the other without truncation error or change of order. That is, any solution of the one agrees exactly with a solution of the other at those time points (sample points) at which the solution of the difference equation is defined.

The transition from differential equation to difference equation (Reference 3) is made in the following manner.

Substitution Rule

Consider the differential equation

$$f(D) y(t) = K g(D) x(t) \quad (1.2)$$

where D is the differential operator, $Dy(t) = dy/dt$, f and g are polynomials of degree p and p' , respectively, each with leading coefficient unity. The functions $x(t)$ and $y(t)$ are filter input and output, and K is a gain constant. Next, consider the difference equation

$$\bar{f}(E) y(n) = K \bar{g}(E) x(n) \quad (1.3)$$

where E is the shifting operator (Reference 4, page 16), $Ef(t) = f(t + T)$, and T is the sampling interval. The functions \bar{f} and \bar{g} are polynomials in the operator E . The steps in the transition from Equation (1.2) to Equation (1.3) are as follows:

- (1) Express $f(D)$ and $g(D)$ as products of linear factors, i.e.,

$$f(D) = \prod_{i=1}^p (D - \rho_i), \quad g(D) = \prod_{j=1}^{p'} (D - \rho_j)$$

- (2) Replace D by E
 (3) Replace each root ρ by $e^{T\rho}$
 (4) Replace K by $K(Te^{1/2})^{p-p'}$
 (5) Expand the result, i.e.,

$$\bar{f}(E) = \prod_i^p (E - e^{T\rho_i})$$

$$\bar{g}(E) = E^{(p-p')/2} \prod_j^{p'} (E - e^{T\rho_j})$$

$$\bar{K} = K T^{p-p'}$$

Frequency Response

The frequency response functions associated with Equations (1.2) and (1.3) are

$$F(\omega) = \frac{K g(j\omega)}{f(j\omega)}$$

$$\bar{F}(\omega) = \frac{\bar{K} \bar{g}(e^{j\omega T})}{\bar{f}(e^{j\omega T})}$$

Numerical comparisons were made for the path from e_{in} to e_2 (Figure 1-1) using the parameters

$$\omega_c = 3 \text{ rad/sec}$$

$$\omega_1 = 4.5 \text{ rad/sec}, \quad \zeta_1 = 0.5$$

$$\omega_2 = 6.0 \text{ rad/sec}, \quad \zeta_2 = 0.6$$

which correspond to Case 37 shown on page 14 of Reference 1-1. Frequency characteristics are shown in Figure 1-5 for sampling frequencies of 24, 48, and 96 rad/sec.

1.3 DIGITAL FILTER PERFORMANCE

Numerical results obtained, using the difference equations and logic developed in the previous section, are presented in this section.

Figure 1-6 shows a signal which is the sum of four sinusoidal components. To form a basis for comparison, the components of this signal are altered by the amplitude and phase characteristics for the continuous filter legs shown in Figure 1-1. Resulting time functions were then sampled at 24 rad/sec and the sequences operated upon by the digital logic previously described. The

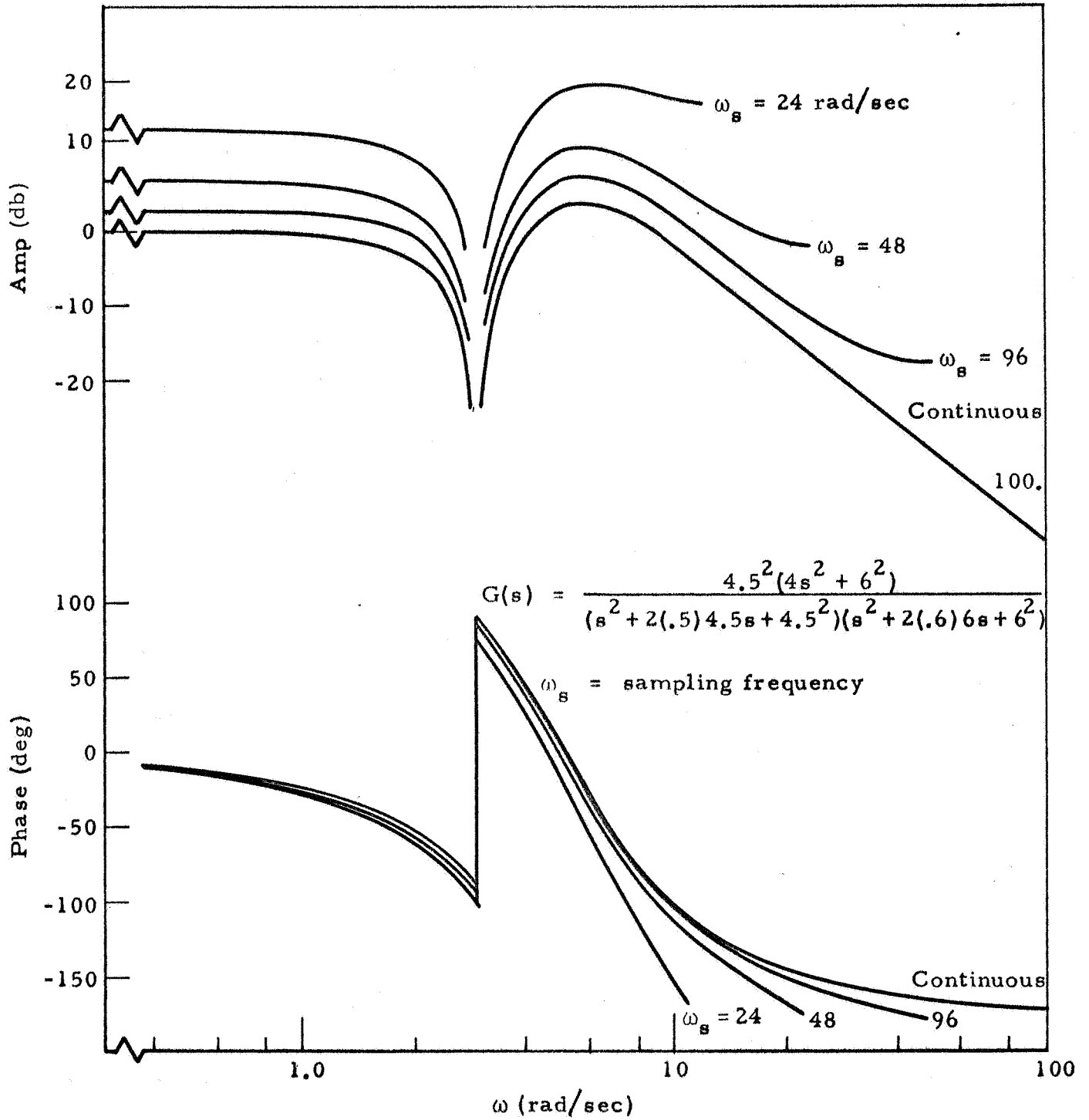
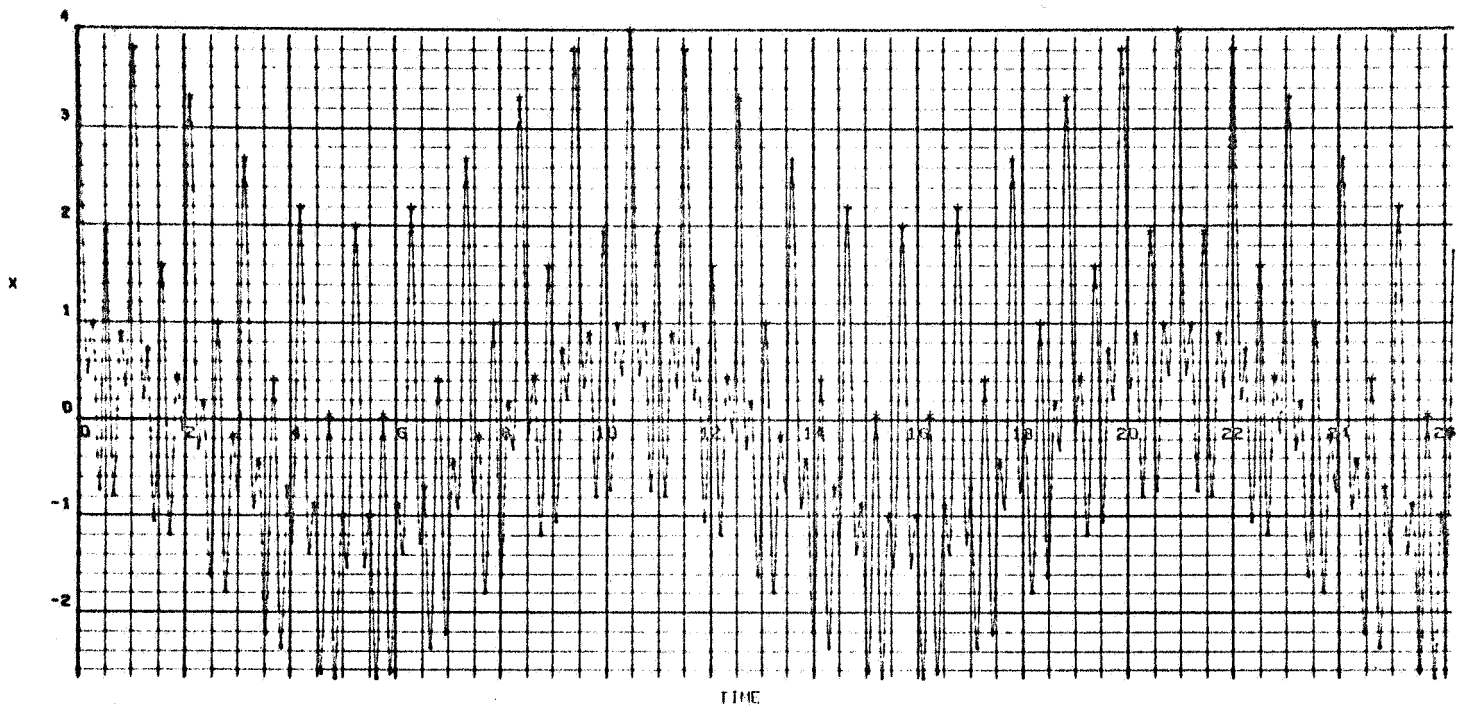


Figure 1-5 - Frequency Characteristics of Discrete Analog of Continuous Filter

470220
000 011



$$x(t) = \cos.6t + \cos6t + \cos12t + \cos24t$$

(*) values are sample points, T = .2618 sec

Figure 1-6 - Input Signal

resulting output sequences are shown by the squares superimposed on the continuous signals in Figure 1-7. Note that even for this low sampling frequency, a fairly respectable sinusoidal sequence is obtained. Responses obtained in a similar manner for sampling frequencies of 48 and 96 rad/sec are shown in Figures 1-8 and 1-9. The output sequence becomes progressively more sinusoidal as the sampling frequency is increased.

Figures 1-10, 1-11 and 1-12 show the result of operating on the input signal with the difference equations. The difference equation coefficients were normalized to have a gain of one at zero frequency and are tabulated in Table 1-2. A steady state envelope was computed by altering the input signal components by the amplitude and phase characteristics associated with the difference equation. These values are tabulated in Tables 1-3 and 1-4. The actual computed solution on the difference equation is shown superimposed on the steady state envelope and is indicated by the (*) points. The output of the digital logic is also superimposed on the plots and marked by a (\square).

Figure 1-10 shows the result of applying the multiple sine wave input to the difference equation computed for a 24 rad/sec sampling frequency. The 24 rad/sec component is passed as a constant, since there is only one sample per cycle. In this particular example, the samples are taken at the peaks of the 24 rad/sec component so that the filter output appears biased at approximately unit amplitude. Figure 1-11 shows a less academic example in which the sampling frequency is 48 rad/sec or twice the highest frequency component in the input. This response coincides almost exactly with the idealized case shown in Figure 1-8. Another run with the sampling frequency increased to 96 rad/sec is shown in Figure 1-12 and gives better definition of the low frequency component.

Table 1-2
DIFFERENCE EQUATION COEFFICIENTS

	$\omega_s = 24 \text{ rad/sec}$		$\omega_s = 48 \text{ rad/sec}$		$\omega_s = 96 \text{ rad/sec}$	
	Filter Leg 1	Filter Leg 2	$D_1(E)$	$D_2(E)$	$D_1(E)$	$D_2(E)$
A_0	0.0	0.0	0.0	0.0	0.0	0.0
A_1	0.0	1.1311	0.0	0.6363	0.0	0.2357
A_2	0.6626	-1.5997	0.0976	-1.1739	0.0091	-0.4623
A_3	-	1.1311	-	0.6363	-	0.2357
B_1	-0.8213		-2.3101		-3.1731	
B_2	0.5995		2.2576		3.8793	
B_3	-0.1623		-1.0670		-2.1621	
B_4	0.0467		0.2162		0.4650	

Form of Difference Equation:

$$y(n) = A_0 x(n) + A_1 x(n-1) + \dots - B_1 y(n-1) - B_2 y(n-2) - \dots$$

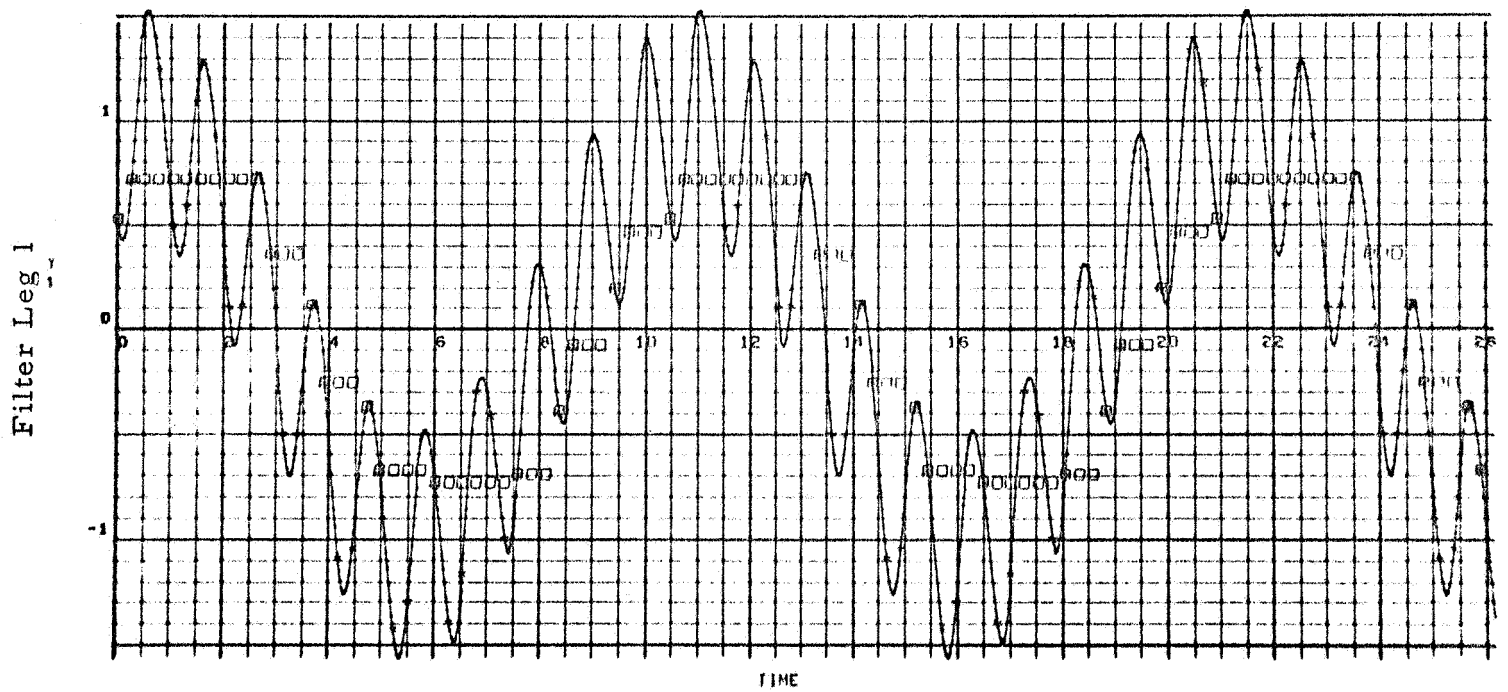
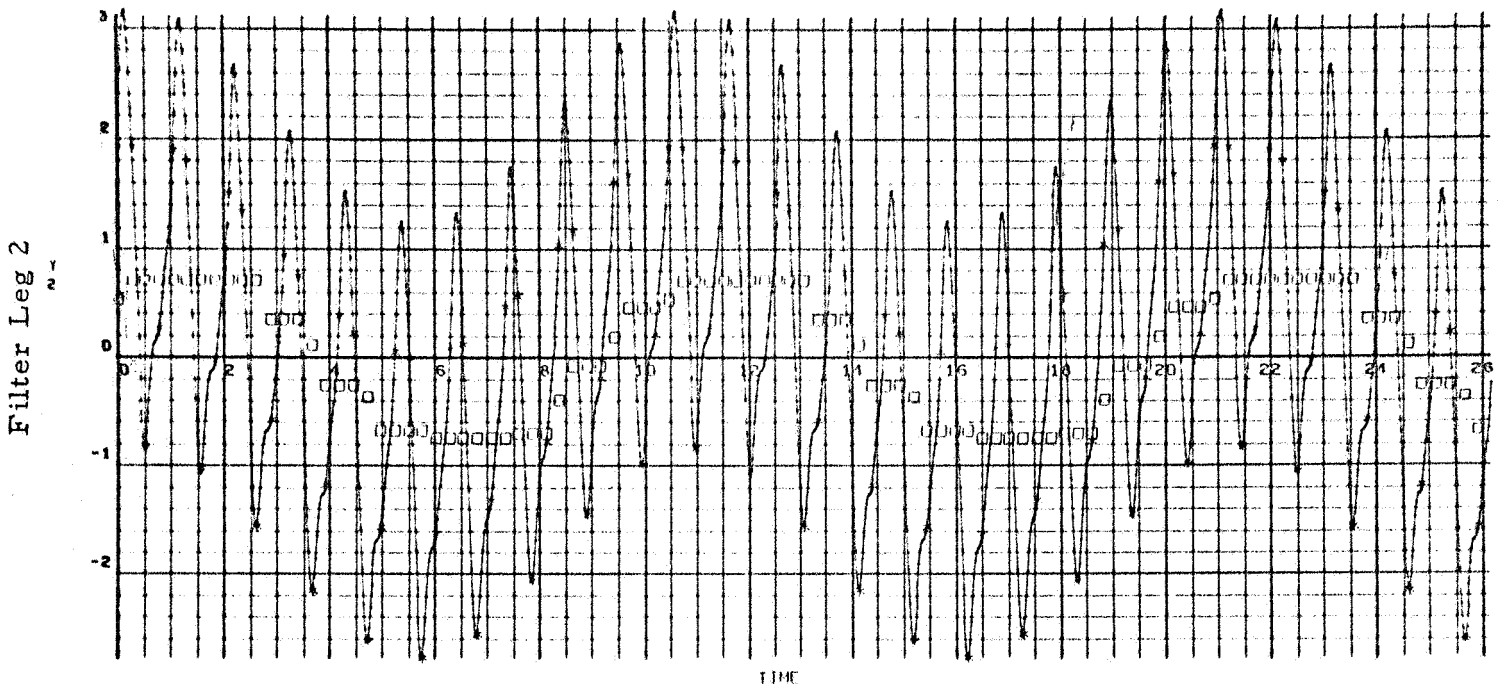
Table 1-3
 FILTER LEG 1 FREQUENCY CHARACTERISTICS ASSOCIATED WITH INPUT SIGNAL COMPONENTS

Frequency (rad/sec)	Continuous		Difference Equation					
			ω_s (rad/sec)					
	Amp	Phase (deg)	24		48		96	
.6	1.0116	-14.64	1.0159	-17.07	1.0127	-15.22	1.0119	-14.79
6.0	.5399	149.74	0.8319	124.16	0.5991	143.85	0.5539	148.30
12.0	.03904	62.23	0.4437	0.00	0.05964	50.04	0.04329	59.32
24.0	.00227	28.74	1.000	0.00	0.01412	0.00	0.00346	22.72

Table 1-4
 FILTER LEG 2 FREQUENCY CHARACTERISTICS ASSOCIATED WITH INPUT SIGNAL COMPONENTS

Frequency (rad/sec)	Continuous		Difference Equation					
			Sampling Frequency, ω_s (rad/sec)					
	Amp	Phase (deg)	24		48		96	
.6	.9712	-14.64	.9731	-17.07	0.9717	-15.22	0.9713	-14.78
6.0	1.6196	-30.26	2.0084	-55.84	1.7062	-36.15	1.6406	-31.70
12.0	0.5856	-117.77	1.4685	180.00	0.7238	-129.95	0.6167	-120.68
24.0	0.1431	-151.13	1.0000	0.00	0.3568	180.00	0.1766	-153.28

T = .262



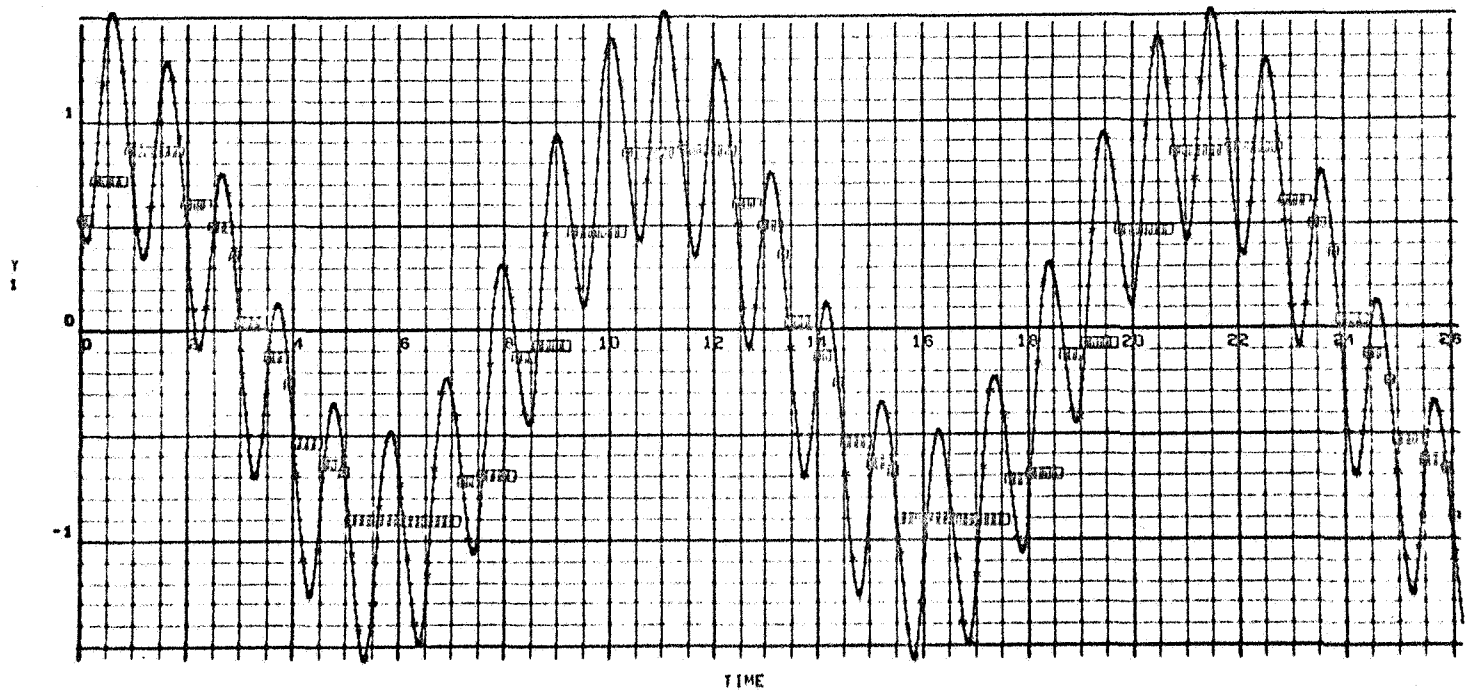
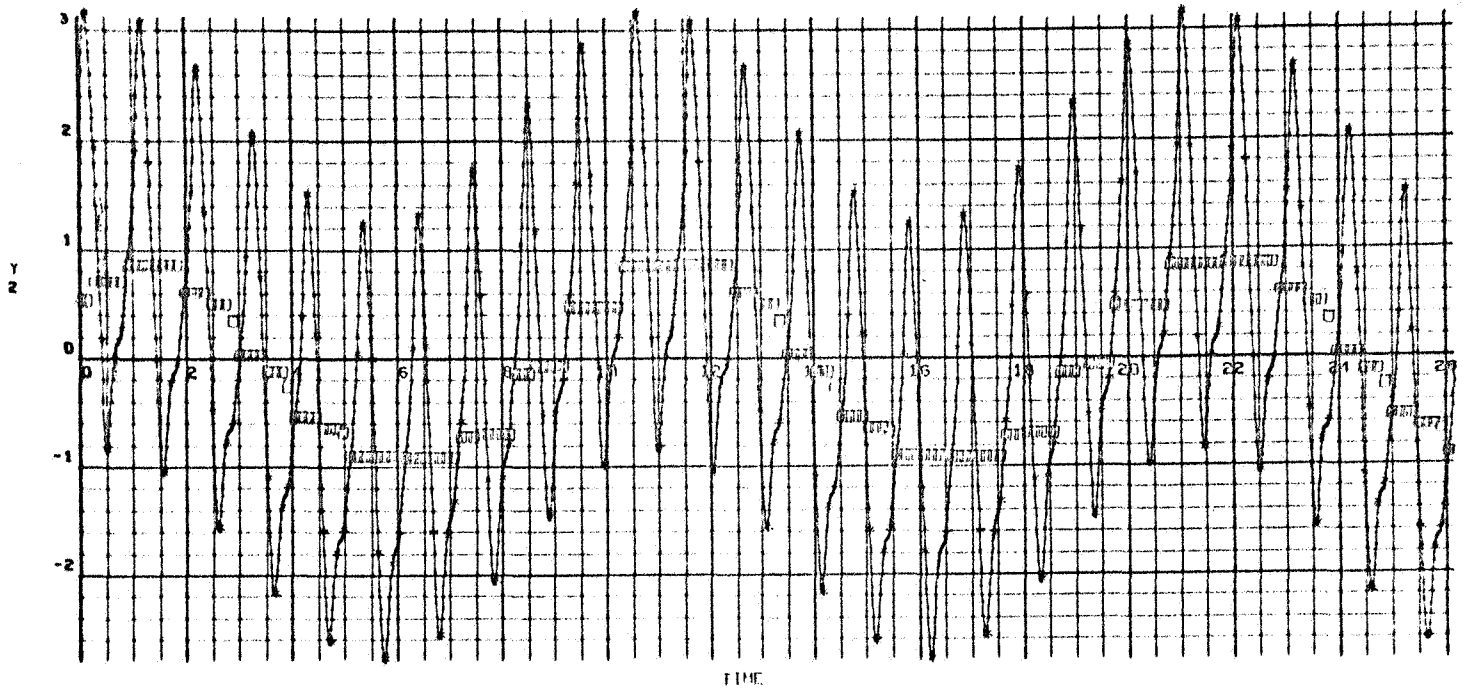
(*) Sampled values (T = .2618 sec)

(□) Output of digital logic

Figure 1-7 - Idealized Filter Response ($\omega_s = 24$ rad/sec)

470220
000 006

T = .131



(*) Sampled values (T = .1309 sec)

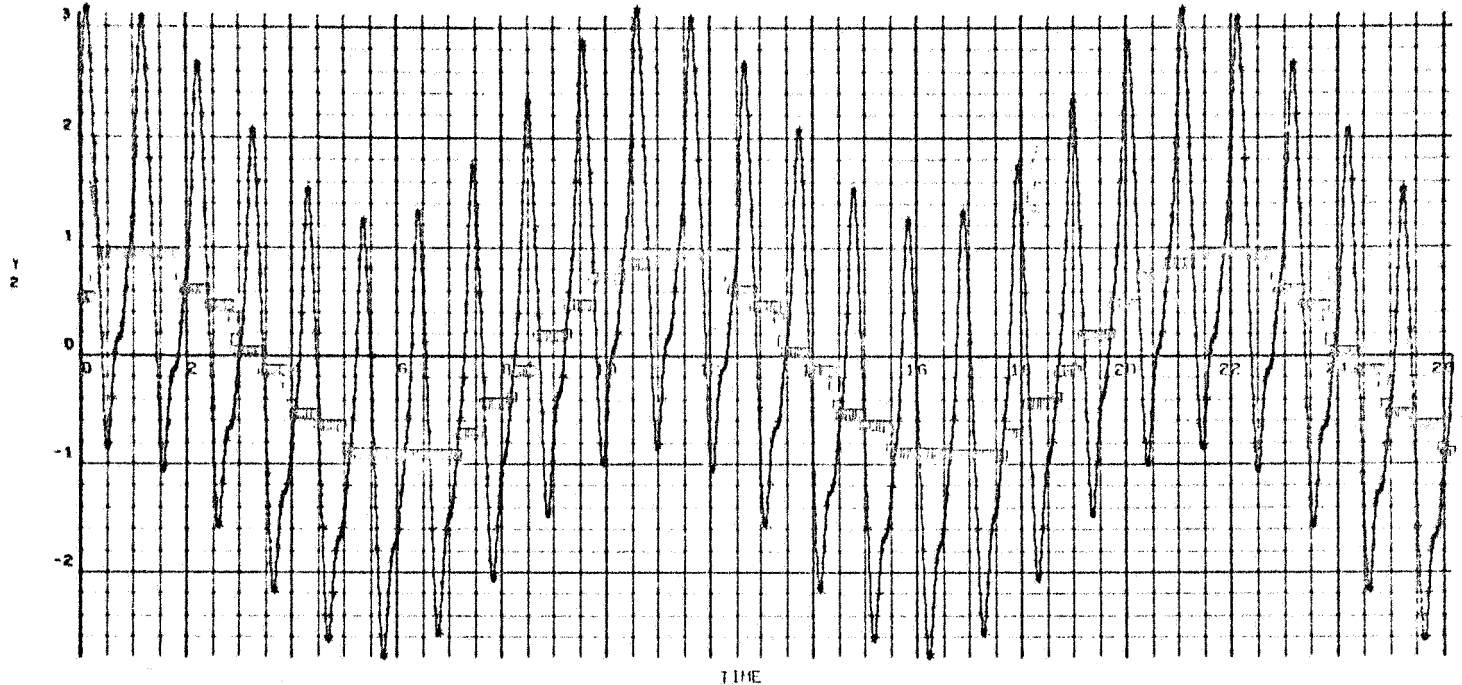
(□) Output of digital logic

Figure 1-8 - Idealized Filter Response ($\omega_s = 48$ rad/sec)

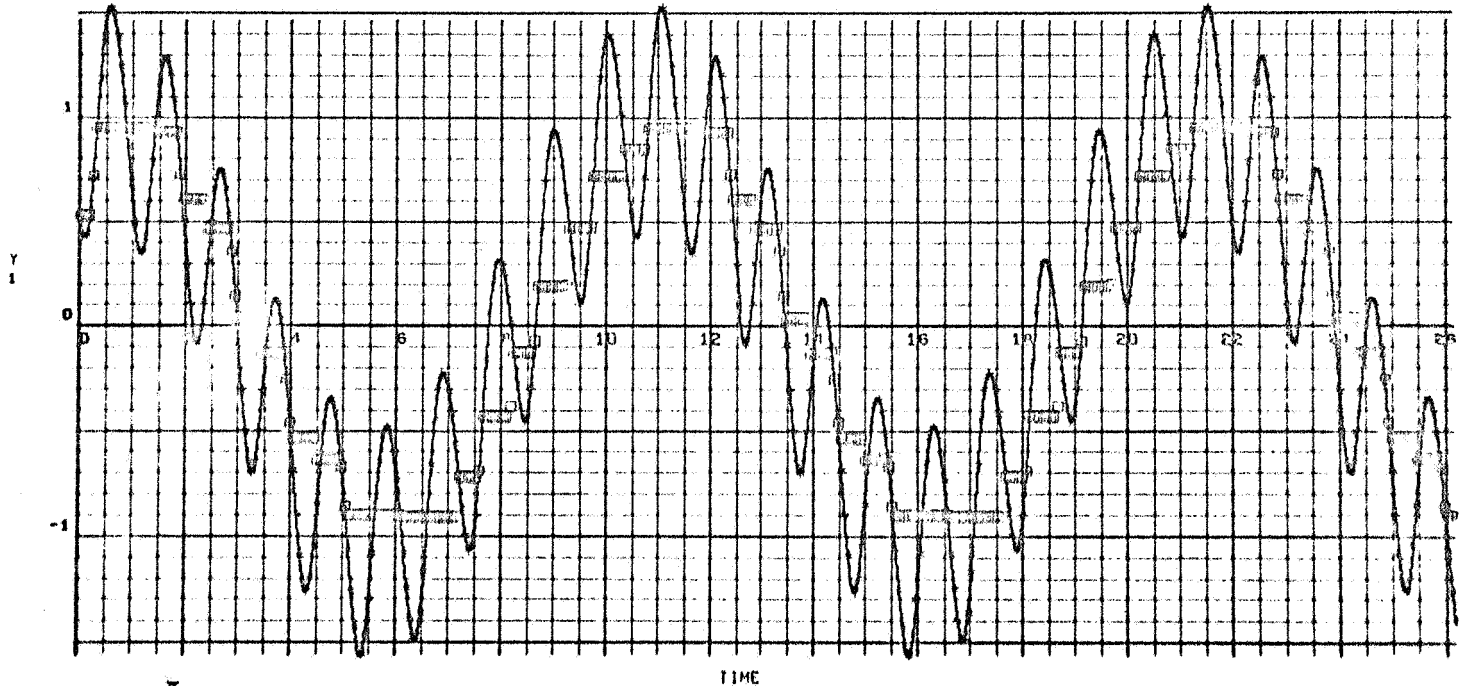
470220
000 110

$T = .0655$

Filter Leg 2



Filter Leg 1

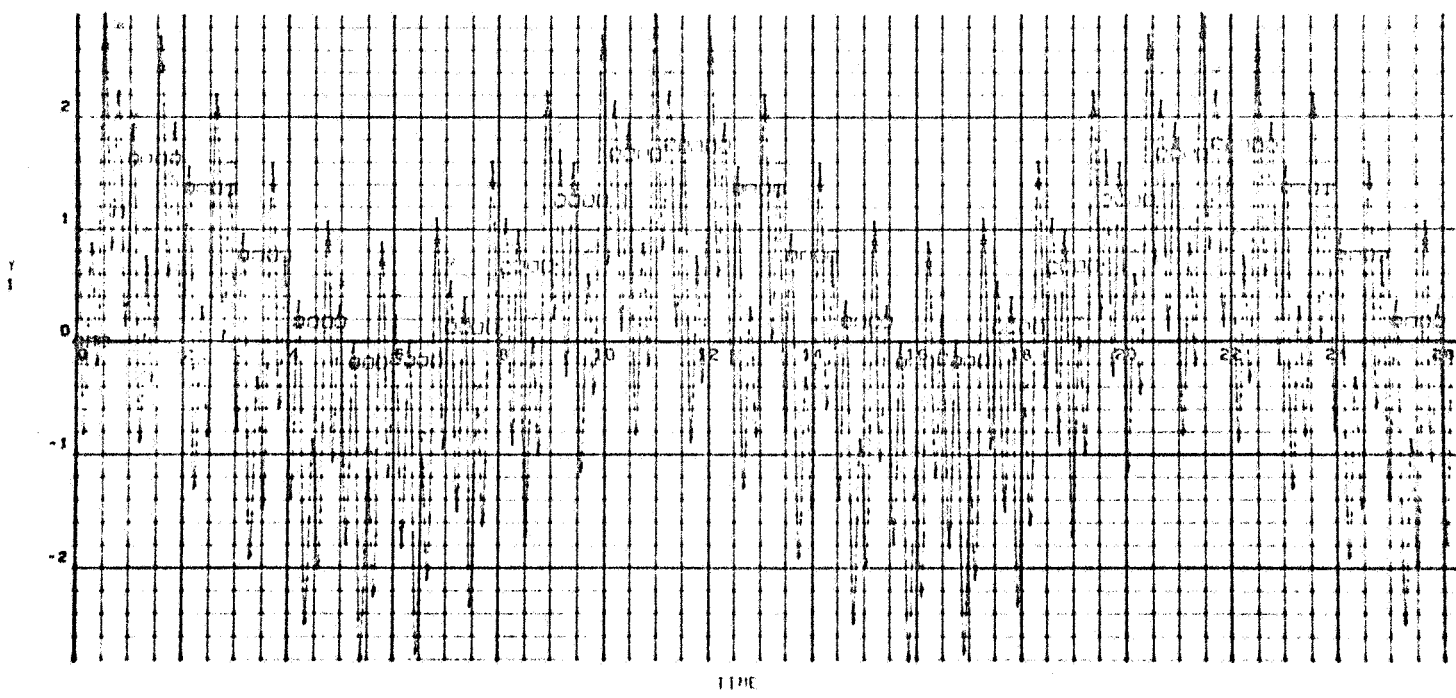
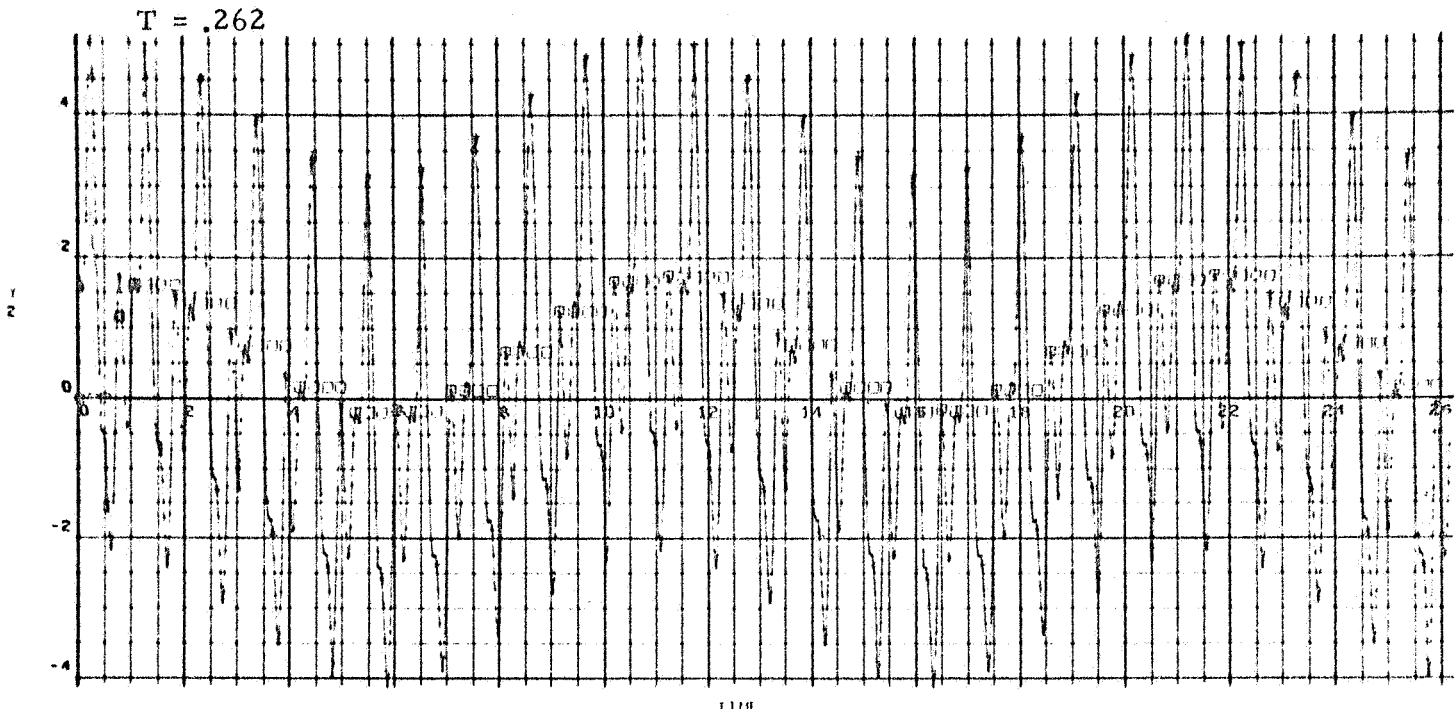


(*) Sampled values ($T = .06545$ sec)

(□) Output of digital logic

Figure 1-9 - Idealized Filter Response ($\omega_s = 96$ rad/sec)

47 225
116 112

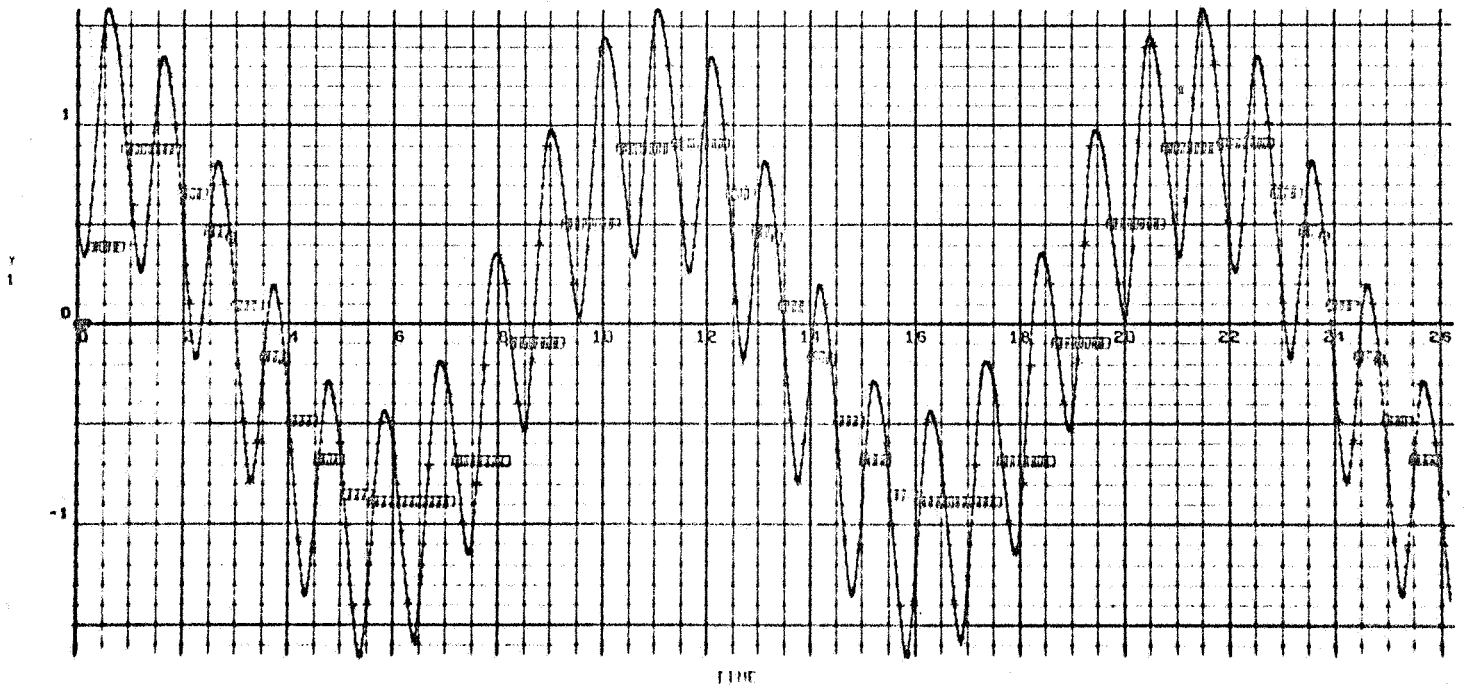
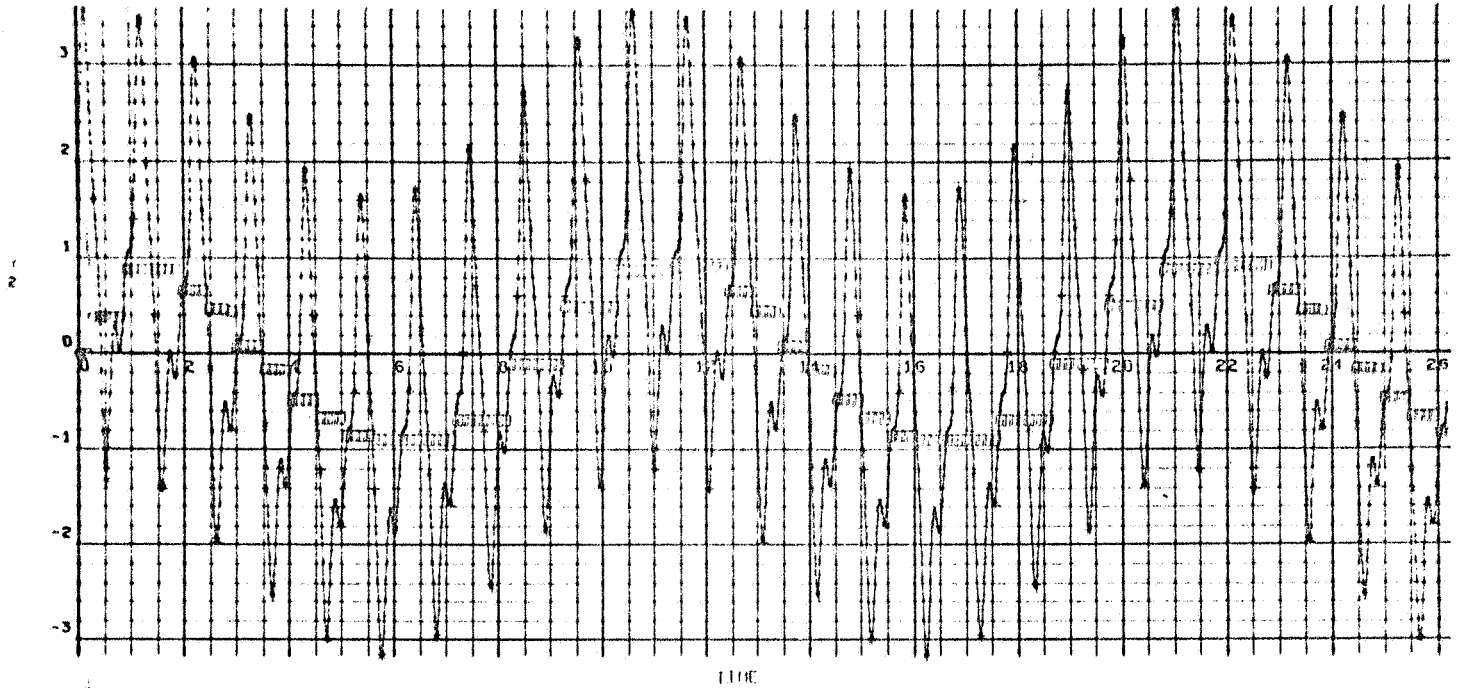


(*) Values computed from difference equations ($T = .2618 \text{ sec}$)

(□) Output of digital logic

Figure 1-10 - Digital Filter Response ($\omega_s = 24 \text{ rad/sec}$)

T = .131

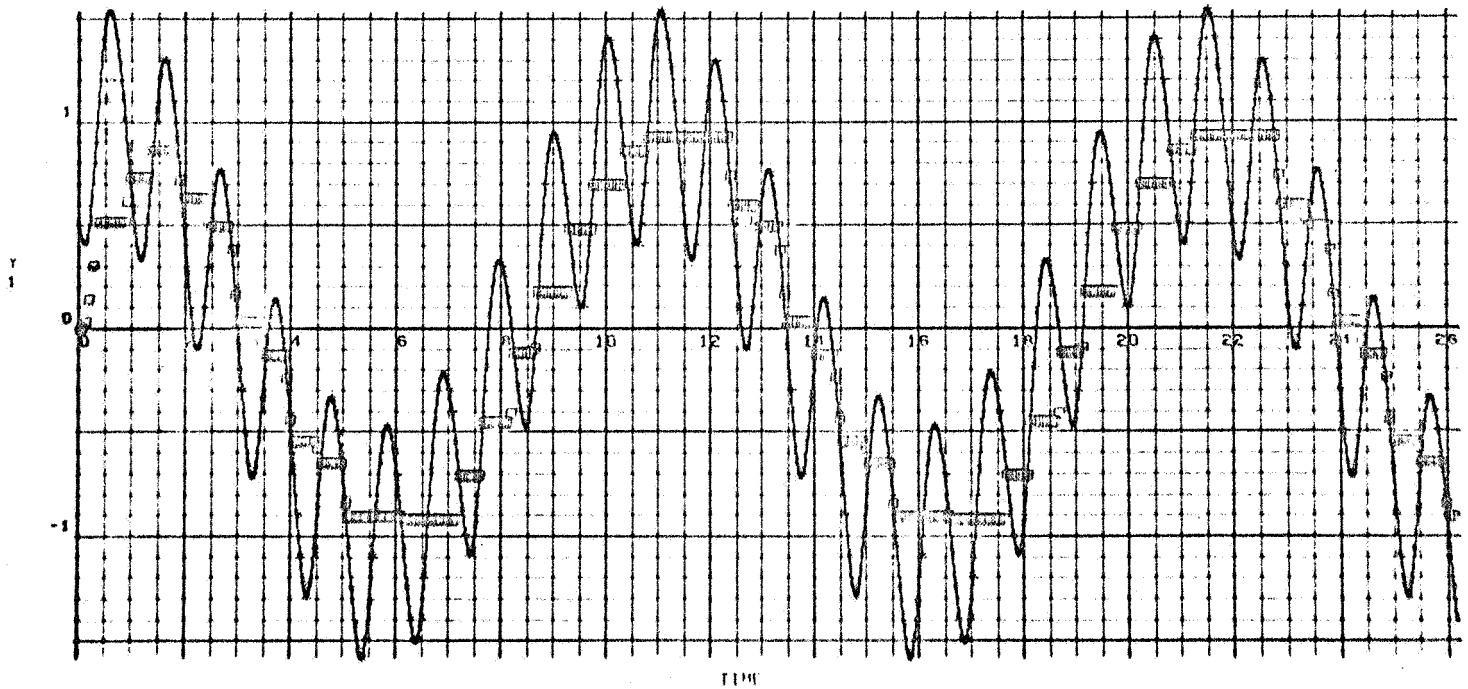
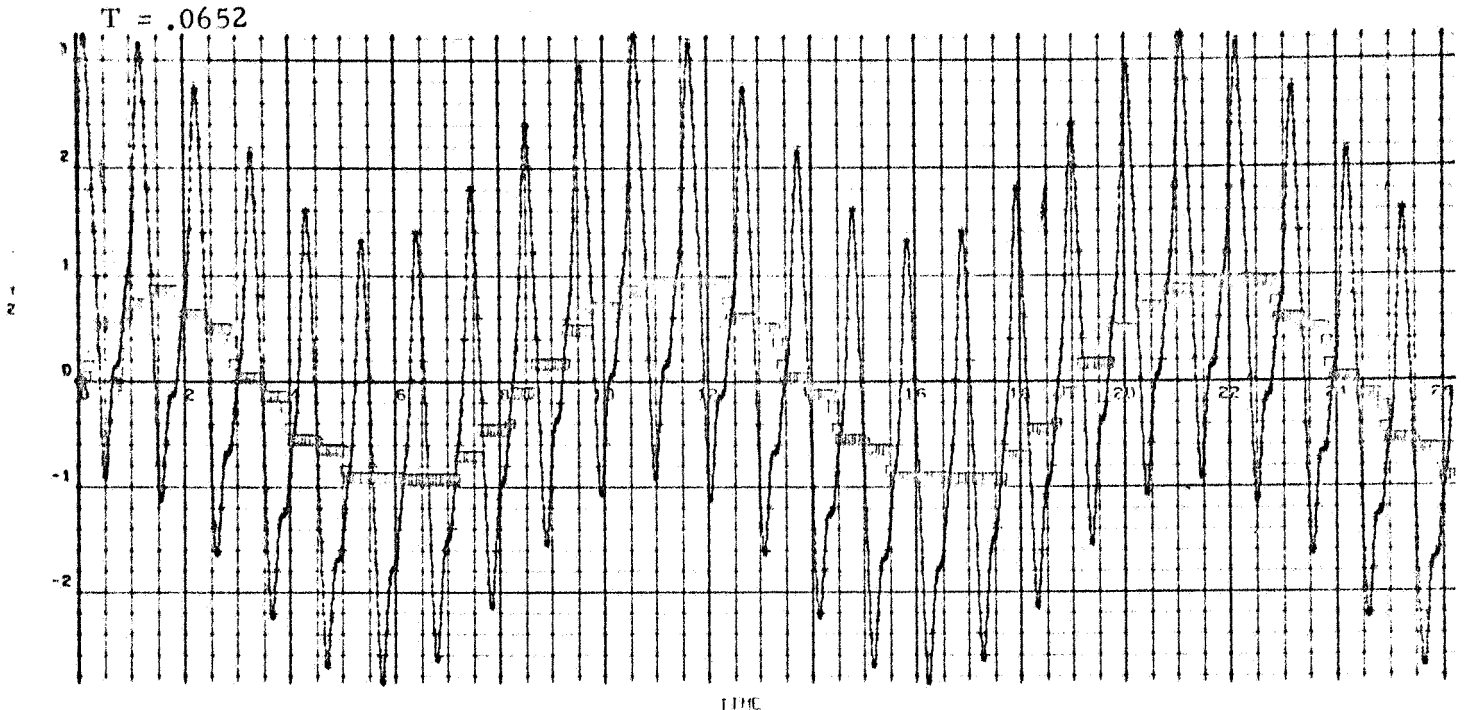


(*) Values computed from difference equations (T = .1309 sec)

(□) Output of digital logic

Figure 1-11 - Digital Filter Response ($\omega_s = 48$ rad/sec)

471221
000 100



(*) Values computed from difference equations ($T = .62545 \text{ sec}$)

(□) Output of digital logic

Figure 1-12 - Digital Filter Response ($\omega_s = 96 \text{ rad/sec}$)

1.4 CONCLUSIONS

When this study was initiated, whether the analog nonlinear filter (Reference 1) could be satisfactorily mechanized on a sampled data basis was uncertain. The performance seemed to depend on rather exact and continuous relationships between the amplitudes and phases of the two signals which were impressed on the diode bridge. The results presented here show that sampling of the signals does not appear to be a major problem. Performance of the filter comparable to the analog mechanization was obtained with relatively low sampling frequencies. The next check of the effect of sampling will be a simulation of the filter and launch vehicle.

Section 2

SIMULATION AND APPLICATION OF NONLINEAR FILTER
TO LAUNCH VEHICLE

- 2.1 Summary
- 2.2 Introduction
- 2.3 Discussion
- 2.4 Results
- 2.5 Conclusions
- 2.6 Illustrations

Section 2

SIMULATION AND APPLICATION OF NONLINEAR FILTER
TO LAUNCH VEHICLE

2.1 SUMMARY

This section presents a study of the effectiveness of the nonlinear filter in the Saturn V attitude control system for the AS-503, S-IC boost phase. This study extends the scope of Reference 2, of Appendix E and investigates the application of a digital version of the filter to the vehicle control system.

The system simulation is completely digital and includes the first three vehicle bending modes in addition to propellant sloshing models for the first three tanks.

Two forms of the filter are investigated; a continuous version which represents an active, electrical network realization, and a corresponding digital version for realization in the onboard digital computer. Both control system versions are subjected to adverse wind disturbances and are also studied in their responses to step attitude commands. Comparisons are made with the AS-503 linear filters. Extreme changes are also made in bending mode characteristics such as reversal of bending modes sign.

Results indicate that the application of the nonlinear filter to the Saturn V attitude control system is feasible in both its forms, the analog version and the digital implementation.

2.2 INTRODUCTION

This study represents the culmination of the work performed in References 1 and 2 of Appendix E. In Reference 1, the nonlinear filter

was evaluated in the Saturn V control system on a fixed-point-in-flight-time basis with three bending modes and one slosh mode included. Reference 2 extended this study to a description of the same system with time-varying coefficients. This study was limited to one bending and sloshing mode since it was performed on an all-analog simulation. Complete background is given in Appendix A. The system simulation for this study is a time-varying coefficient digital program and includes three bending modes and three propellant sloshing modes.

The study makes use of the simulation to compare the control system responses of the nonlinear filter implemented in two forms:

- A continuous form which represents the filter in an application as an active electrical network located in the Saturn V flight control computer.
- A digital form which describes the filter by difference equations and can be programmed into the Saturn V onboard digital flight computer.

Included also are the associated control system responses of the AS-503 linear control filters.

The ability of the digital form of the filter to stabilize the control system is directly a function of the sampling rate of the system computer. Therefore, the three cases examined in Section 1, $\omega_s = 24, 48, 96$ rad/sec, are used to determine the relative effectiveness of the digital nonlinear filter.

2.3 DISCUSSION

2.3.1 Saturn V Attitude Control System

General

The vehicle attitude control system of the Saturn V, S-IC stage, is shown in Figure 2-1* in block diagram form. The system provides control

* Illustrations are presented in Section 2.6, beginning on page 2-8.

in the pitch, yaw, and roll planes; and each channel contains a rate and position gyro. Since the vehicle is symmetrical in pitch and yaw, the study is confined to the pitch channel.

Equations and Input Data

The equations of motion for the pitch plane are presented in Appendix B and the associated nomenclature is given in Appendix C. The time-varying coefficients include the mass parameters, aerodynamics, and bending and slosh mode parameters for AS-503. Plots of these coefficients are shown in Appendix D as a function of flight time. The AS-503 Reference Trajectory of Reference 11 in Appendix E was used for the nominal trajectory in the simulation.

The control gains, a_0 and a_1 , and associated gain-change schedule for the linear filters are given below and agree with Reference 6, in Appendix E.

<u>a_0</u>	<u>a_1</u>	<u>Time</u>
.90	.69	$0 < t \leq 105$
.45	.44	$105 < t \leq 120$
.32	.30	$t > 120$

The control gains and gain-change schedule used for the nonlinear filter are given in the following and represent the result of several trial computer runs to determine an adequate set of gains for the particular set of nonlinear filter parameters used in this study.

<u>a_0</u>	<u>a_1</u>	<u>Time</u>
.25	.60	$0 < t \leq 105$
.20	.30	$t > 105$

The instrument locations are in the Instrument Unit, Station 3240. Although the rate gyro has a bandwidth much higher than the control and flexibility frequencies, its frequency characteristics are included in the simulation; the position gyro is considered frequency insensitive. The rate gyro damping ratio, ζ_G , and undamped natural frequency, ω_G , are 0.7 and 188 rad/sec, respectively.

The actuator transfer function is presented in Appendix B and is the same approximated transfer function used in previous studies.

2.3.2 Nonlinear Filter Equations

The nonlinear filter is shown in Figure 1.1 of Section 1 in block diagram form. Discussion of the operation of the filter and analyses of the analog and digital forms have been covered in Section 2 and previous material. Selection of the parameters for linear portions of the nonlinear filter is in agreement with case 37 of Reference 1 of Appendix E. Values are given below.

$\underline{\omega_1}$	$\underline{\zeta_1}$	$\underline{\omega_2}$	$\underline{\zeta_2}$	$\underline{\omega_c}$
4.5	.5	6	.6	3

where $\omega_1, \omega_2, \omega_c$ are radians/second.

The nonlinear portion of the filter is simulated ideally as presented in Section 1 and is used for both the continuous and digital version of the nonlinear filter.

The continuous form of the nonlinear filter represents the analog version of the filter. When used in the control system, its transfer is evaluated every computational pass through the digital program in the simulation. The digital version represents the filter in difference equation form; and its transfer is not updated every computation pass but at specific intervals which correspond to a computer computational cycle in an applied system. A range of values for the sampling interval are examined and concur with those analyzed in Section 1 (shown below).

$\underline{T \text{ (sec)}}$	$\underline{\omega_s \text{ (rad/sec)}}$
0.2617994	24
0.1308997	48
0.06544985	96

The difference equation form and associated difference equation coefficients are given in Table 1-2 of Section 1.

2.4 RESULTS

2.4.1 General

Comments are made with respect to a series of time response runs presented in Figures 2-4 through 2-17. Two forms of excitations are used in the study. The wind disturbance time history is shown in Figure 2-2 and the ϕ_c time history is given in Figure 2-3.

2.4.2 Effects of Wind Disturbances

Figures 2-4 and 2-5 show the Saturn V responses to a wind disturbance. Response of the linear filters are shown in Figure 2-4 and that of the continuous version of the nonlinear filter in Figure 2-5. As may be observed, the only significant difference in the two responses is in the second bending mode in the region around 90 seconds. Overall system sensitivity in the region about maximum q (77.25 seconds) is slightly higher for the continuous nonlinear filter. This can be attributed to the difference in rigid body characteristics since different control gains are used in each case.

Figures 2-6 through 2-8 show the Saturn V responses to a wind disturbance with the digital nonlinear filter for the three sampling frequencies. All three cases exhibit virtually the same amount of attitude control as the continuous nonlinear filter of Figure 2-5. The second bending mode oscillation in the 90 to 110 second is slightly more pronounced in the digital filter.

2.4.3 Effect of Attitude Step Commands at 58, 80 and 126 Seconds

Figures 2-9 and 2-10 show the Saturn V response to the ϕ_c time schedule. As may be seen the case with the linear filters in Figure 2-9 exhibits a significant amount of oscillation in the region preceding maximum q. Severest ringing exists in the third sloshing mode and the first bending mode which couples a noticeable amount of oscillation into the engine gimbal

angle, β . Responses to the step changes at 80 and 126 seconds are normal. It should be noted that the negative of the ϕ_c time schedule was input to the system; however, this has no effect on the use of the run for comparison purposes. Inspection of Figure 2-10 shows the continuous nonlinear filter to be similarly responsive with the exceptions of less oscillations in the sloshing modes and an increase in the bending mode ringing. Note also that the oscillation after 126 seconds at the rigid body frequency is slightly increased.

Figures 2-11 through 2-13 illustrate the Saturn V responses to ϕ_c with the three digital versions of the nonlinear filter. As may be seen, the 96 rad/sec case response is virtually the same as in the continuous case. Examination of all three cases shows that as the sampling frequency is decreased the rigid body frequency oscillation after 126 seconds increases. However, the large amount of ringing in the third slosh mode after the step at 58 seconds that occurred in the linear filter case now assumes a normal response in the 24 rad/sec case.

2.4.4 Effects of Bending Mode Variations

Figure 2-14 shows the Saturn V response to ϕ_c with all bending mode signs reversed for the 96 rad/sec digital filter case. This condition has been shown previously to be unstable when linear filters were used and stable for the continuous nonlinear filter (Reference 2 of Appendix E). Although there are slight differences, Figure 2-14 shows a stable response similar to the response shown in Figure 2-13 which is the same run but with correct bending mode signs. Figure 2-15 shows the response to ϕ_c with bending mode signs reversed with the 24 rad/sec digital filter case. The response is unstable at the rigid body frequencies after 90 seconds and indicates that the relatively long time between samples for this filter case is inadequate for controlling a vehicle which is rapidly becoming unstable in the interval between samples.

Figure 2-16 further demonstrates the ability of the digital filter to perform under adverse conditions. All bending mode damping ratios have been decreased by the factor 10 (from .005 to .0005). This run when compared with Figure 2-13 shows very little difference in response in the system variables which couple with bending. As may be observed, the bending mode oscillations are increased by the reduction in damping.

2.4.5 Digital Nonlinear Filter with Revised Control Gains

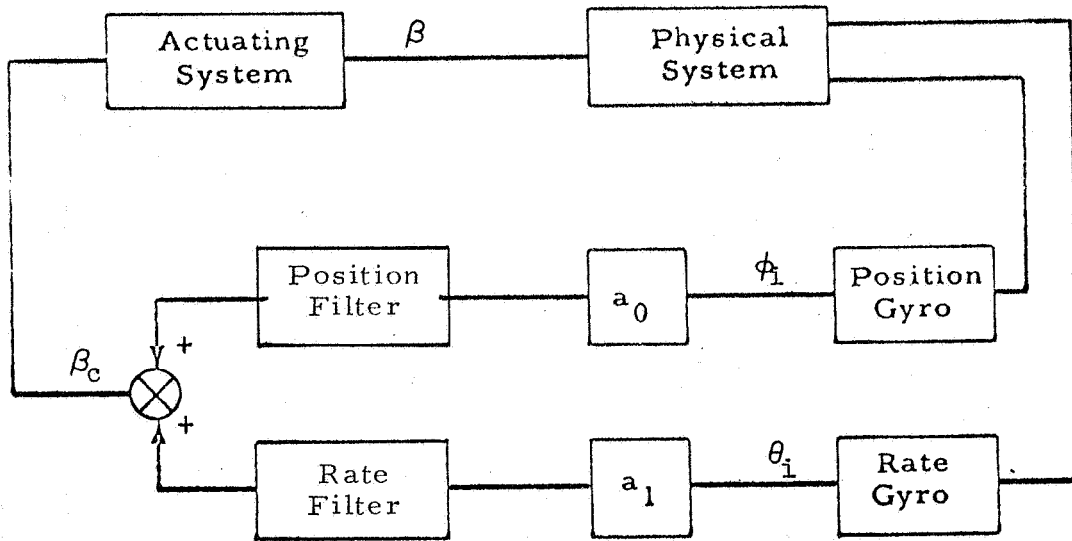
Figure 2-17 shows the Saturn V response to a wind disturbance with a revised control gains schedule using the 96 rad/sec case. The purpose of this run is to show that a higher position gain can be used in the region below maximum q . An advantage of higher position gain is the increased correction of thrust misalignment. Optimization of the control gains and gain-change schedule can be achieved by further study and consideration of other cases than case 37 of the nonlinear filter.

2.5 CONCLUSIONS

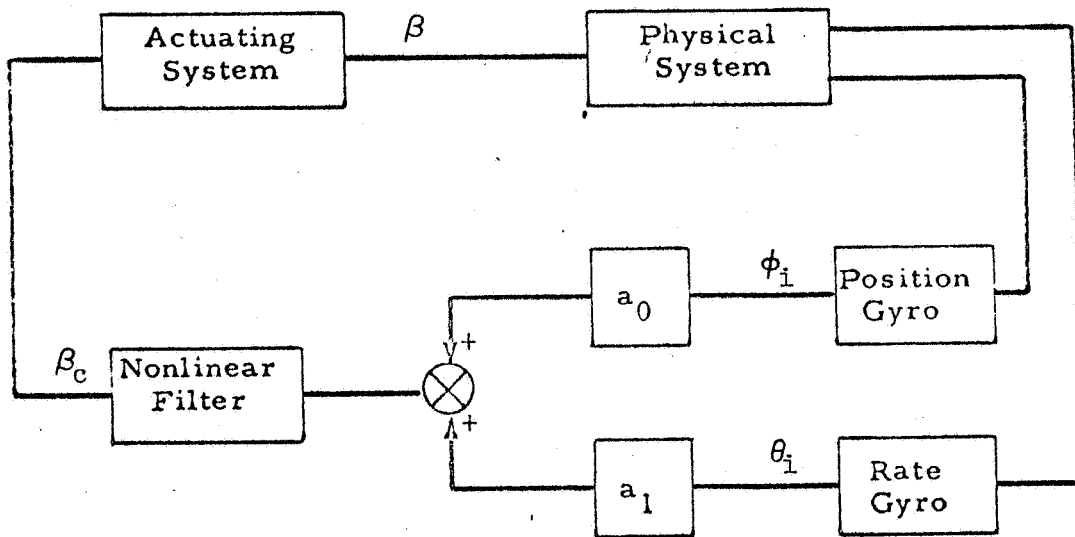
The nonlinear filter in its continuous and digital forms adequately stabilizes the Saturn V, S-IC control system in a time-varying coefficient simulation which includes three modes of bending and sloshing. The ability of the digital filter to stabilize the system under adverse conditions such as bending mode sign reversal has been shown to be a function of sampling frequency. It appears that the 24 rad/sec case filter lacks sufficient separation from the bending mode frequencies; however, the 96 rad/sec case filter performed well under this condition. This form of the filter would be readily adaptable to the Launch Vehicle Digital Computer (LVDC) since the LVDC minor loop computational interval is 40 milliseconds. The corresponding sampling frequency for the digital filter would be 157 rad/sec which is higher than the 96 rad/sec case in this study and would exhibit increased system control. A primary application of the digital nonlinear filter would be as a back-up to the existing linear filters in the flight control computer.

2.6 ILLUSTRATIONS

Figure	Title	Page
2-1	Simplified Diagram of Saturn V Attitude Control System	2-9
2-2	S-IC Stage Wind Disturbance Peaking at $t = 80$ Seconds	2-10
2-3	ϕ_c Time Schedule	2-11
2-4	Saturn V, S-IC Stage Response to Wind Disturbance — AS-503 Linear Filters	2-12
2-5	Saturn V, S-IC Stage Response to Wind Disturbance — Continuous Nonlinear Filter	2-15
2-6	Saturn V, S-IC Stage Response to Wind Disturbance — Digital Nonlinear Filter ($\omega_s = 24$ rad/sec)	2-18
2-7	Saturn V, S-IC Stage Response to Wind Disturbance — Digital Nonlinear Filter ($\omega_s = 48$ rad/sec)	2-21
2-8	Saturn V, S-IC Stage Response to Wind Disturbance — Digital Nonlinear Filter ($\omega_s = 96$ rad/sec)	2-24
2-9	Saturn V, S-IC Stage Response to ϕ_c — AS-503 Linear Filters	2-27
2-10	Saturn V, S-IC Stage Response to ϕ_c — Continuous Nonlinear Filter	2-30
2-11	Saturn V, S-IC Stage Response to ϕ_c — Digital Nonlinear Filter ($\omega_s = 24$ rad/sec)	2-33
2-12	Saturn V, S-IC Stage Response to ϕ_c — Digital Nonlinear Filter ($\omega_s = 48$ rad/sec)	2-36
2-13	Saturn V, S-IC Stage Response to ϕ_c — Digital Nonlinear Filter ($\omega_s = 96$ rad/sec)	2-39
2-14	Saturn V, S-IC Stage Response to ϕ_c with all Bending Mode Signs Reversed — Digital Nonlinear Filter ($\omega_s = 96$ rad/sec)	2-42
2-15	Saturn V, S-IC Stage Response to ϕ_c with all Bending Mode Signs Reversed — Digital Nonlinear Filter ($\omega_s = 24$ rad/sec)	2-45
2-16	Saturn V, S-IC Stage Response to ϕ_c with all Bending Mode Damping Ratios Reduced by a Factor 10 — Digital Nonlinear Filter ($\omega_s = 96$ rad/sec)	2-46
2-17	Saturn V, S-IC Stage Response to Wind Disturbance with a Revised Control Gains Schedule — Digital Nonlinear Filter ($\omega_s = 96$ rad/sec)	2-49



(a) with Linear Filter



(b) with Nonlinear Filter

Figure 2-1 - Simplified Diagram of Saturn V Attitude Control System

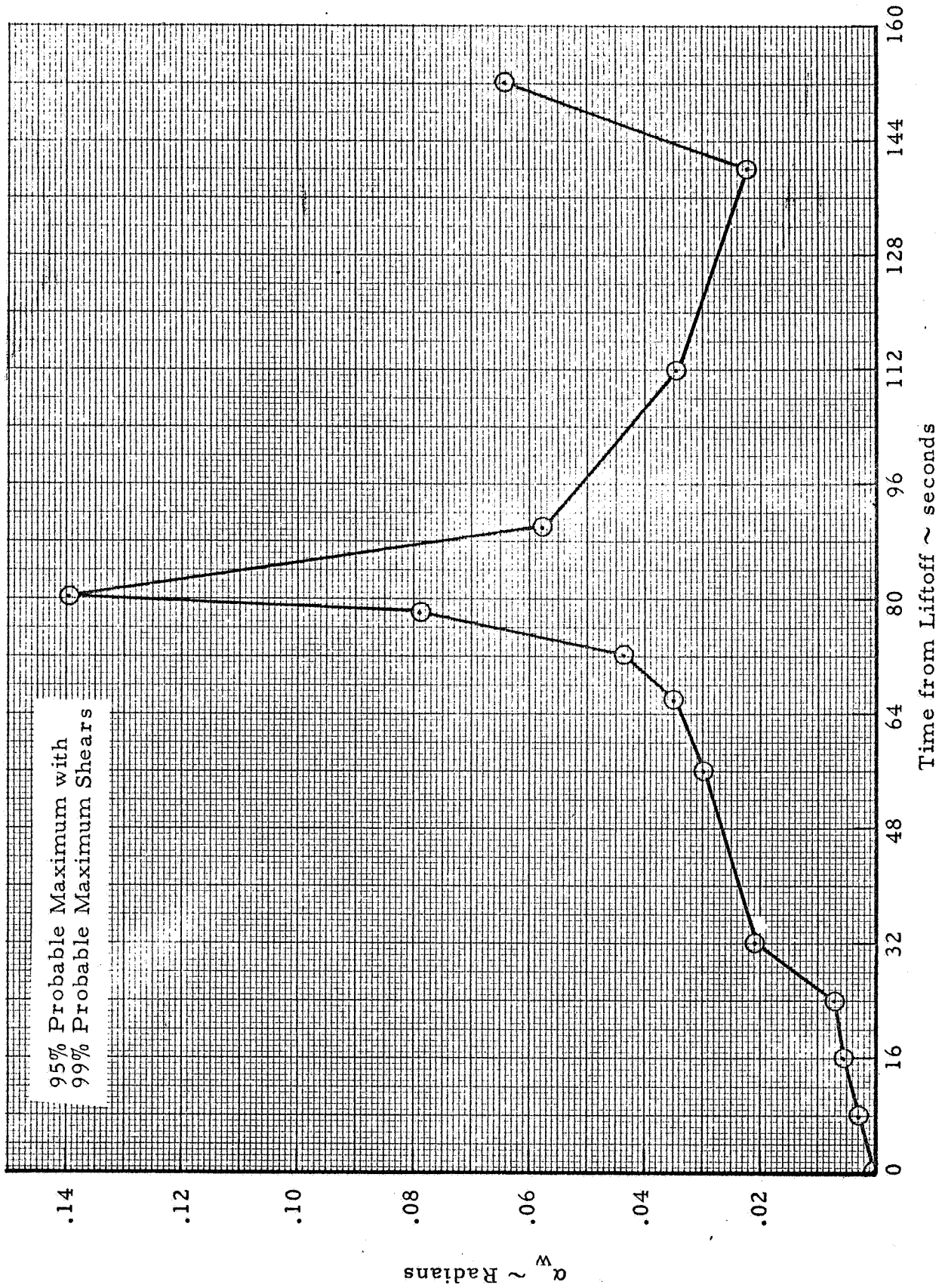


Figure 2-2 - S-IC Stage Wind Disturbance Peaking at t = 80 seconds

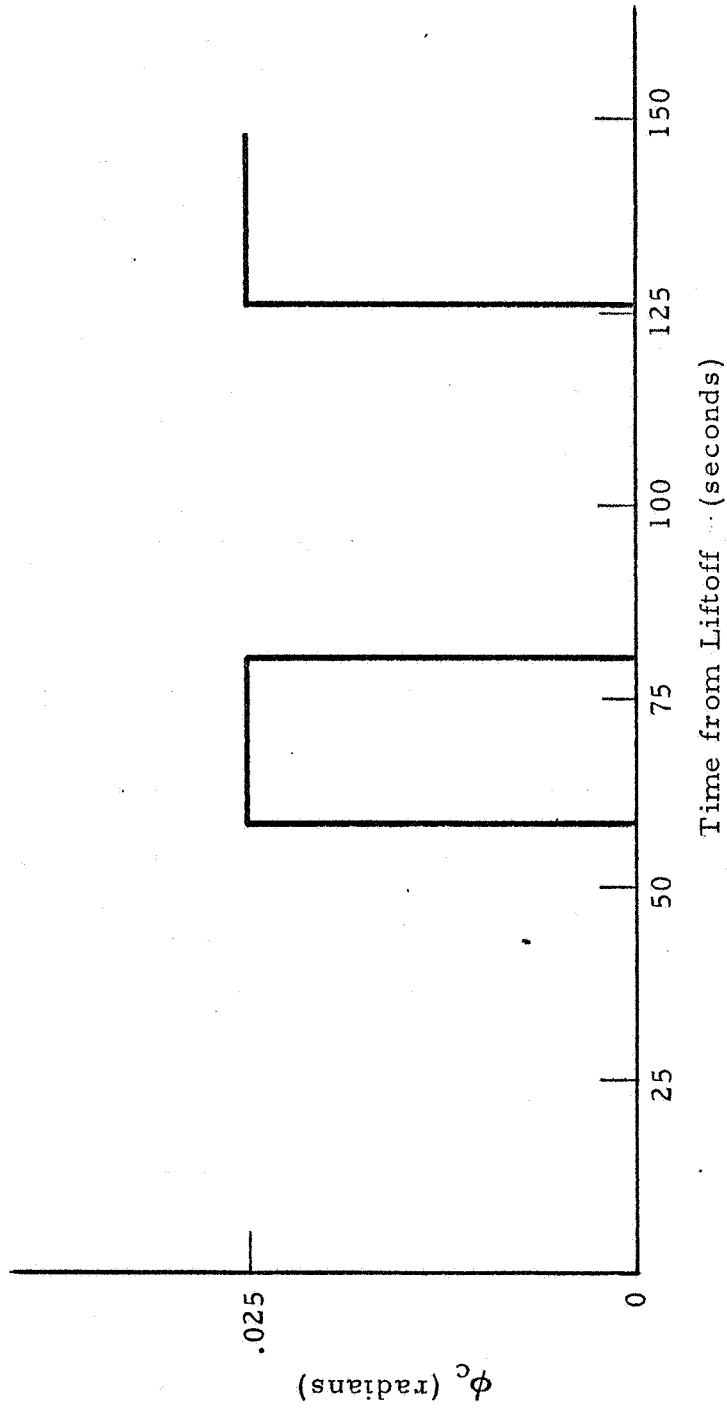


Figure 2-3 - ϕ_c Time Schedule

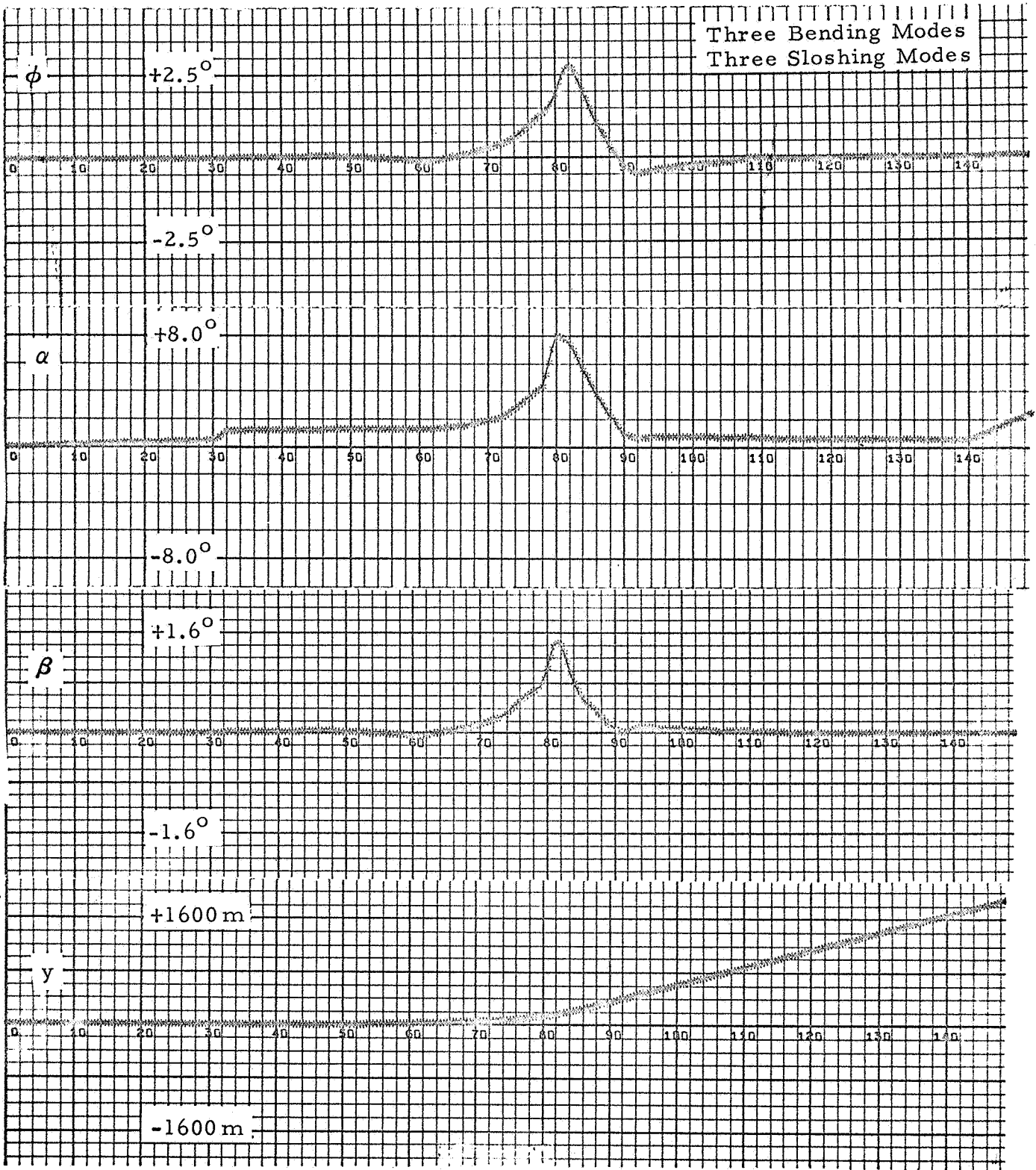


Figure 2-4a - Saturn V, S-IC Stage Response to Wind Disturbance - AS-503 Linear Filters

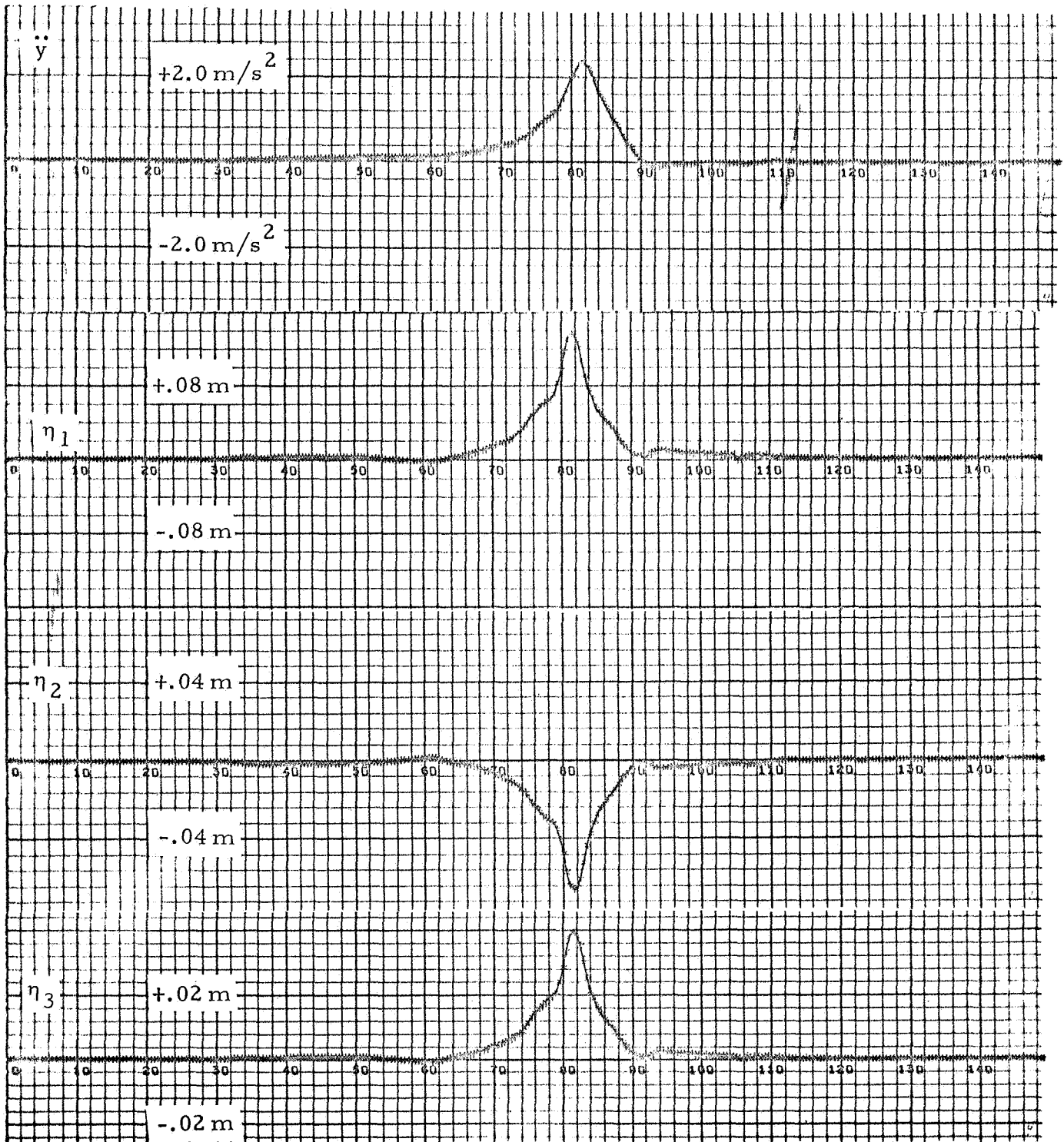


Figure 2-4b - Saturn V, S-IC Stage Response to Wind Disturbance - AS-503 Linear Filters

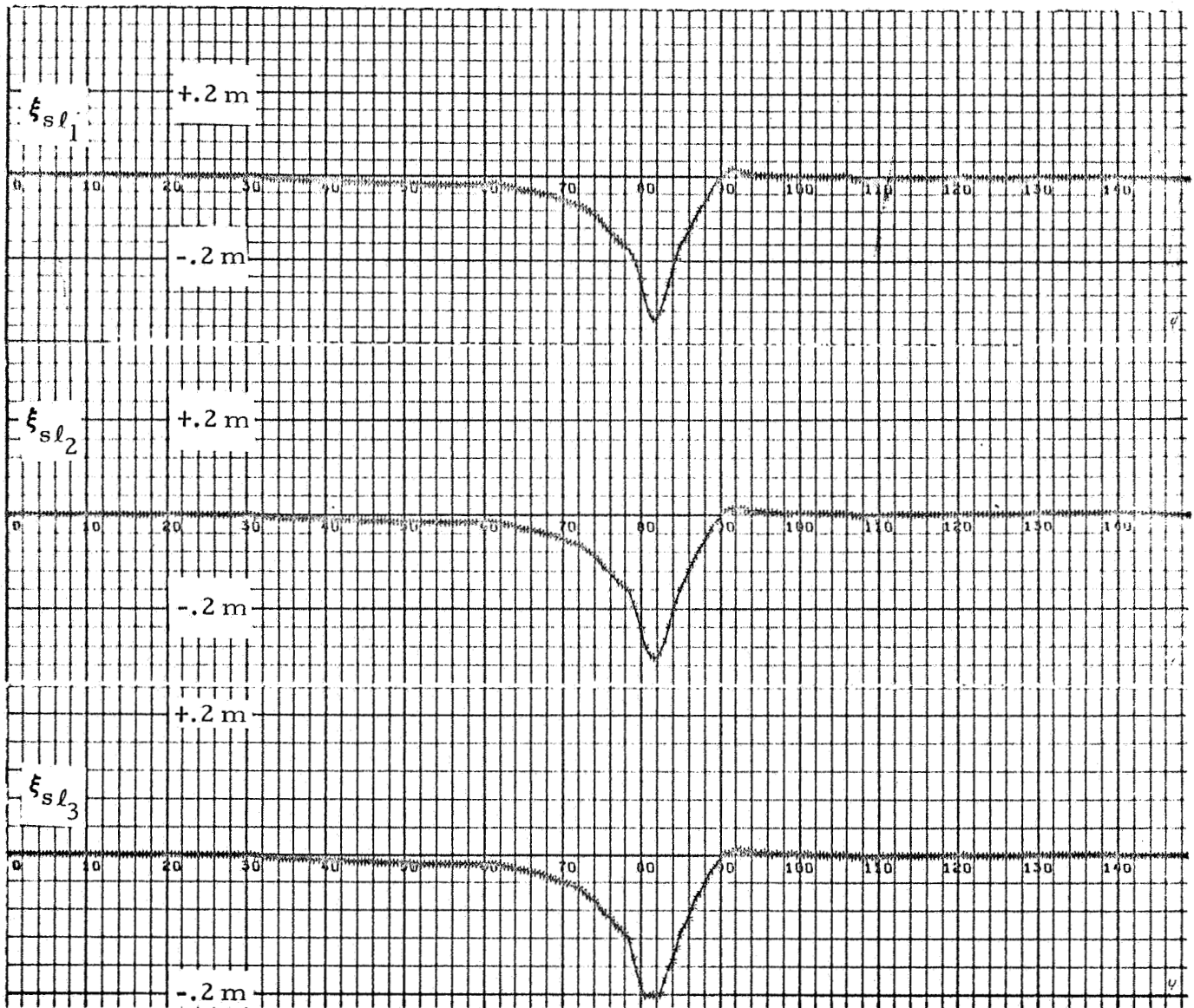


Figure 2-4c - Saturn V, S-IC Stage Response to Wind Disturbance - AS-503
Linear Filters

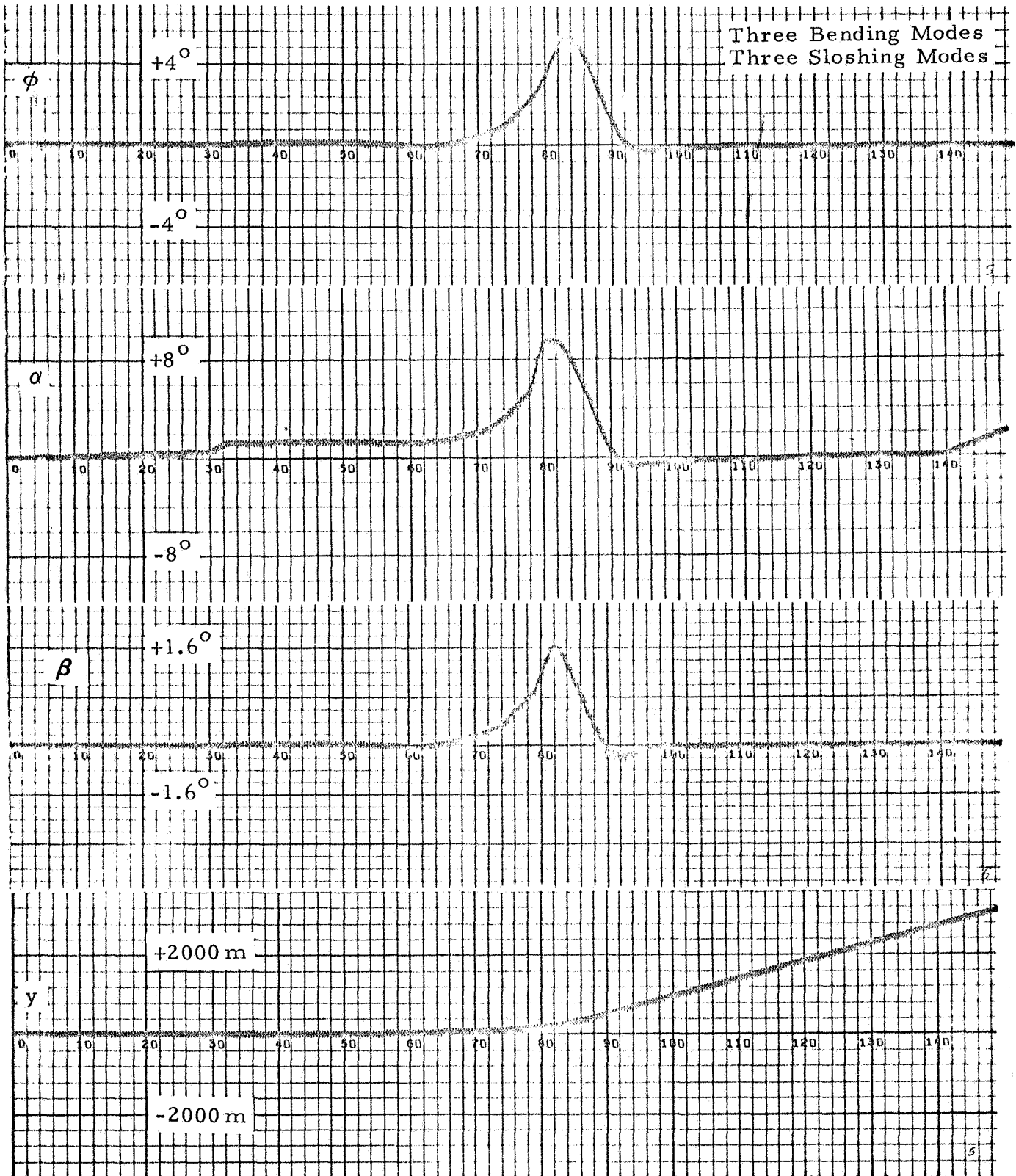


Figure 2-5a - Saturn V, S-IC Stage Response to Wind Disturbance - Continuous Nonlinear Filter

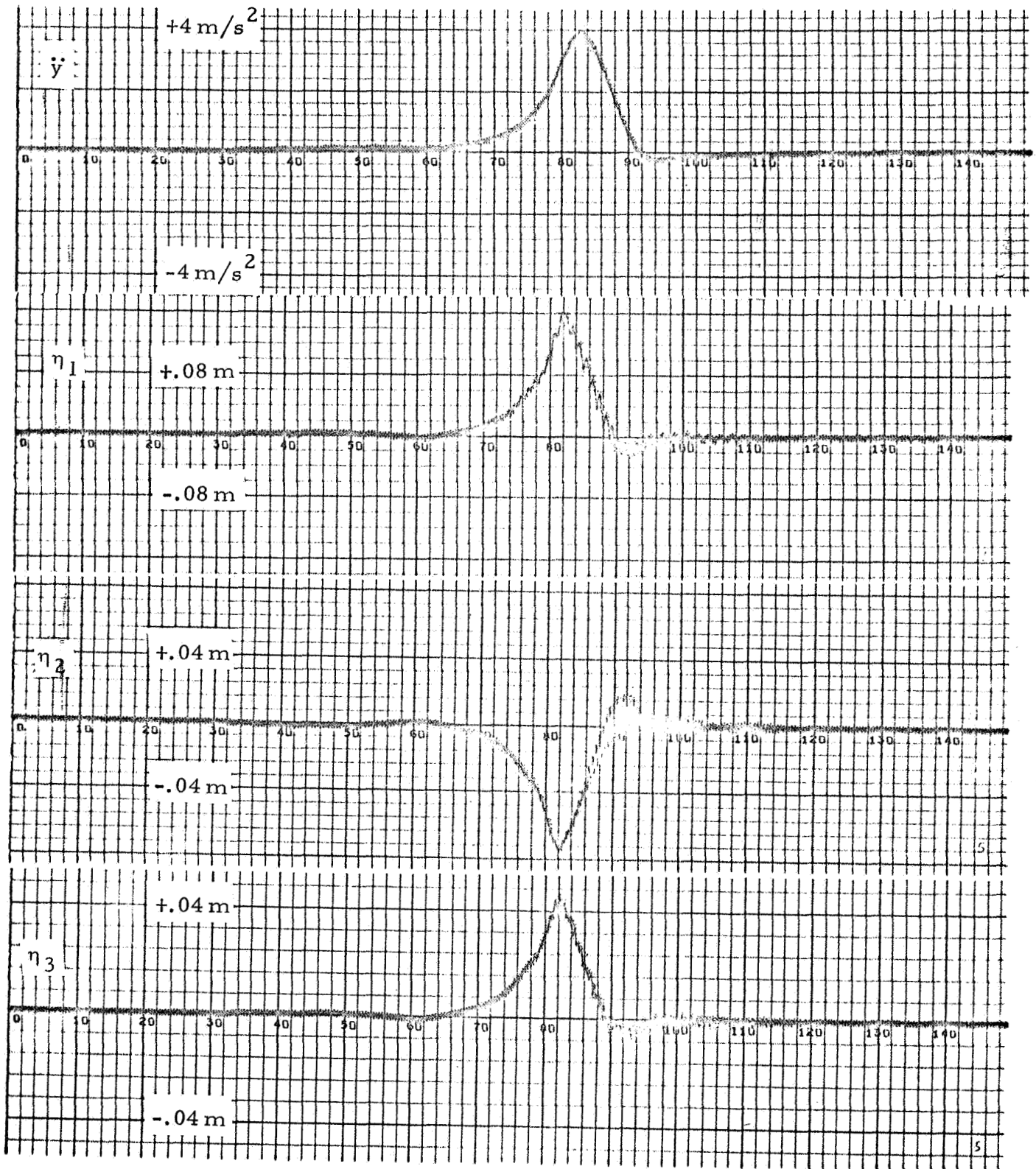


Figure 2-5b - Saturn V, S-IC Stage Response to Wind Disturbance - Continuous Nonlinear Filter

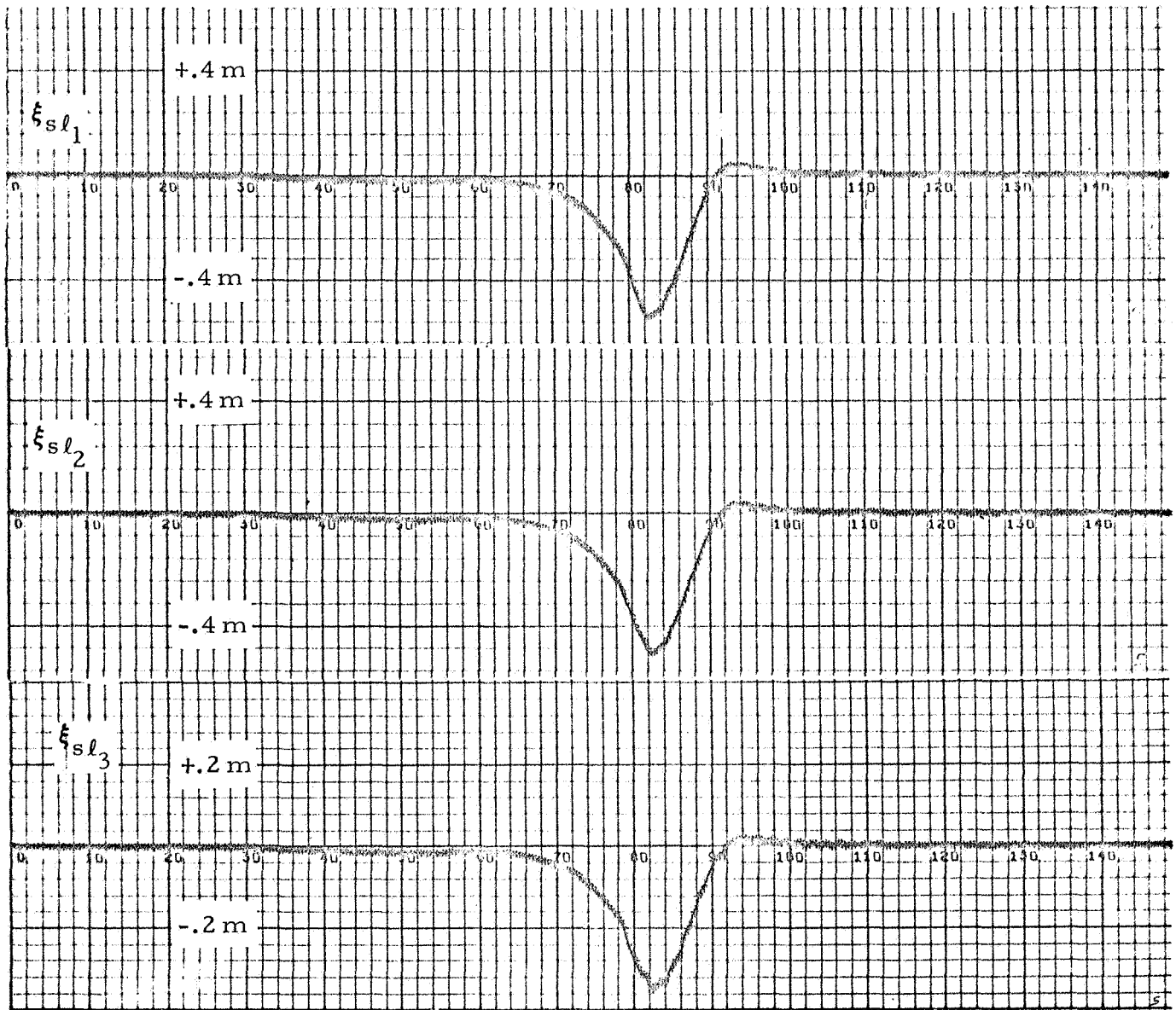


Figure 2-5c - Saturn V, S-IC Stage Response to Wind Disturbance -
Continuous Nonlinear Filter



Figure 2-6a - Saturn V, S-IC Stage Response to Wind Disturbance - Digital Nonlinear Filter ($\omega_s = 24$ rad/sec).

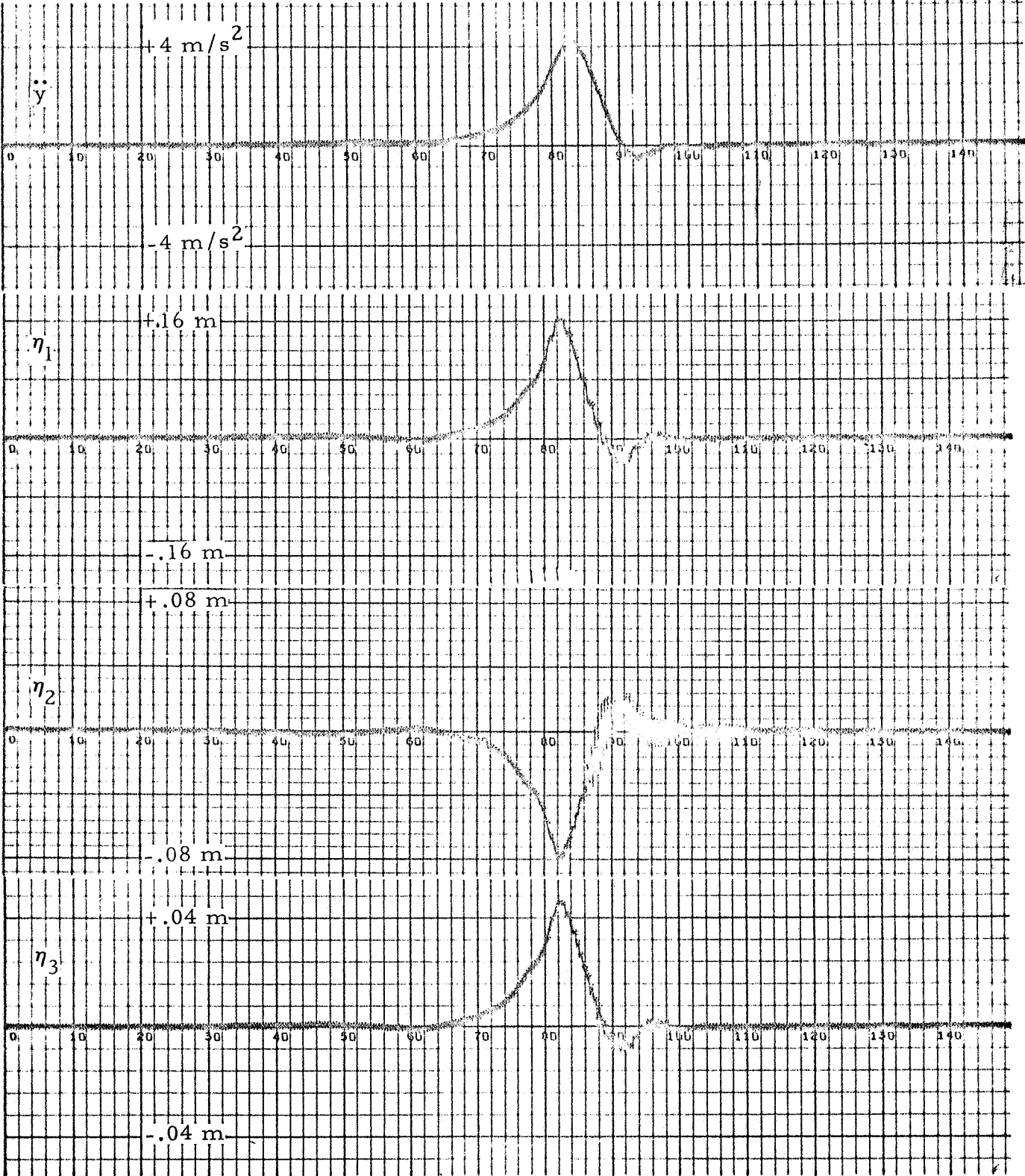


Figure 2-6b - Saturn V, S-IC Stage Response to Wind Disturbance - Digital Nonlinear Filter ($\omega_s = 24 \text{ rad/sec}$).

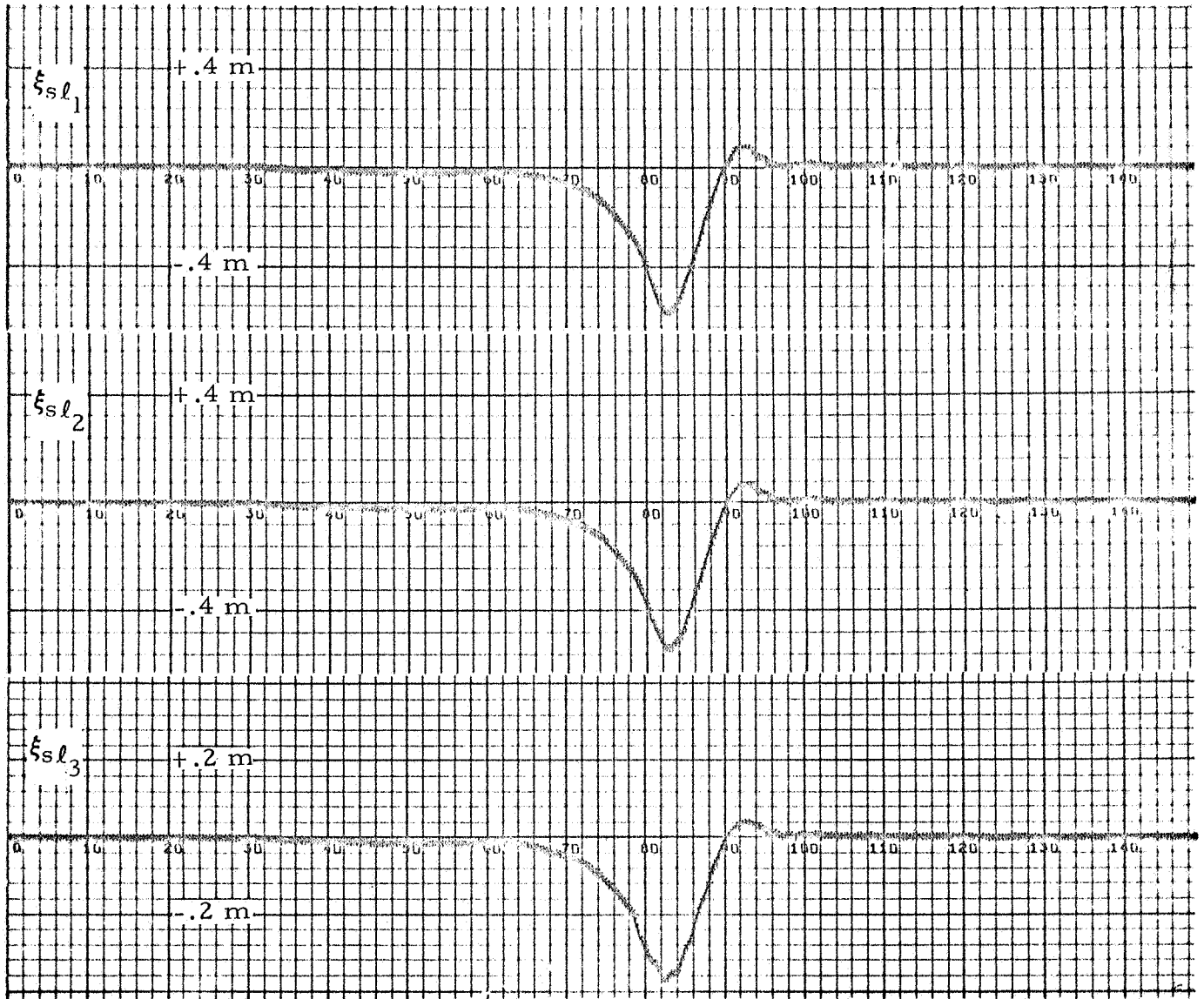


Figure 2-6c - Saturn V, S-IC Stage Response to Wind Disturbance - Digital Nonlinear Filter ($\omega_s = 24$ rad/sec).

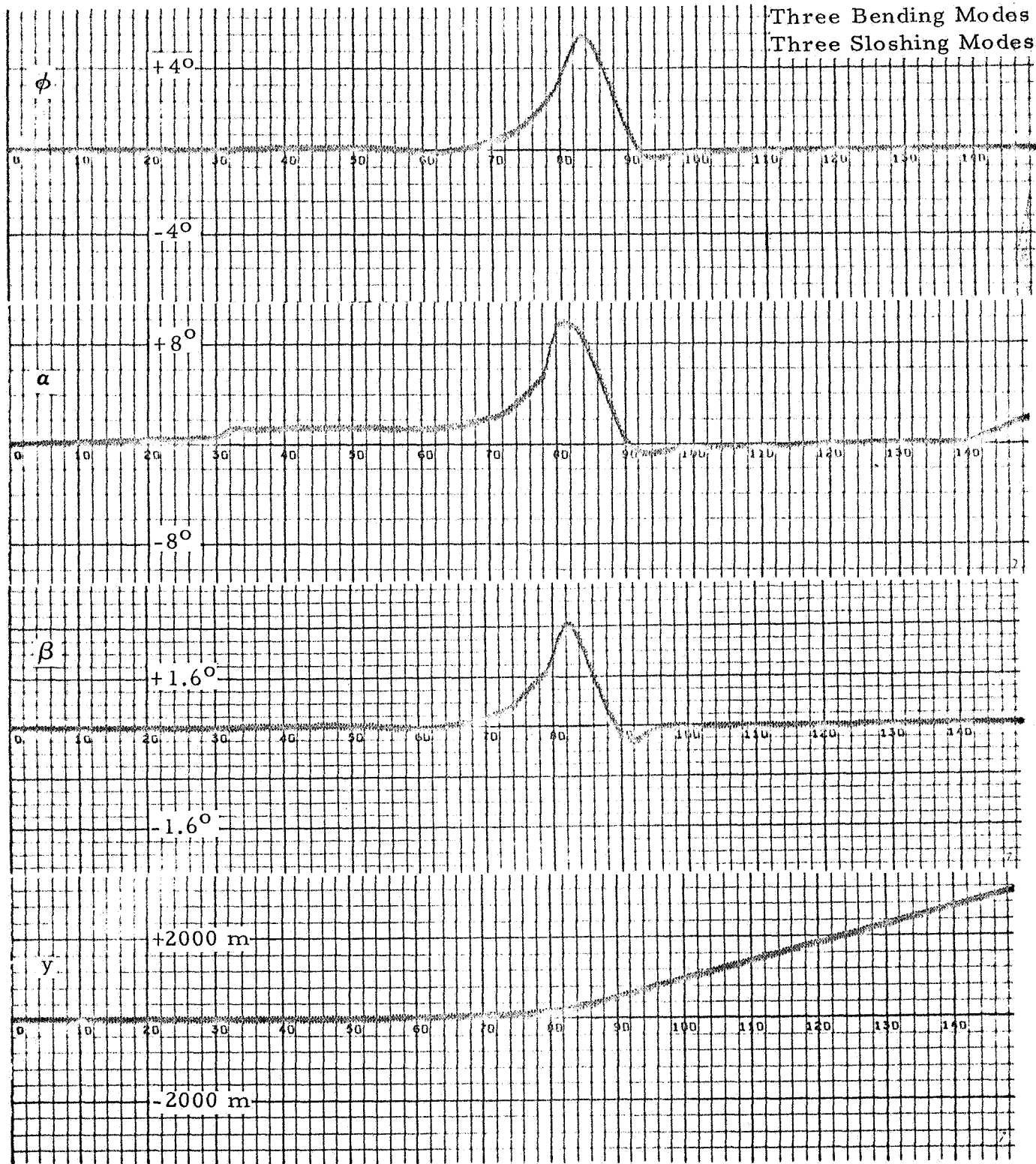


Figure 2-7a - Saturn V, S-IC Stage Response to Wind Disturbance - Digital Nonlinear Filter ($\omega_s = 48$ rad/sec).



Figure 2-7b - Saturn V, S-IC Stage Response to Wind Disturbance - Digital Nonlinear Filter ($\omega_s = 48 \text{ rad/sec}$).

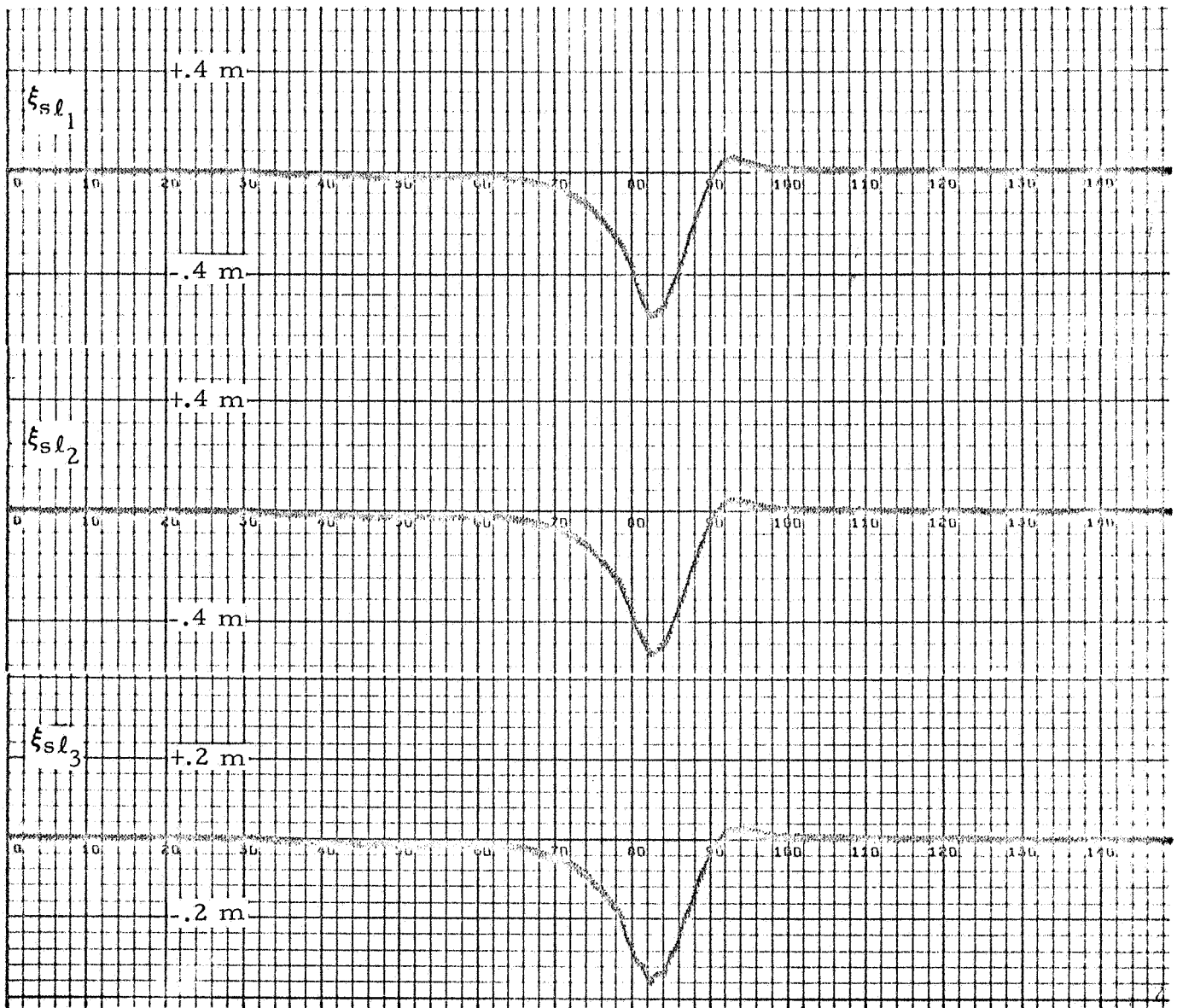


Figure 2-7c - Saturn V, S-IC Stage Response to Wind Disturbance - Digital Nonlinear Filter ($\omega_s = 48$ rad/sec).

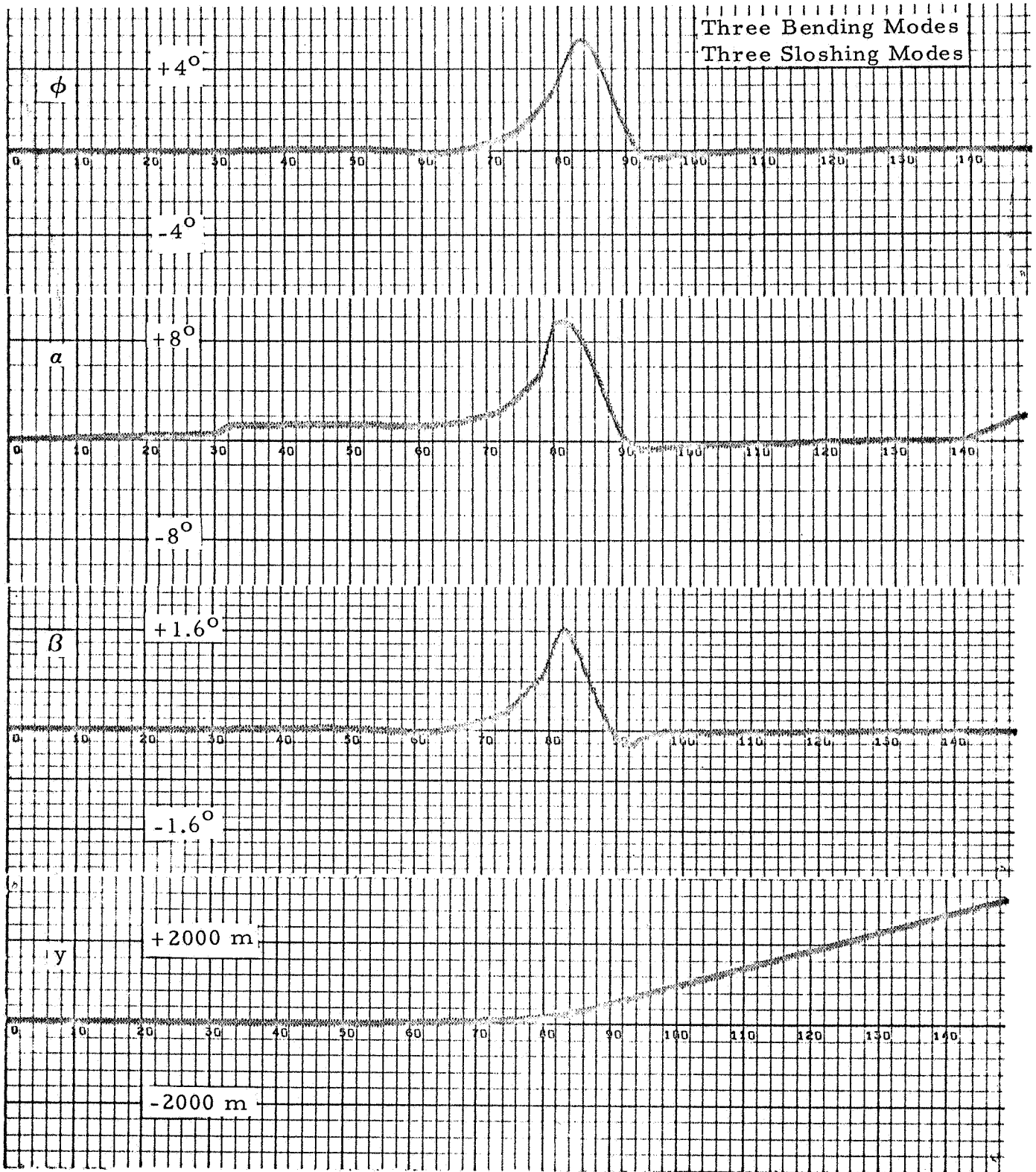


Figure 2-8a - Saturn V, S-IC Stage Response to Wind Disturbance - Digital Nonlinear Filter ($\omega_s = 96$ rad/sec).

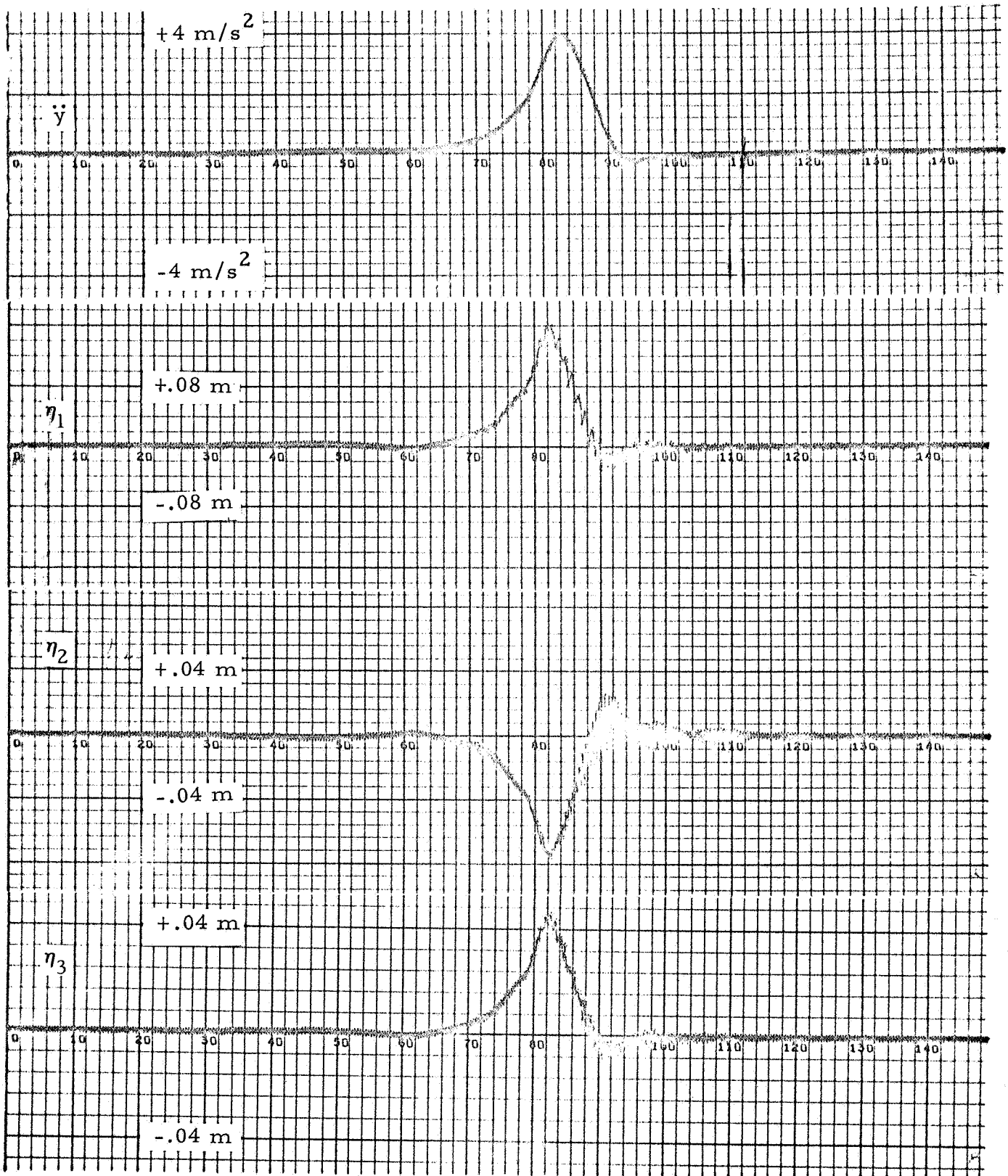


Figure 2-8b - Saturn V, S-IC Stage Response to Wind Disturbance - Digital Nonlinear Filter ($\omega_s = 96 \text{ rad/sec}$).

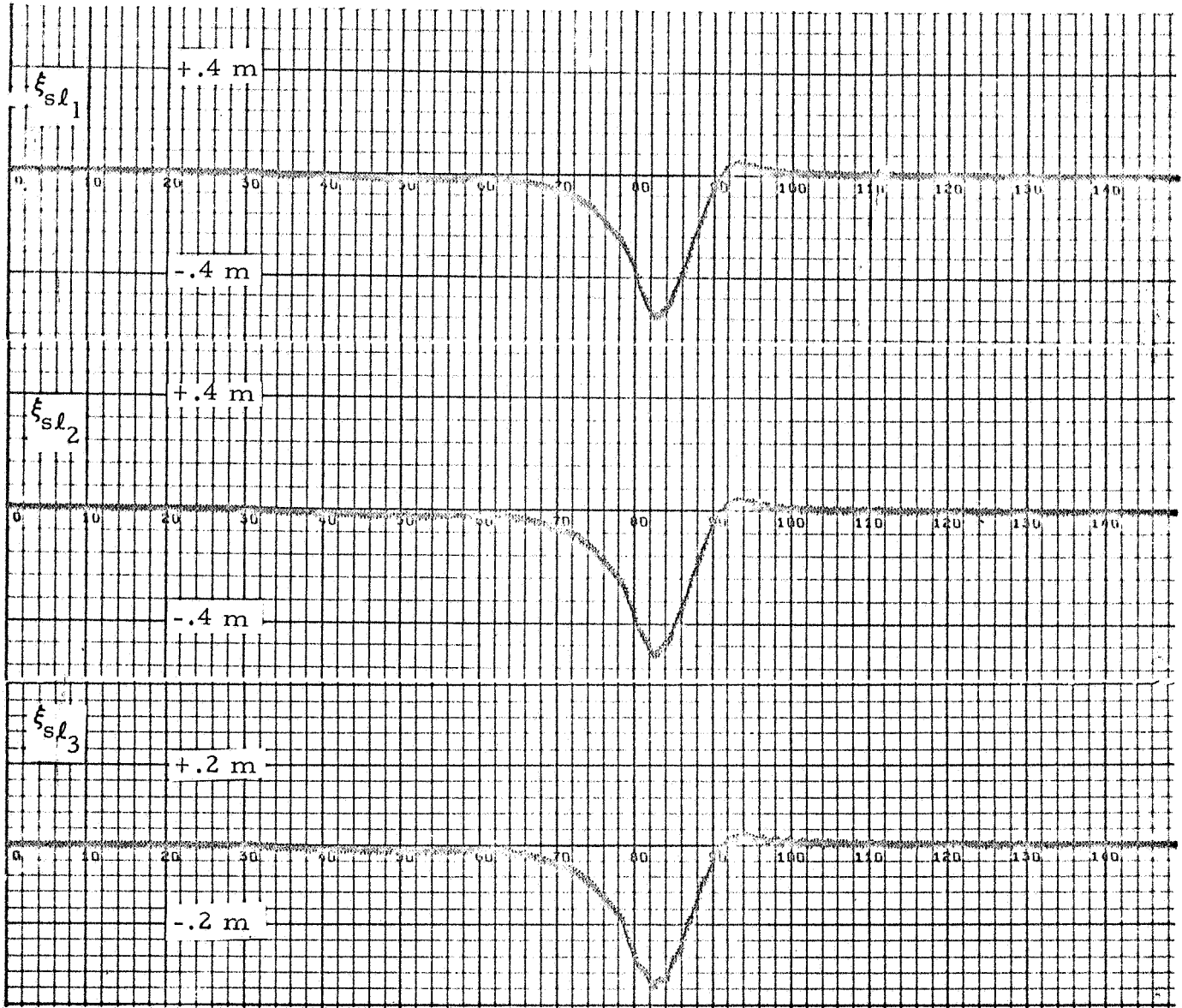


Figure 2-8c - Saturn V, S-IC Stage Response to Wind Disturbance - Digital Nonlinear Filter ($\omega_s = 96$ rad/sec).

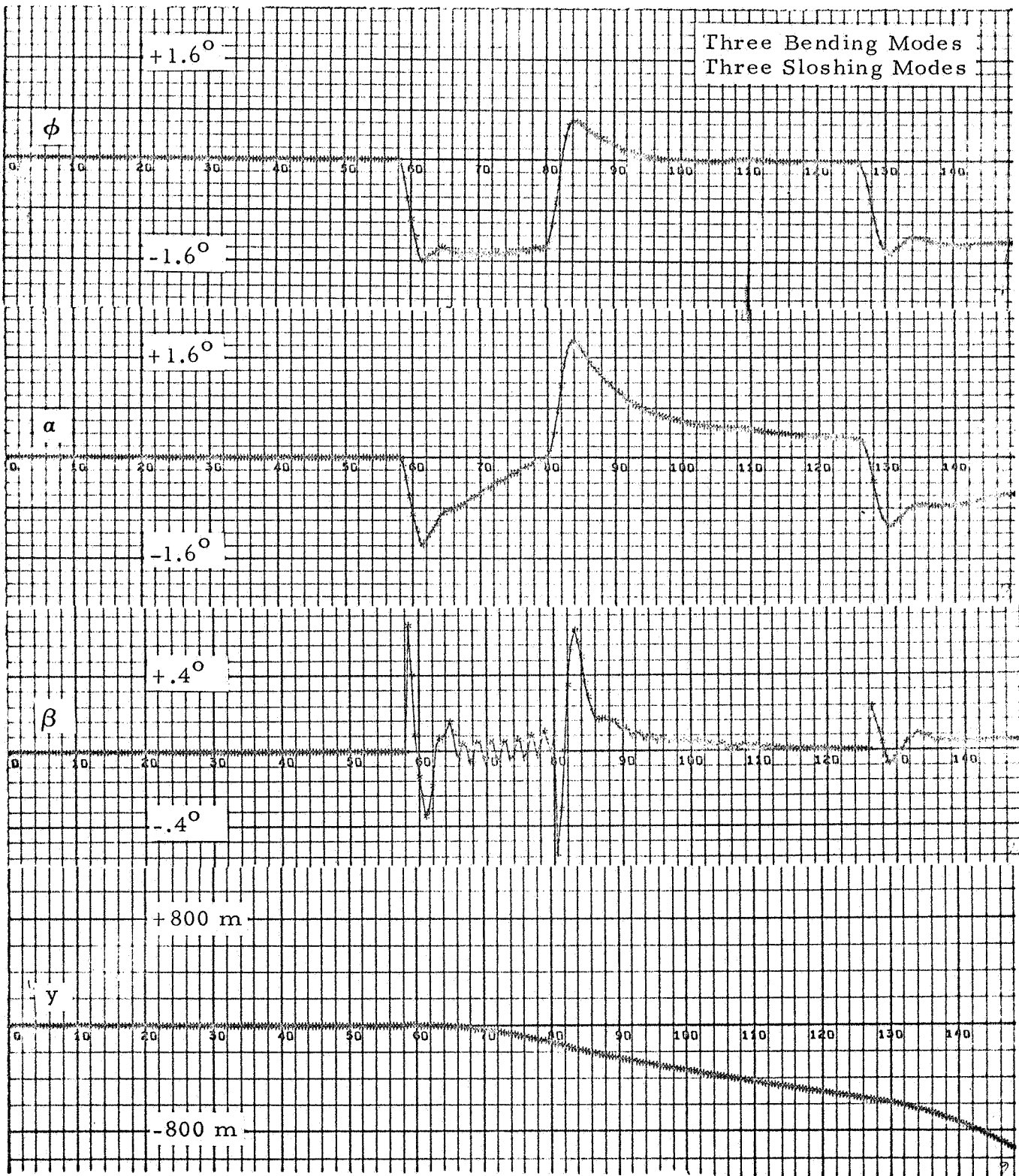


Figure 2-9a - Saturn V, S-IC Stage Response to ϕ_c - AS-503 Linear Filters.



Figure 2-9b - Saturn V, S-IC Stage Response to ϕ_C - AS-503 Linear Filters.

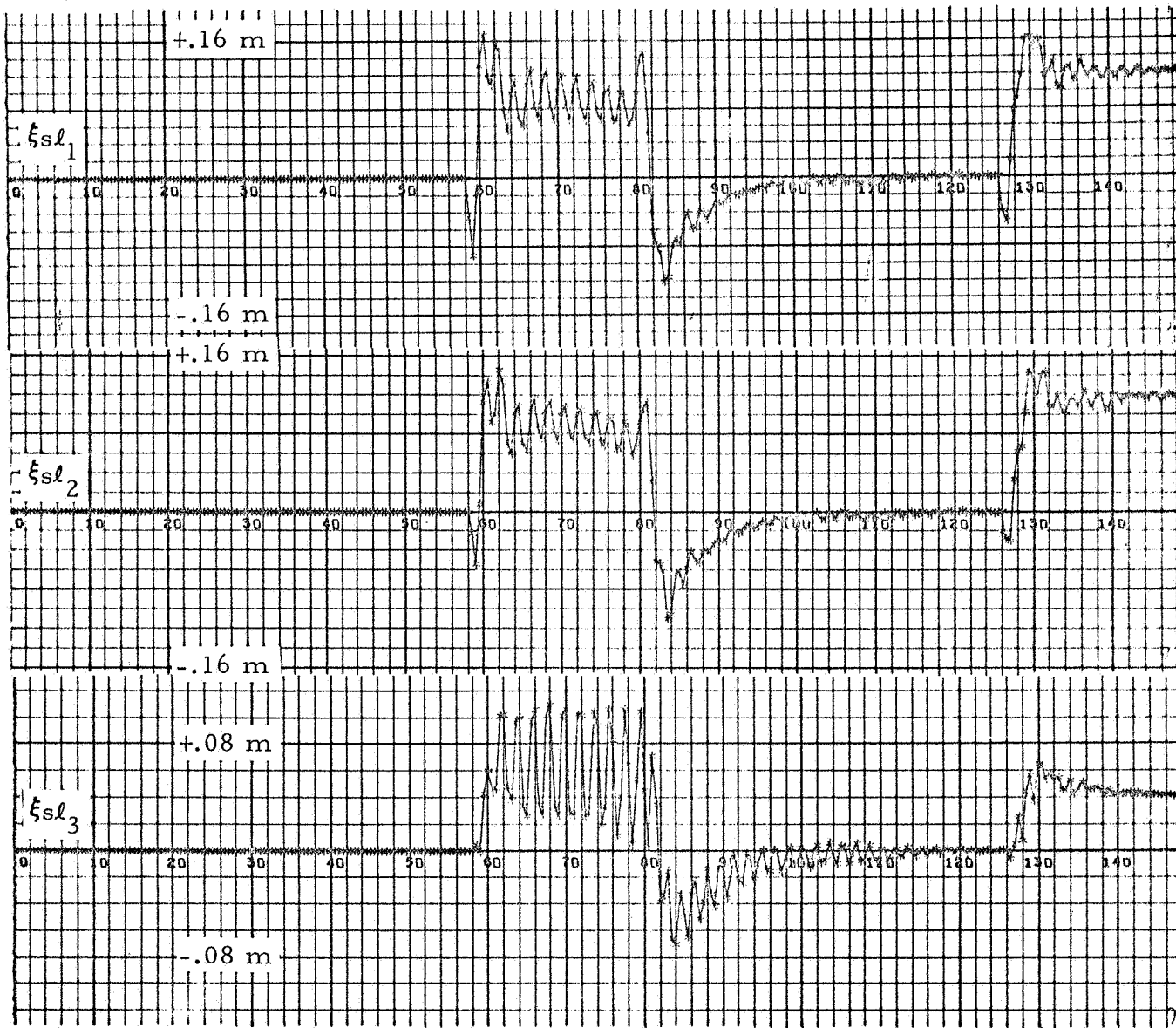


Figure 2-9c - Saturn V, S-IC Stage Response to ϕ_c - AS-503 Linear Filters.

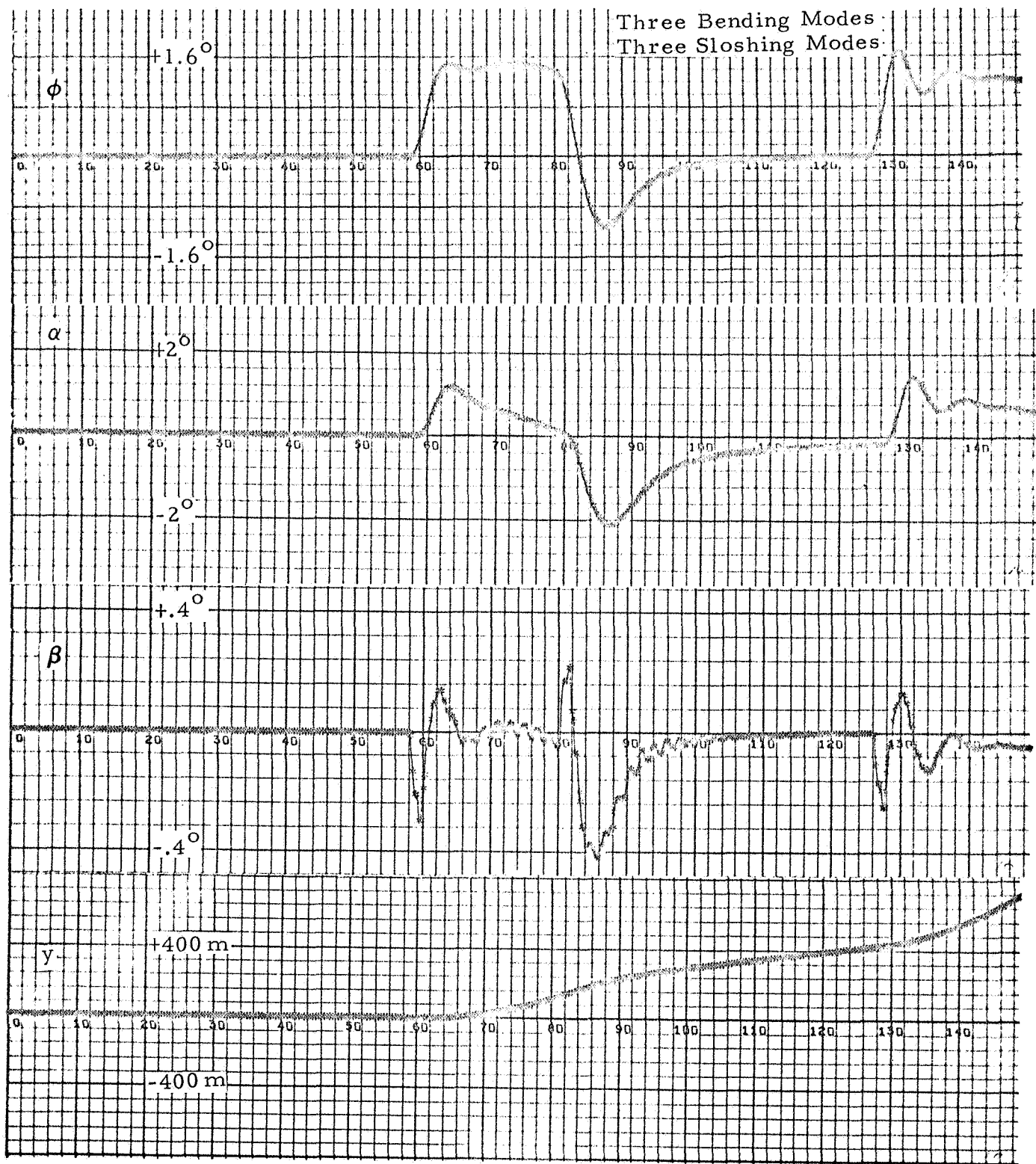


Figure 2-10a - Saturn V, S-IC Stage Response to ϕ_c , Continuous Nonlinear Filter



Figure 2-10b - Saturn V, S-IC Stage Response to ϕ_c , Continuous Nonlinear Filter



Figure 2-10c - Saturn V, S-IC Stage Response to ϕ_c , Continuous Nonlinear Filter



Figure 2-11a - Saturn V, S-IC Stage Response to ϕ_c - Digital Nonlinear Filter ($\omega_s = 24$ rad/sec).



Figure 2-11b - Saturn V, S-IC Stage Response to ϕ_c - Digital Nonlinear Filter ($\omega_s = 24$ rad/sec).



Figure 2-11c - Saturn V, S-IC Stage Response to ϕ_c - Digital Nonlinear Filter ($\omega_s = 24$ rad/sec).

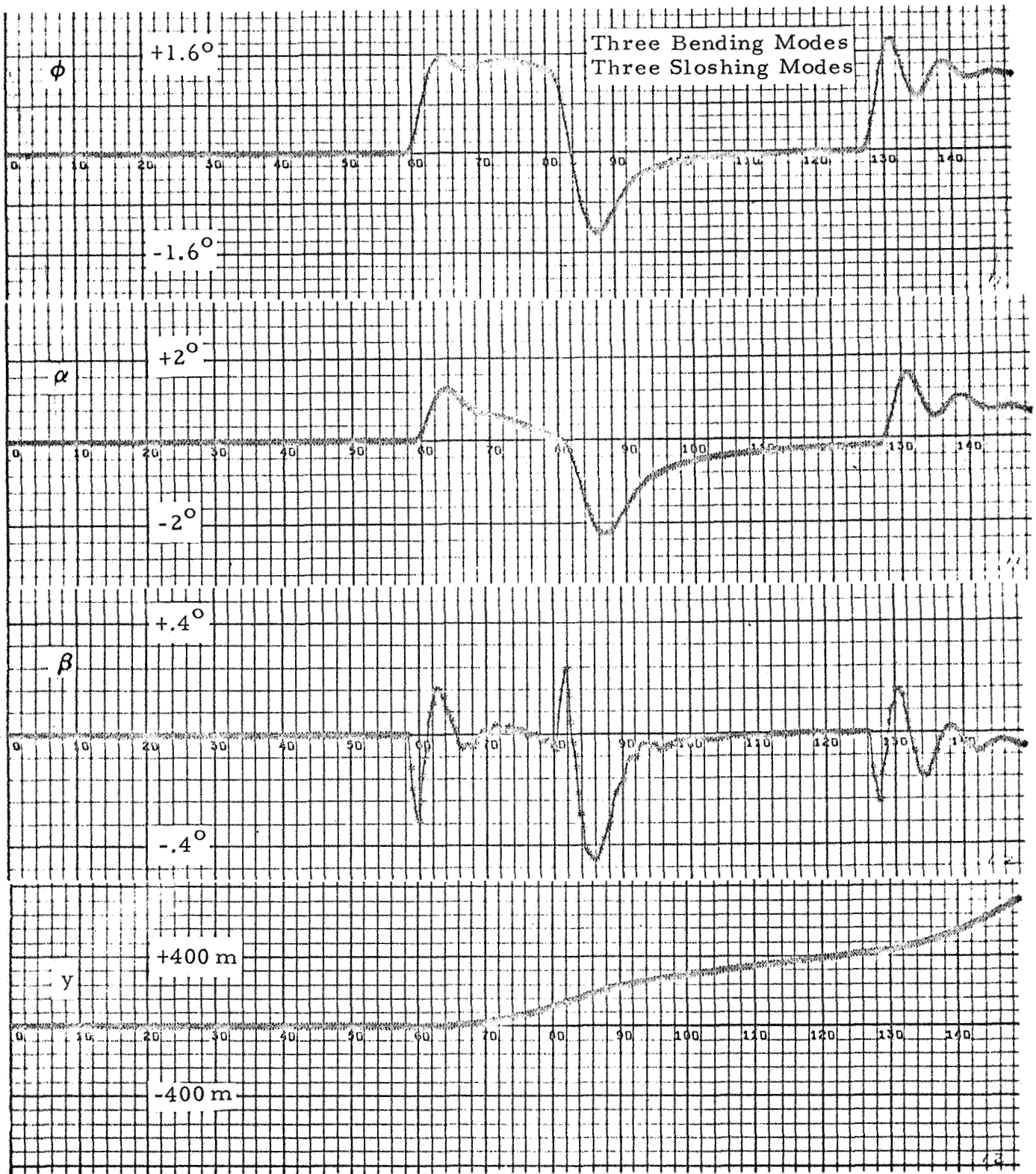


Figure 2-12a - Saturn V, S-IC Stage Response to ϕ_c - Digital Nonlinear Filter ($\omega_s = 48 \text{ rad/sec}$)

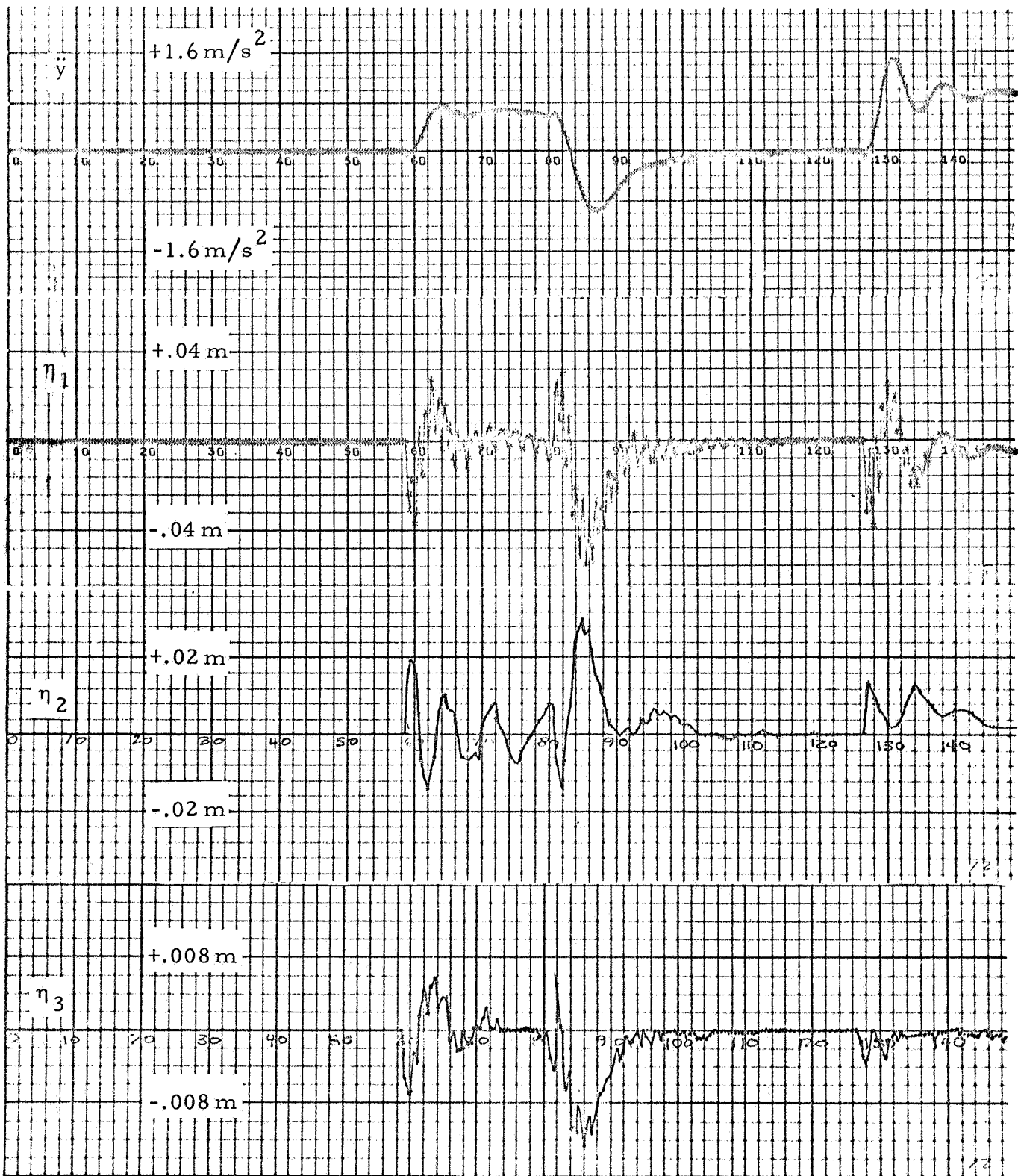


Figure 2-12b - Saturn V, S-IC Stage Response to ϕ^c - Digital Nonlinear Filter ($\omega_s = 48$ rad/sec)^c



Figure 2-12c - Saturn V, S-IC Stage Response to ϕ^c - Digital Nonlinear Filter ($\omega_s = 48 \text{ rad/sec}$)^c

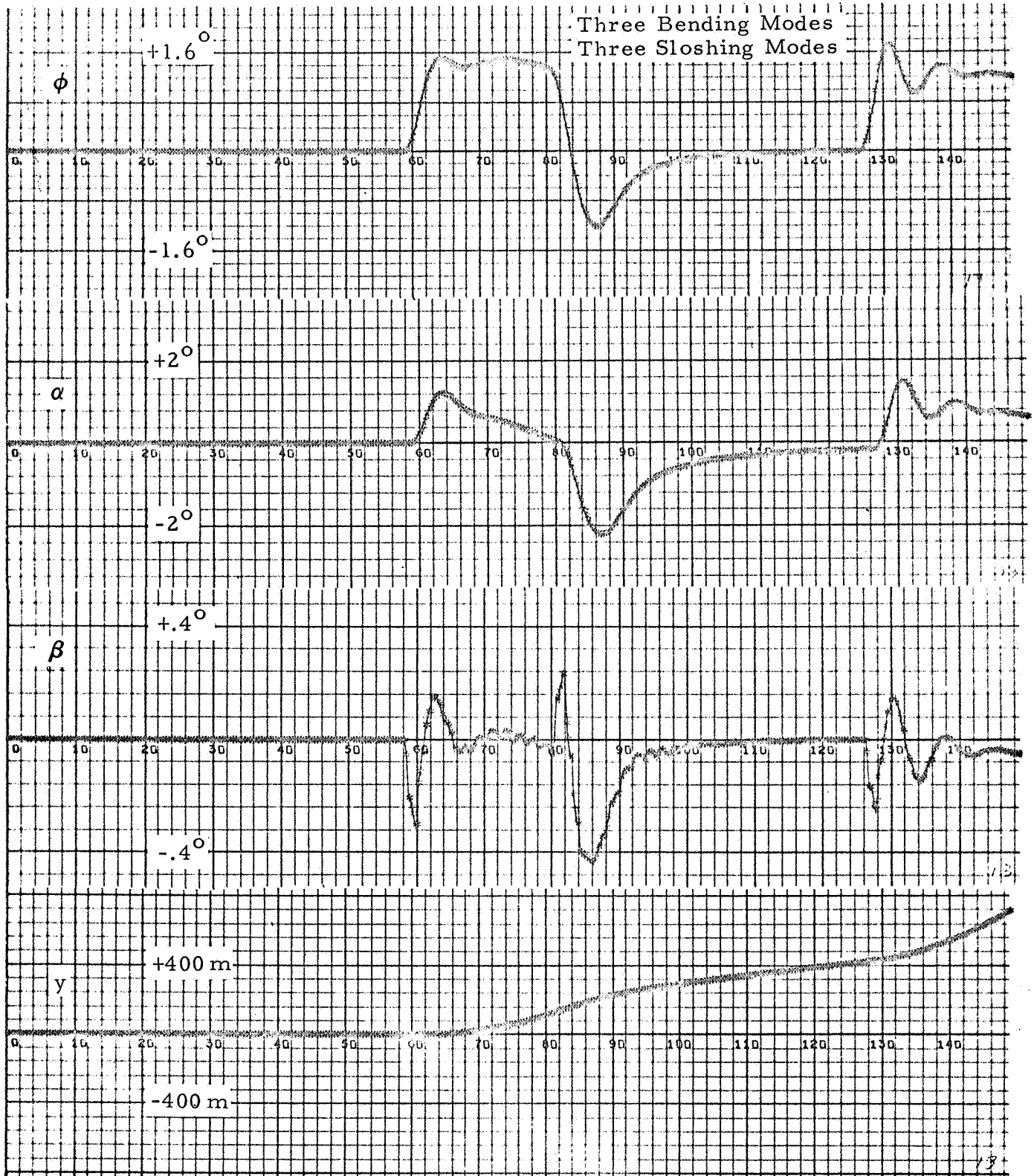


Figure 2-13a - Saturn V, S-IC Stage Response to ϕ_c - Digital Nonlinear Filter ($\omega_s = 96$ rad/sec)

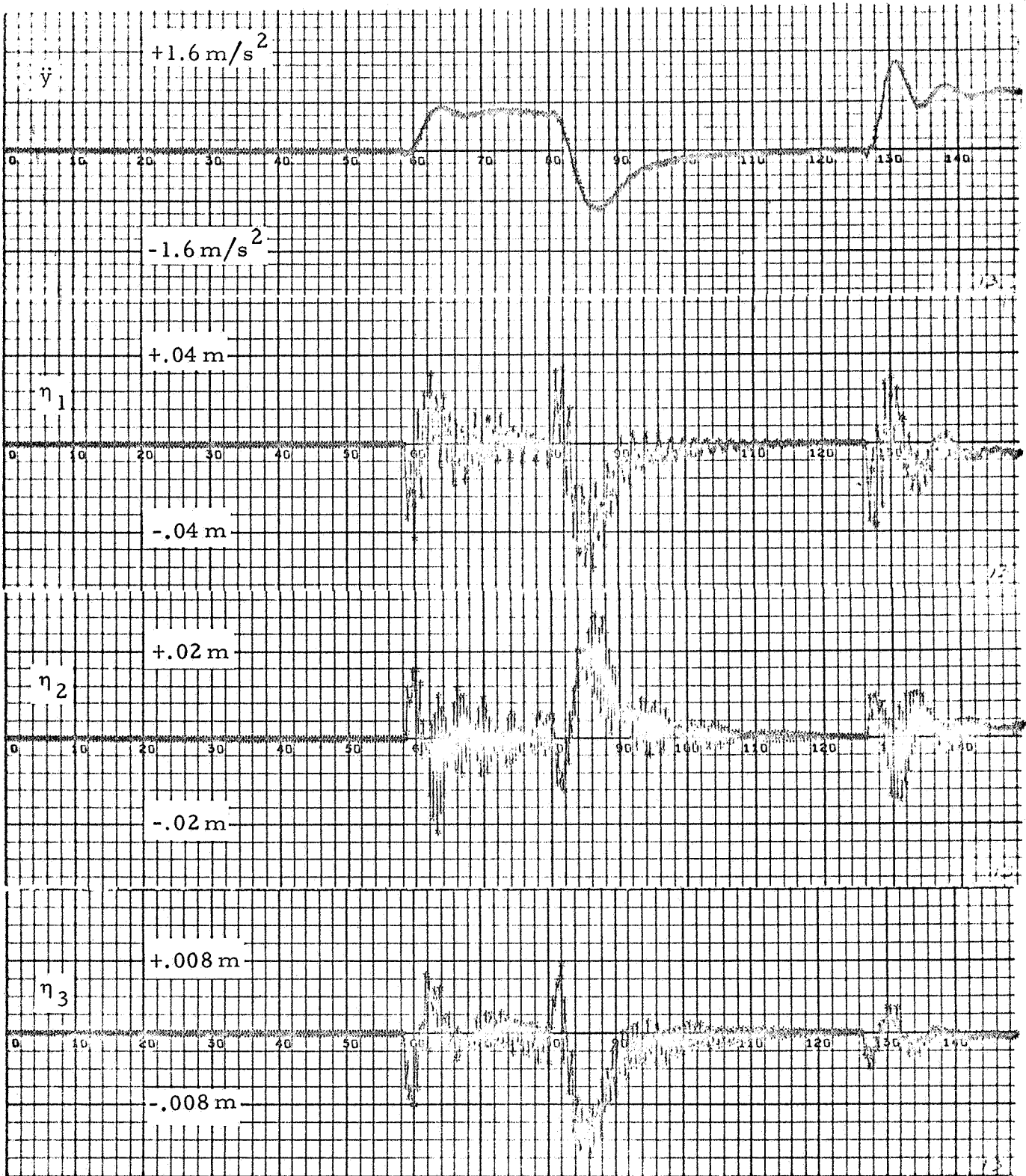


Figure 2-13b - Saturn V, S-IC Stage Response to ϕ_c - Digital Nonlinear Filter ($\omega_s = 96$ rad/sec)



Figure 2-13c - Saturn V, S-IC Stage Response to ϕ_c - Digital Nonlinear Filter ($\omega_s = 96\text{ rad/sec}$)



Figure 2-14a - Saturn V, S-IC Stage Response to ϕ_c with all Bending Mode Signs Reversed - Digital Nonlinear Filter ($\omega_s = 96$ rad/sec)



Figure 2-14b - Saturn V, S-IC Stage Response to ϕ_c with all Bending Mode Signs Reversed - Digital Nonlinear Filter ($\omega_s = 96$ rad/sec)



Figure 2-14c - Saturn V, S-IC Stage Response to ϕ_c with all Bending Mode Signs Reversed - Digital Nonlinear Filter ($\omega_s = 96$ rad/sec)

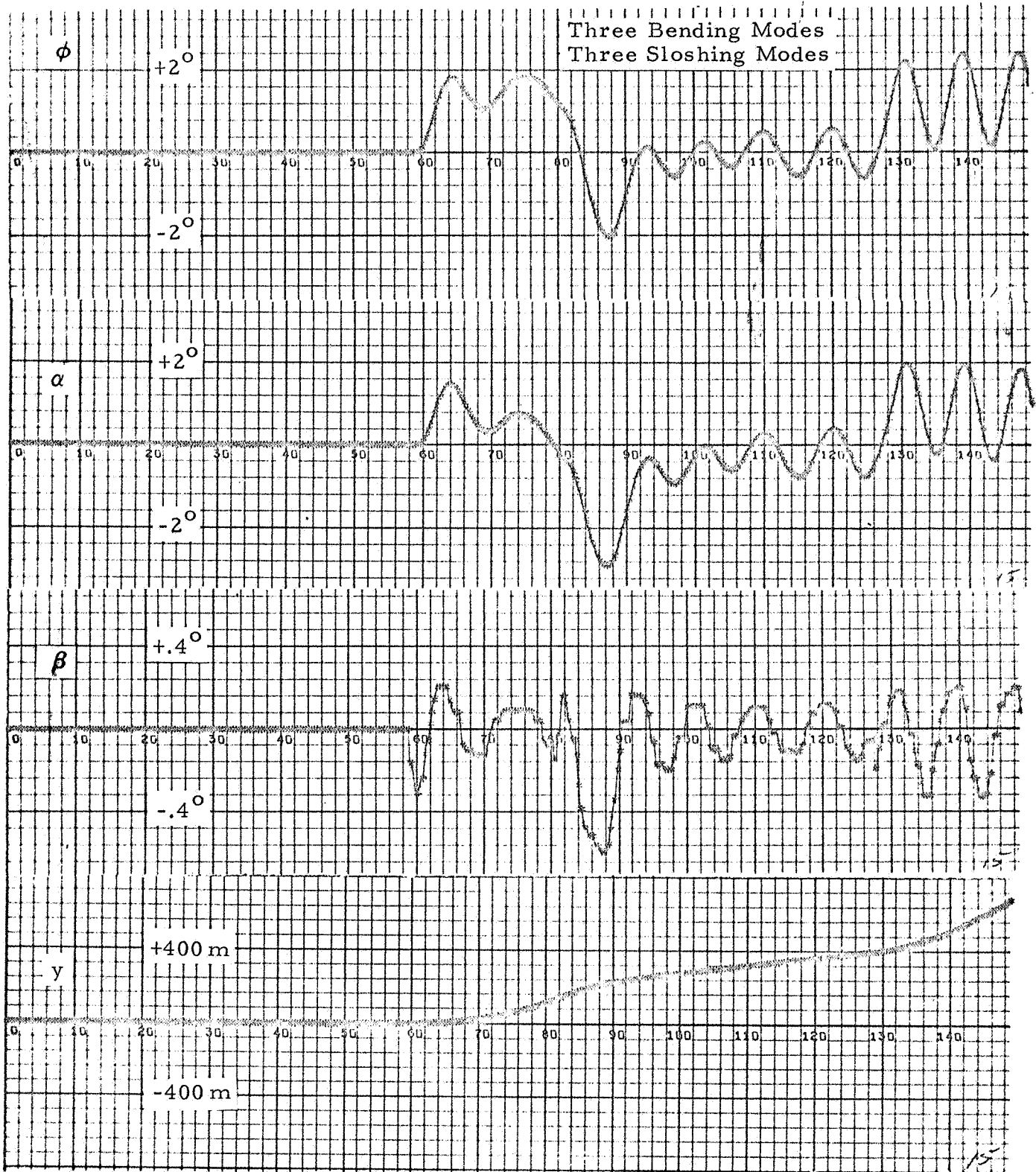


Figure 2-15 - Saturn V, S-IC Stage Response to ϕ_c with all Bending Mode Signs Reversed - Digital Nonlinear Filter ($\omega_s = 24$ rad/sec)

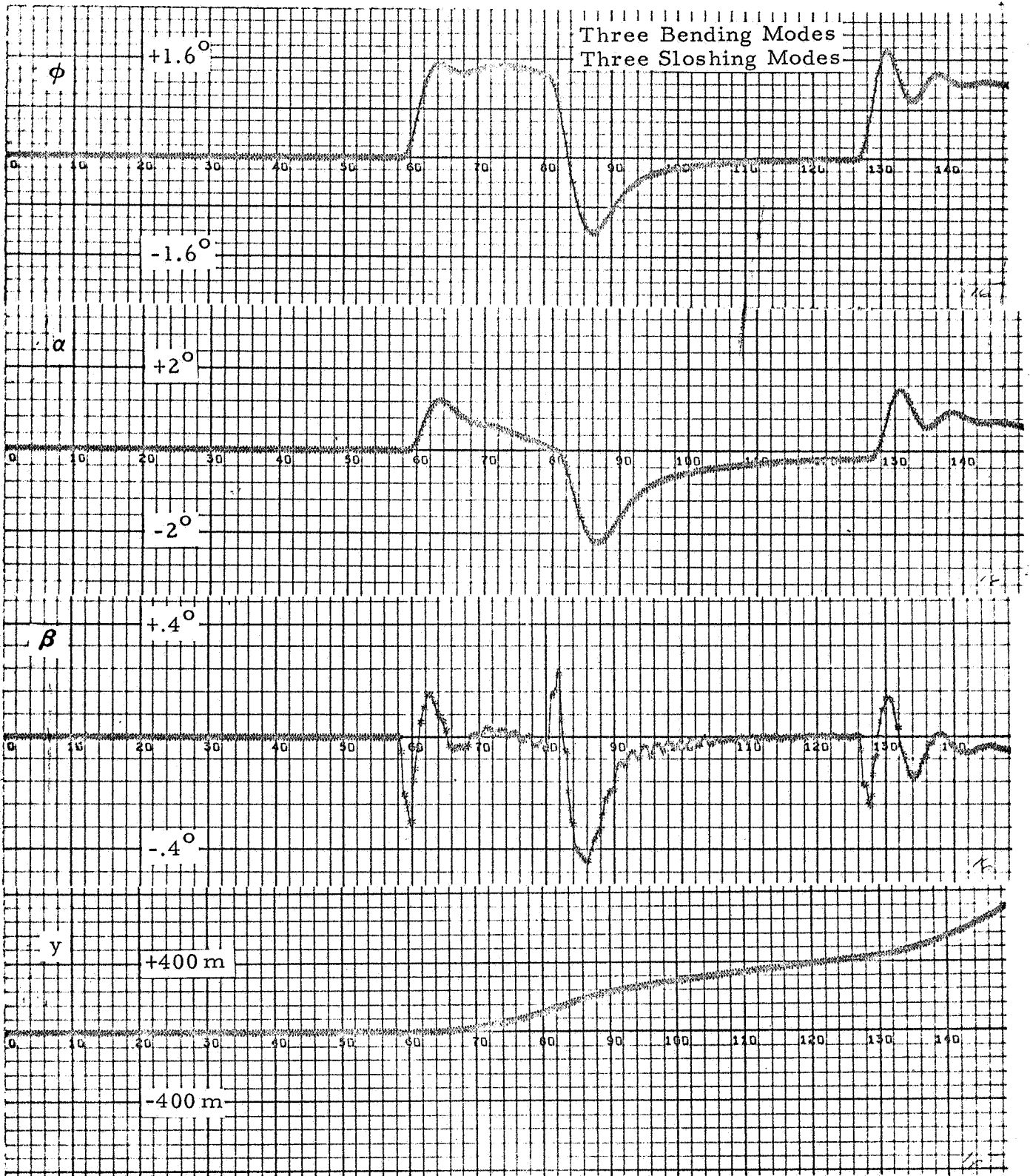


Figure 2-16a - Saturn V, S-IC Stage Response to ϕ_c with all Bending Mode Damping Ratios Reduced by a Factor 10 - Digital Nonlinear Filter ($\omega_s = 96$ rad/sec)



Figure 2-16b - Saturn V, S-IC Stage Response to ϕ_c with all Bending Mode Damping Ratios Reduced by a Factor 10 - Digital Nonlinear Filter ($\omega_s = 96$ rad/sec)

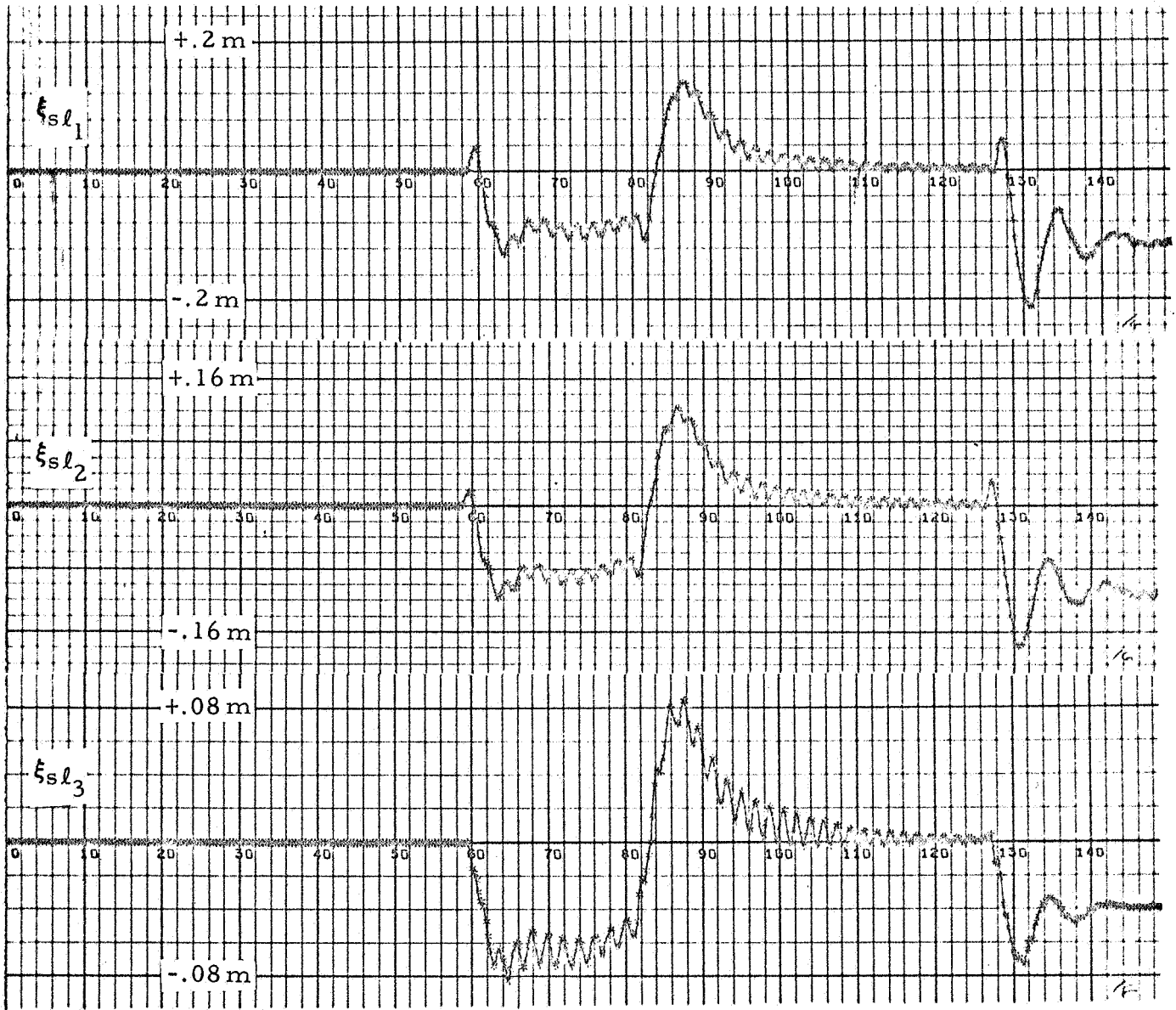


Figure 2-16c - Saturn V, S-IC Stage Response to ϕ_c with all Bending Mode Damping Ratios Reduced by a Factor 10 - Digital Nonlinear Filter ($\omega_s = 96\text{ rad/sec}$)

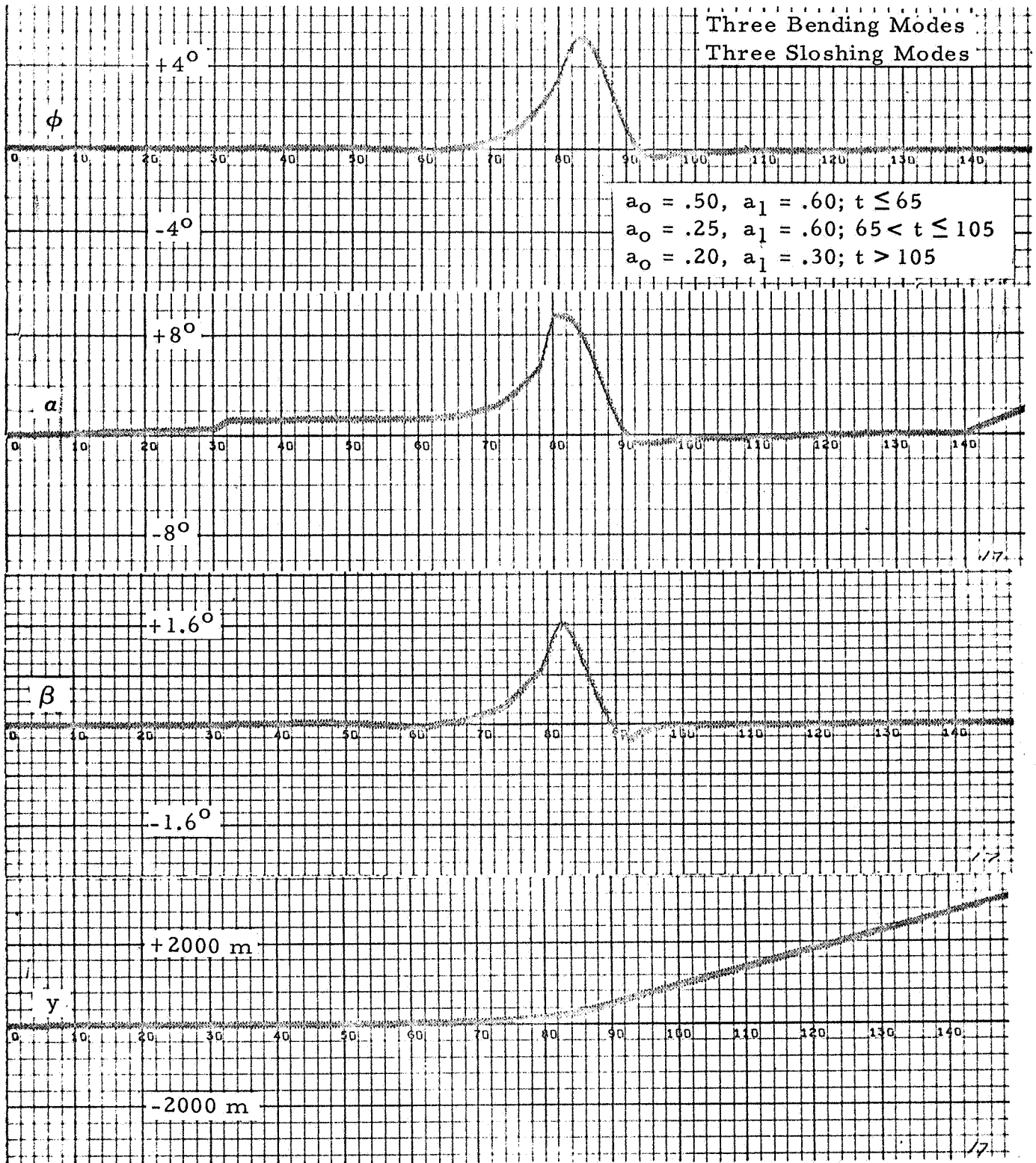


Figure 2-17a - Saturn V, S-IC Stage Response to Wind Disturbance with a Revised Control Gains Schedule - Digital Nonlinear Filter ($\omega_s = 96$ rad/sec).

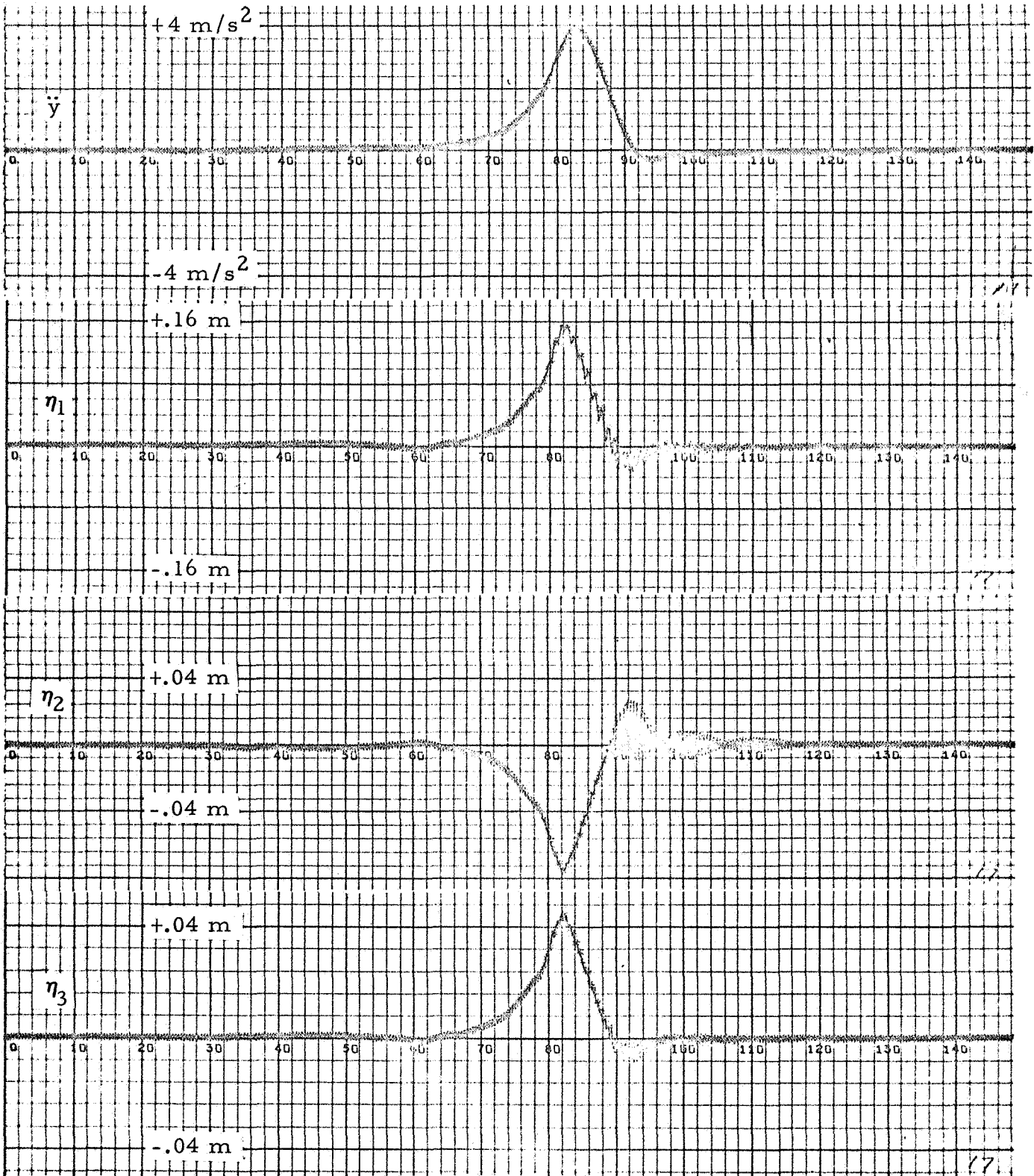


Figure 2-17b - Saturn V, S-IC Stage Response to Wind Disturbance with a Revised Control Gains Schedule - Digital Nonlinear Filter ($\omega_s = 96$ rad/sec).

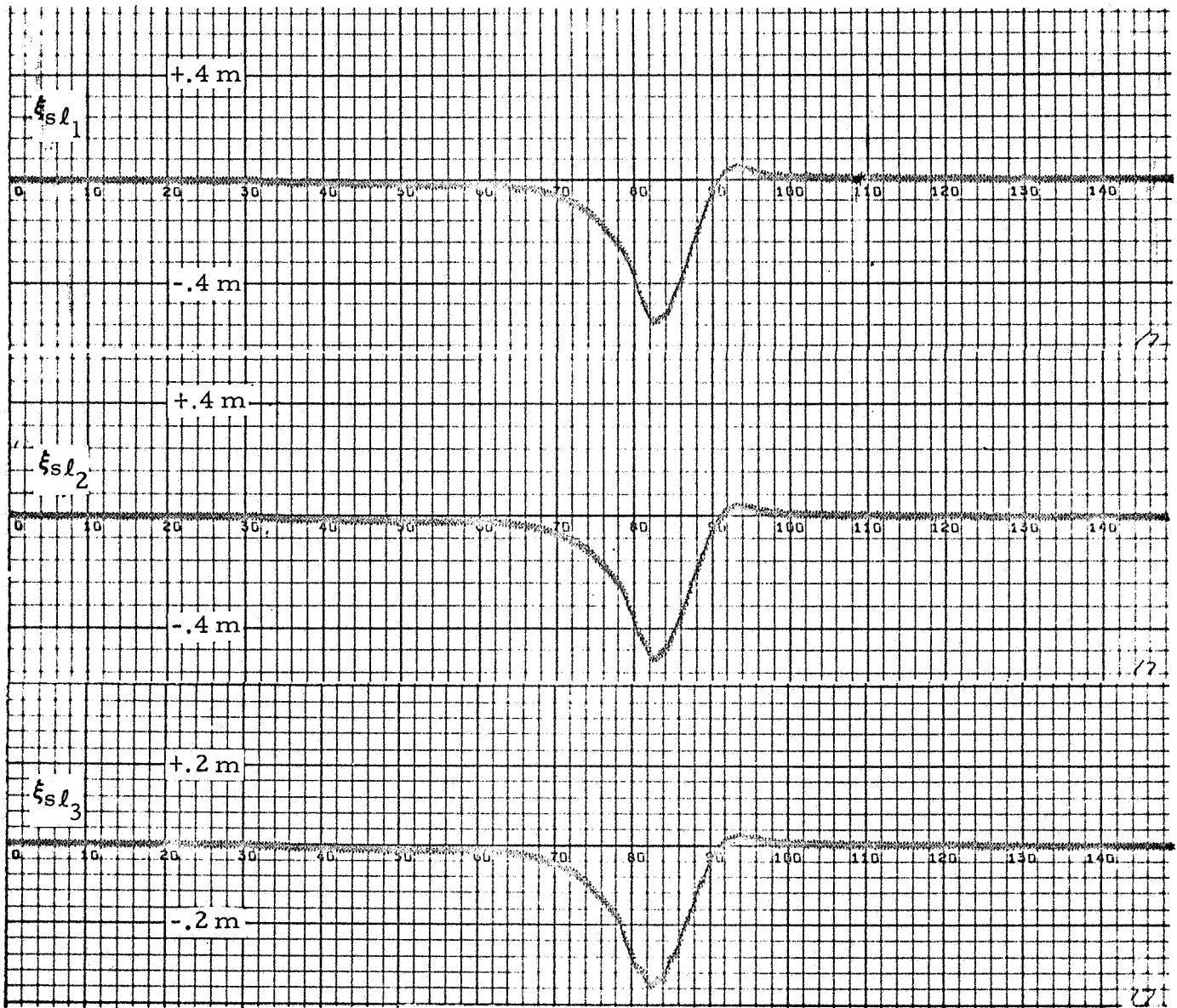


Figure 2-17c - Saturn V, S-IC Stage Response to Wind Disturbance with a Revised Control Gains Schedule - Digital Nonlinear Filter ($\omega_s = 96$ rad/sec).

Appendix A

NONLINEAR FILTER CONCEPT DEVELOPMENT

A.1 Introduction

A.2 Study No. 1 (NAS8-20268)

A.3 Study No. 2 (NAS8-20082)

Appendix A
NONLINEAR FILTER CONCEPT DEVELOPMENT

A.1 INTRODUCTION

Two previous studies have been performed on the subject of the non-linear filter; the first under NASA Contract NAS8-20268 and the second and most recent study under NASA Contract NAS8-20082. The content of these studies is presented in the following in order to describe the concept development for application of the filter to the Saturn V attitude control system and to provide background for the present study.

A.2 STUDY NO. 1 (NAS8-20268)

A.2.1 Title

"A Nonlinear Filter for High Frequency Cut-Off," Lockheed Missiles & Space Company, Huntsville Research & Engineering Center, LMSC/HREC A782442, 13 April 1966.

A.2.2 Duration

Work reported on the nonlinear filter study was for the period from 13 October 1965 through 13 April 1966.

A.2.3 Scope of Study

The purpose of the study was to determine low and high frequency characteristics of the filter, network requirements for the linear portions of the filter and cutoff characteristics; and to establish a design of the filter to obtain suppression of multiple high frequency signals such as vehicle bending modes in the Saturn V control system.

A.2.4 Report Content

The study analyses included the following items:

- Presentation of Filter Concept and Design

The filter has the function of providing "cut-off" of a signal with frequency above its characteristic cut-off frequency. A signal below cut-off is passed with decreasing phase lag as the frequency becomes smaller. The filter is shown in Figure 1-1 of Section 1. A split-signal path is provided for the input to the filter. The two outputs of the linear networks, e_1 and e_2 , are in phase when the input contains frequencies below the filter cut-off. This relationship causes biasing of the diode bridge network so as to pass e_1 on the positive half cycle and e_2 on the negative half cycle. Low frequencies near the cut-off are passed but with insertion of hysteresis. Frequencies above cut-off are 180 degrees out-of-phase. This relationship causes biasing of the bridge so that output voltages are not developed and therefore precludes passage through the filter. Multiple high and low frequencies are treated similarly except the low frequency signal is passed in a "quasi-sampled" form. These special effects are described comprehensively in the report.

Figures A-1 and A-2 are excerpts from the report and demonstrate the low pass characteristics of the filter. As can be seen, a direct application for the filter is the suppression of bending mode frequencies in a vehicle control system. Selection of the cut-off frequency, and subsequently the parameters of the linear networks, is determined by the value of the lowest frequency to be subdued. Variation in the bending mode frequencies during flight requires no change in the filter parameters since cut-off occurs for all frequencies beyond the selected cut-off frequency.

- Performance Evaluation

Design criteria were imposed on the filter to cut-off the first three Saturn V bending modes during first stage flight. The performance of the filter was evaluated for numerous severe excitations of these modes and compared to corresponding performances by the then existent linear control filters.

- Theoretical Derivations

Included in the report are theoretical derivations of the nonlinear filter concept and its high and low frequency patterns, hysteresis effects in the filter, and the quasi-sampling characteristics of the filter.

A.2.5 Simulation

The facility used for the study was a fixed-point-in-flight-time analog simulation with the first three Saturn V bending modes and fuel tank slosh during first stage flight included. The simulation of the vehicle equations of motion represented the pitch plane for the first stage of flight.

A.2.6 Results

The filter was shown to be effective in that it:

- Passed low frequency components of multiple frequency inputs while cutting off high frequencies.
- Attenuated multiple high frequencies increasingly as the amplitude of the lowest expected high frequency component was increased.
- Performed satisfactorily in the Saturn V control system — stabilized bending modes regardless of mode sign.

A.2.7 Conclusions and Recommendations

Development of the nonlinear filter is based on the establishment of a high frequency attenuation pattern related to typical, multiple bending modes characteristic of the Saturn V class of vehicles. When this objective is achieved, the filter is seen to provide stabilization of the excited vehicle bending modes even under adverse conditions such as extreme changes in damping and slope characteristics.

It was recommended that the filter be analyzed with a time-varying coefficient system simulation in order to evaluate the filter in a system where the bending mode characteristics, aerodynamics, and mass parameters are changing with flight time. The need also exists to build a bread-board prototype of the filter in order to study any hardware limitations.

A.3 STUDY NO. 2 (NAS8-20082)

A.3.1 Title

"The Nonlinear Filter in the Saturn V Vehicle with Time Varying Coefficients," Lockheed Missiles & Space Company, Huntsville Research & Engineering Center, LMSC/HREC A783123, August 1966.

A.3.2 Duration

Work reported on the nonlinear filter study was for the period 16 May 1966 through 23 July 1966.

A.3.3 Scope of Study

The purpose of the study was to perform a preliminary study of the effectiveness of the nonlinear filter in the Saturn V, S-IC stage control system with time varying coefficients.

A.3.4 Report Content

The report contains the following items:

- General equations for the pitch channel and the associated time varying parameters for the AS-501 vehicle equations of motion.
- Performance Evaluation

Two sets of network parameters for the nonlinear filter were selected from Study No. 1 and examined for their ability to suppress the first bending mode in Saturn V first stage boost phase. Comparisons were made with corresponding linear filter performances. Severe conditions were created by alternately reversing the bending mode sign and reducing the damping to a very small value. These parameter changes were accompanied by large excitations in attitude command and wind disturbances. The evaluations are essentially the same as those conducted in Study No. 1 except that time-varying parameters are included.

A.3.5 Simulation

The facility used for study was a time-varying coefficient analog simulation which contained one bending and one slosh mode due to limited availability of equipment.

A.3.6 Results

The nonlinear filter was shown to perform adequately in the S-IC boost phase of the flight. The filter was effective in stabilizing the first bending mode excited by variable wind disturbances accompanied by abrupt changes in commanded vehicle attitude. Extreme changes in bending mode characteristics did not alter the performance of the nonlinear filter; whereas the then existent linear filters did not perform as well. Reversal of sign of the bending mode resulted in stabilization by the nonlinear filter, but divergence occurred when the linear filter was used.

A.3.7 Conclusions and Recommendations

Essentially, the results of Study No. 1 are confirmed for the same physical system except with time-varying parameters. The study revealed the nonlinear filter's comparable effectiveness with the linear filters in stabilizing a single bending mode in the first stage boost phase.

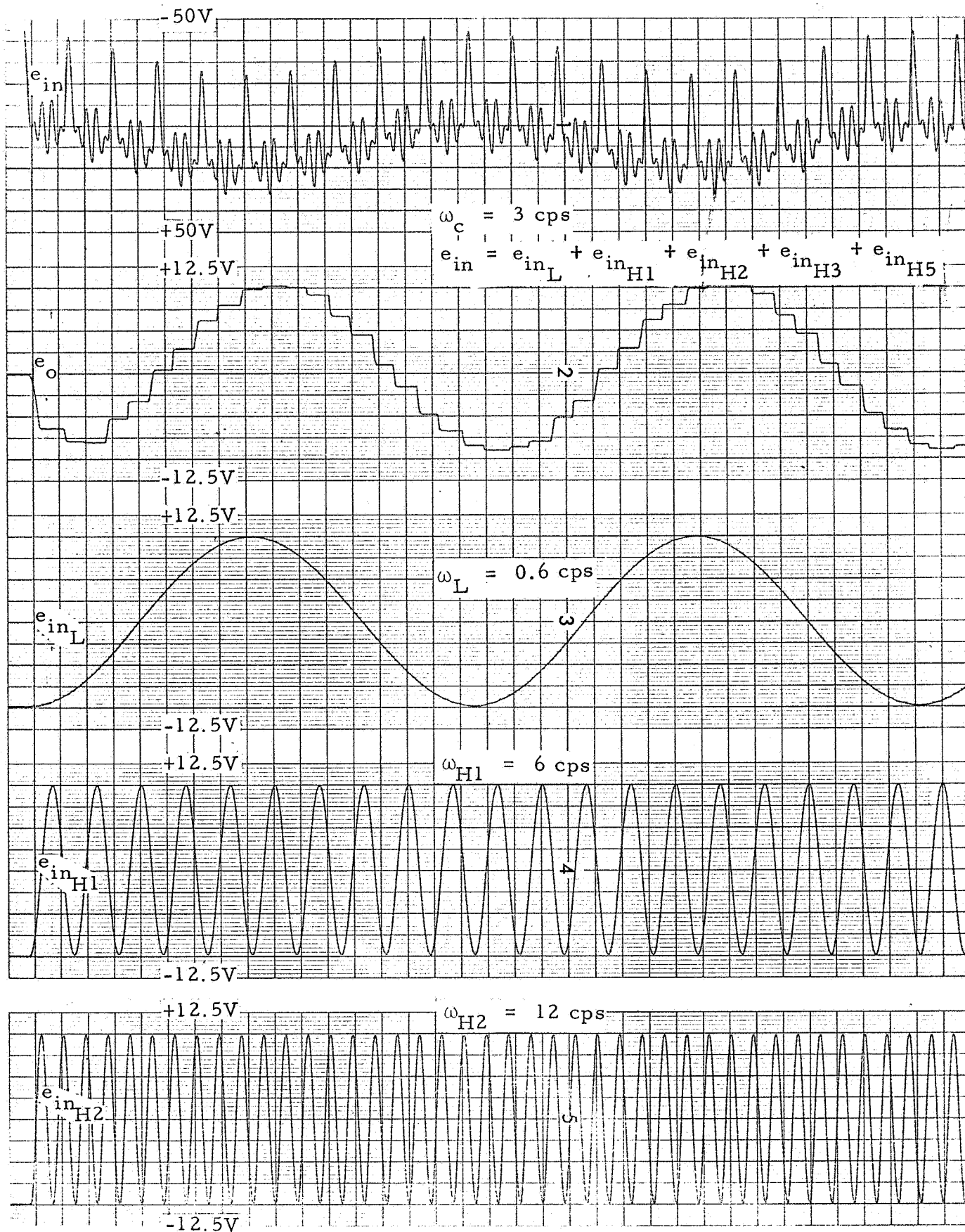


Figure A-1 - Response of Nonlinear Filter to Low Frequency Signal of 0.6 cps and Multiple High Frequency

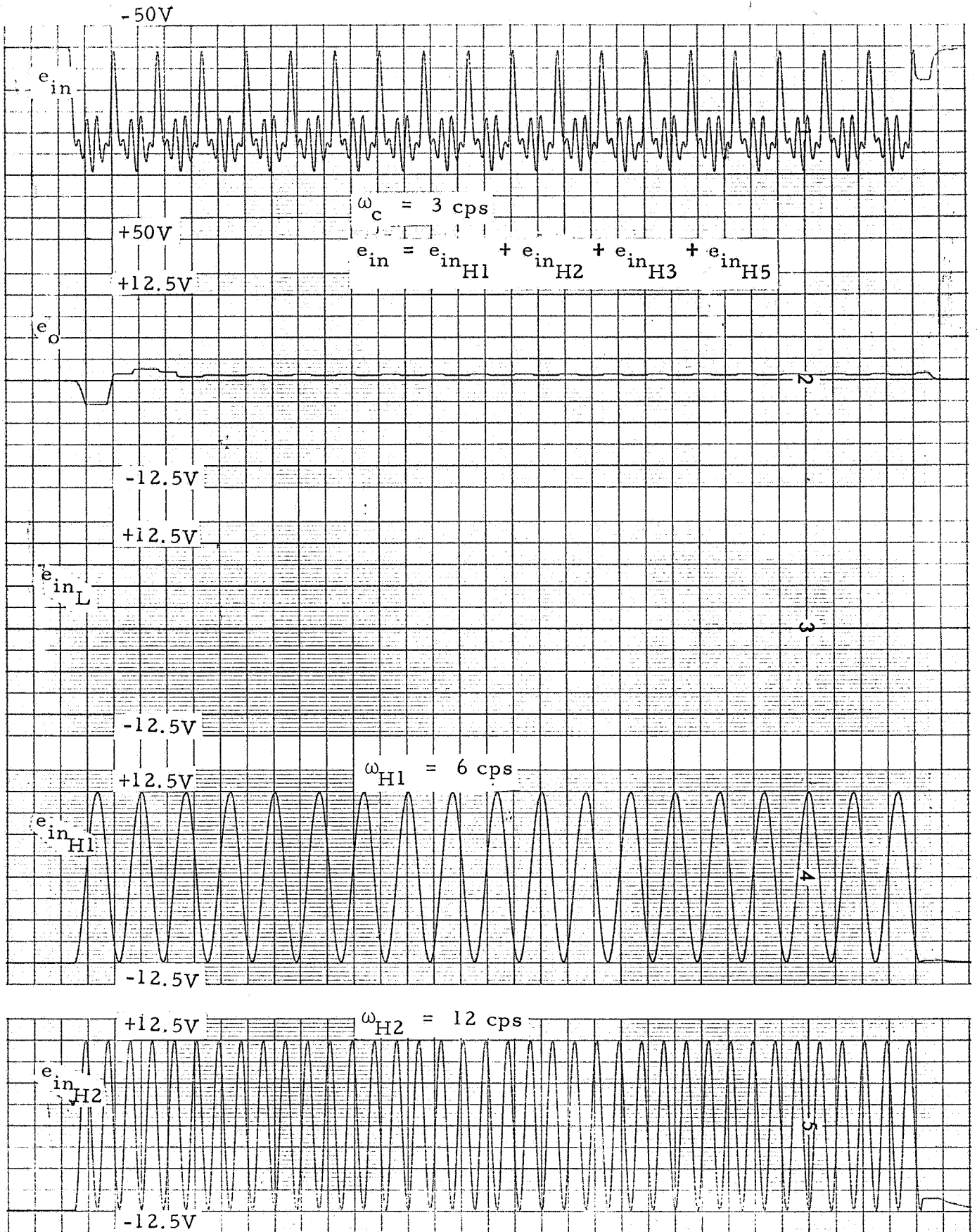


Figure A-2- Response of Nonlinear Filter to Multiple High Frequency Inputs

Appendix B

EQUATIONS OF MOTION FOR LAUNCH VEHICLE
WITH BENDING AND SLOSHING

Appendix B
EQUATIONS OF MOTION FOR LAUNCH VEHICLE
WITH BENDING AND SLOSHING

The general equations for the Saturn V 1st stage control system are shown below. The equations are consistent with those given in Reference 1 and are based on a vehicle coordinate system in the pitch plane only (yaw plane is similar). The pitch plane relationships are depicted in Figures B-1 and B-2.

Translational:

$$\ddot{y} = U_t \phi + A_t \alpha + B_t \beta - \bar{N}_{tl1} \ddot{\xi}_{sl1} - \bar{N}_{tl2} \ddot{\xi}_{sl2} - \bar{N}_{tl3} \ddot{\xi}_{sl3} - G_{tl1} \eta_1 - G_{tl2} \eta_2 - G_{tl3} \eta_3$$

Rotational:

$$\ddot{\phi} = -A_r \alpha - B_r \beta + \bar{N}_{rl1} \ddot{\xi}_{sl1} + \bar{N}_{rl2} \ddot{\xi}_{sl2} + \bar{N}_{rl3} \ddot{\xi}_{sl3} + N_{rl1} \dot{\xi}_{sl1} + N_{rl2} \dot{\xi}_{sl2} + N_{rl3} \dot{\xi}_{sl3} + G_{rl1} \eta_1 + G_{rl2} \eta_2 + G_{rl3} \eta_3$$

Angle of Attack:

$$\alpha = \phi - \dot{y}/V^i + \alpha_w$$

Propellant Sloshing:

$$\begin{aligned} \ddot{\xi}_{sl_1} = & -\bar{N}_{sl_1} \dot{\xi}_{sl_1} - N_{sl_1} \xi_{sl_1} - \ddot{y} + \bar{U}_{sl_1} \ddot{\phi} \\ & - \bar{G}_{sl_{11}} \ddot{\eta}_1 - \bar{G}_{sl_{12}} \ddot{\eta}_2 - \bar{G}_{sl_{13}} \ddot{\eta}_3 \end{aligned}$$

$$\begin{aligned} \ddot{\xi}_{sl_2} = & -\bar{N}_{sl_2} \dot{\xi}_{sl_2} - N_{sl_2} \xi_{sl_2} - \ddot{y} + \bar{U}_{sl_2} \ddot{\phi} \\ & - \bar{G}_{sl_{21}} \ddot{\eta}_1 - \bar{G}_{sl_{22}} \ddot{\eta}_2 - \bar{G}_{sl_{23}} \ddot{\eta}_3 \end{aligned}$$

$$\begin{aligned} \ddot{\xi}_{sl_3} = & -\bar{N}_{sl_3} \dot{\xi}_{sl_3} - N_{sl_3} \xi_{sl_3} - \ddot{y} + \bar{U}_{sl_3} \ddot{\phi} \\ & - \bar{G}_{sl_{31}} \ddot{\eta}_1 - \bar{G}_{sl_{32}} \ddot{\eta}_2 - \bar{G}_{sl_{33}} \ddot{\eta}_3 \end{aligned}$$

Vehicle Bending:

$$\begin{aligned} \ddot{\eta}_1 = & -\bar{G}_{bl_1} \ddot{\eta}_1 - G_{bl_1} \eta_1 + B_{bl_1} \beta \\ & - \bar{N}_{bl_{11}} \ddot{\xi}_{sl_1} - \bar{N}_{bl_{12}} \ddot{\xi}_{sl_2} - \bar{N}_{bl_{13}} \ddot{\xi}_{sl_3} \end{aligned}$$

$$\begin{aligned} \ddot{\eta}_2 = & -\bar{G}_{bl_2} \ddot{\eta}_2 - G_{bl_2} \eta_2 + B_{bl_2} \beta \\ & - \bar{N}_{bl_{21}} \ddot{\xi}_{sl_1} - \bar{N}_{bl_{22}} \ddot{\xi}_{sl_2} - \bar{N}_{bl_{23}} \ddot{\xi}_{sl_3} \end{aligned}$$

$$\begin{aligned} \ddot{\eta}_3 = & -\bar{G}_{bl_3} \ddot{\eta}_3 - G_{bl_3} \eta_3 + B_{bl_3} \beta \\ & - \bar{N}_{bl_{31}} \ddot{\xi}_{sl_2} - \bar{N}_{bl_{32}} \ddot{\xi}_{sl_2} - \bar{N}_{bl_{33}} \ddot{\xi}_{sl_3} \end{aligned}$$

Control:

$$\beta_c = a_0 F_{pg} \phi_i + a_1 F_{rg} \theta_i : \text{Linear Filter Cases}$$

$$\beta_c = F_{nl}(a_0 \phi_i + a_1 \theta_i) : \text{Nonlinear Filter Cases}$$

$$\beta = A(s) \beta_c ; \quad \beta_{\max} = \pm .090008 \text{ radians}$$

Position Gyro:

$$\phi_i = \phi - Y_1'(X_G) \eta_1 - Y_2'(X_G) \eta_2 - Y_3'(X_G) \eta_3 - \phi_c$$

Rate Gyro:

$$\begin{aligned} \ddot{\theta}_i = & -2\zeta_G \omega_G \dot{\theta}_i - \omega_G^2 \theta_i + \omega_G^2 \dot{\phi} - \omega_G^2 Y_1'(X_{RG}) \dot{\eta}_1 \\ & - \omega_G^2 Y_2'(X_{RG}) \dot{\eta}_2 - \omega_G^2 Y_3'(X_{RG}) \dot{\eta}_3 \end{aligned}$$

Actuator Transfer Function:

$$A(s) = \frac{3.3(10^3)(s^2 + 5.35s + 2547)}{(s^2 + 29.9s + 1188)(s^2 + 135s + 7090)}$$

Position Filter Transfer Function:

$$F_{pg}(s) = \frac{84.531 (s + .1)(s^2 + 2(.45)(14)s + 14^2)}{(s + .0499)(s + 11.99)(s + 47.24)(s + 58.62)}$$

Rate Filter Transfer Function:

$$F_{rg}(s) = \frac{16.393 (s^2 + 2(.034)(10.1)s + 10.1^2)(s^2 + 2(.086)(20.7s + 20.7^2))}{(s + 2.857)(s + 5.835)(s + 11.67)(s + 55.87)(s + 66.5)}$$

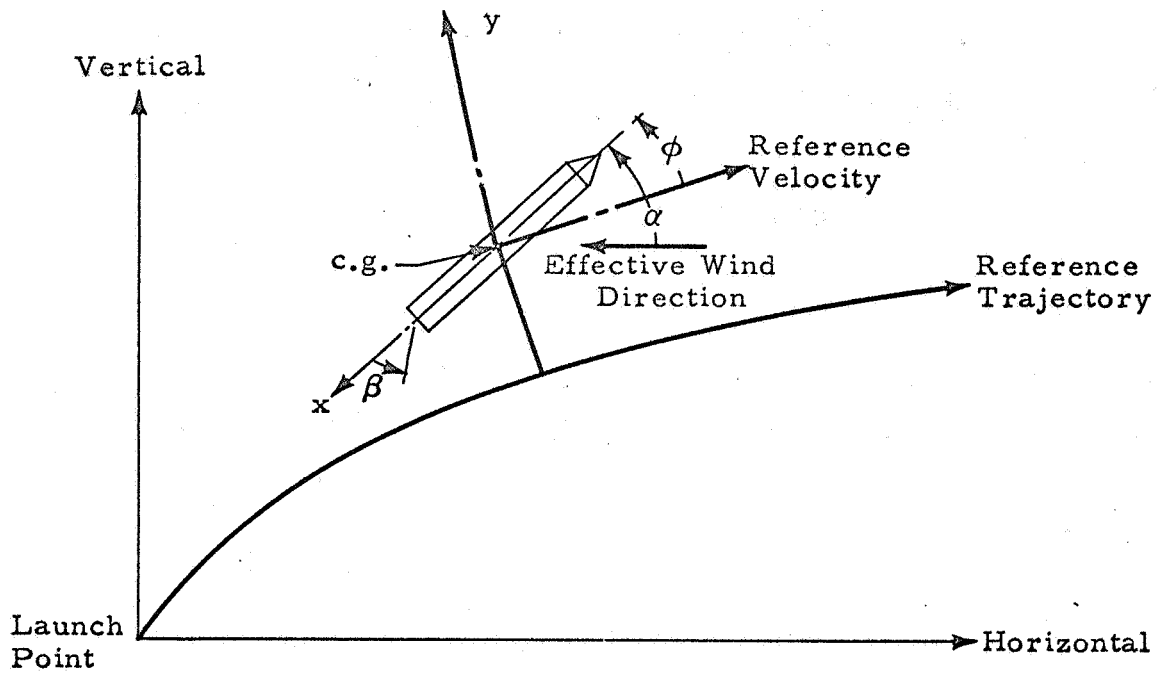


Figure B-1 - Pitch Plane Geometry

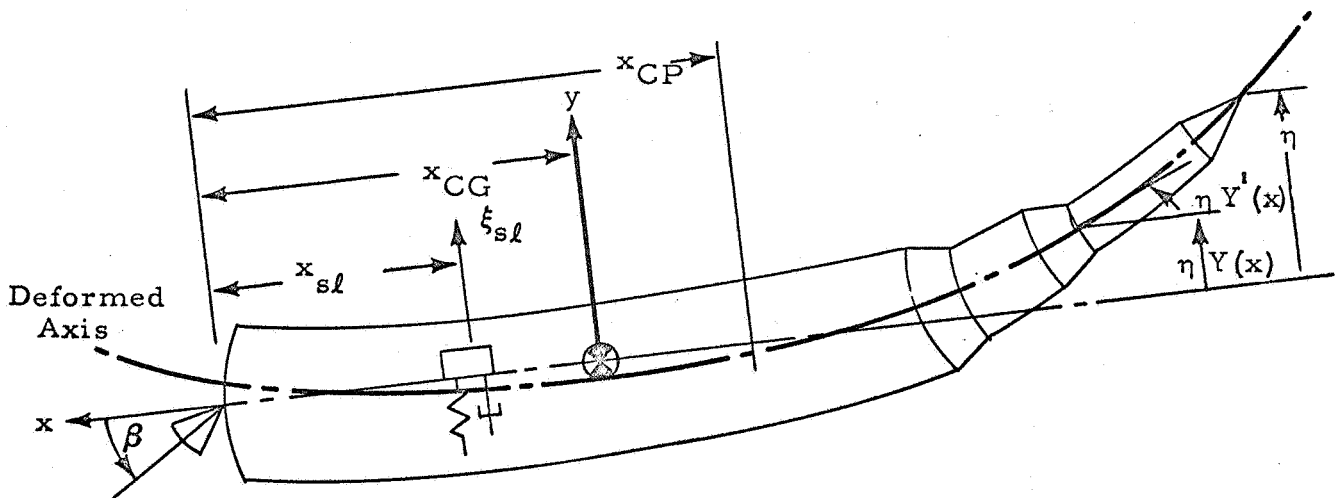


Figure B-2 - Pitch Plane Flexibility

Appendix C
NOMENCLATURE

Appendix C

NOMENCLATURE

$A(s)$	actuator transfer function
a_o, a_1	Saturn V, S-IC attitude and attitude rate control gains, respectively
A_t	$qS_A C_{N_\alpha}/m$
A_r	$qS_A C_{N_\alpha} (x_{CG} - x_{CP})/I$
B_{bl}	$F_s Y(x_E)/T$
B_r	$F_s (x_{CG} - x_E)/I$
B_t	F_s/m
C	electric capacitance
C_{N_α}	normal force coefficient gradient
D	differential operator, $Dy(t) = dy/dt$
$D_1(z),$ $D_2(z)$	operators of z (see Figure 1-3)
E	shifting operator $Ef(t) = f(t+T)$
$e_o(t)$	general output signal
$e_1(t)e_2(t)$	input signals to leg of diode bridge of nonlinear filter
F	total thrust of S-IC engines
F_{nl}	nonlinear filter transfer
F_{pg}	position filter transfer function

F_{rg}	rate filter transfer function
F_s	total thrust of S-IC control engines
\bar{G}_{bl}	$2\zeta_b \omega_b$
G_{bl}	ω_b^2
G_{rl}	$U_t m \left[(x_{CG} - x_E) Y'(x_E) - Y(x_E) \right] / I$
\bar{G}_{sl}	$Y(x_s)$
G_{tl}	$U_t Y'(x_E)$
I	vehicle pitch mass moment of inertia
K	ω_2^2 / ω_0^2
m	total vehicle mass
m_{sl}	modal slosh mass
\bar{N}_{bl}	$m_{sl} Y(x_{sl}) / T$
\bar{N}_{rl}	$m_{sl} (x_{CG} - x_{sl}) / I$
N_{rl}	$m_{sl} U_t / I$
\bar{N}_{sl}	$2\zeta_{sl} \omega_{sl}$
N_{sl}	ω_{sl}^2
\bar{N}_{tl}	m_{sl} / m
q	dynamic pressure
R	ohmic resistance
S_A	S-IC stage aerodynamic reference area
s	Laplacian operator

T	bending mode generalized mass
U_t	$(F-X)/m$
\bar{U}_{sl}	$x_{CG} - x_{sl}$
V'	longitudinal vehicle velocity
X	aerodynamic drag
x_E	S-IC control engines gimbal plane longitudinal coordinate
x_G	position gyro longitudinal coordinate
x_{CG}	vehicle center-of-gravity longitudinal coordinate
x_{CP}	vehicle center-of-pressure longitudinal coordinate
$x_1(t),$ $x_2(t)$	signals in legs of diode bridge (see Figure 1-1)
$x(t)$	continuous input function to filter
$x(n)$	sequence of numerical values at input to filter
x_{RG}	attitude rate gyro longitudinal coordinate
x_{sl}	modal slosh mass longitudinal coordinate
\dot{y}, \ddot{y}	lateral velocity and acceleration with respect to nominal trajectory
Y	bending mode normalized deflection
Y'	slope of bending mode normalized deflection curve
<u>Greek</u>	
α	vehicle angle of attack
α_w	angle between wind velocity vector and vehicle longitudinal velocity vector

β	S-IC control engines gimbal angle
β_C	commanded S-IC control engines gimbal angle
ζ_G	rate gyro damping ratio
ζ_{bl}	bending mode damping ratio
ζ_{sl}	slosh mode damping ratio
ζ_1, ζ_2	damping ratios of linear portion in the nonlinear filter
$\eta, \dot{\eta}, \ddot{\eta}$	amplitude, amplitude rate, amplitude acceleration, respectively, of bending mode at nose of vehicle
θ_i	rate gyro output
$\xi_{sl}, \dot{\xi}_{sl}, \ddot{\xi}_{sl}$	amplitude, amplitude rate, amplitude acceleration, respectively, of slosh mass lateral displacement
ϕ	rigid body vehicle attitude
ϕ_C	vehicle attitude command
ϕ_i	attitude gyro output
$\dot{\phi}$	vehicle attitude rate
ω_{bl}	bending mode undamped natural frequency
ω_c	nonlinear filter cut-off frequency
ω_1, ω_2	undamped natural frequencies of linear portion in the nonlinear filter
ω_s	sampling frequency
ω_G	rate gyro undamped natural frequency
ω_{sl}	slosh mode undamped natural frequency

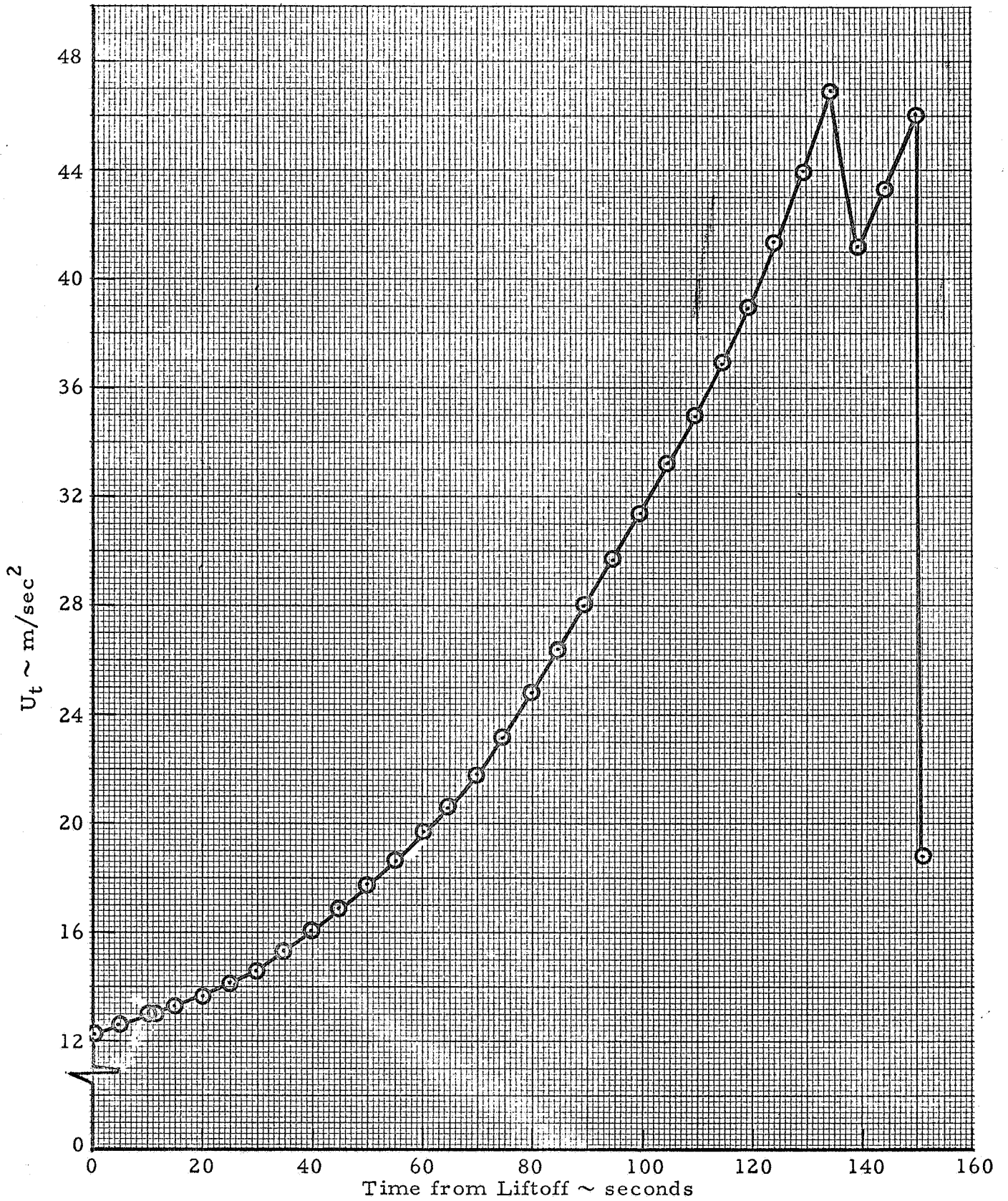
Numerical subscripts, when affixed to bending terms, denote the particular vehicle bending mode. Numerical subscripts affixed to slosh terms denote a particular tank; where Tank 1 is the S-IC fuel tank, Tank 2 is the S-IC LOX tank, Tank 3 is the S-II LOX tank.

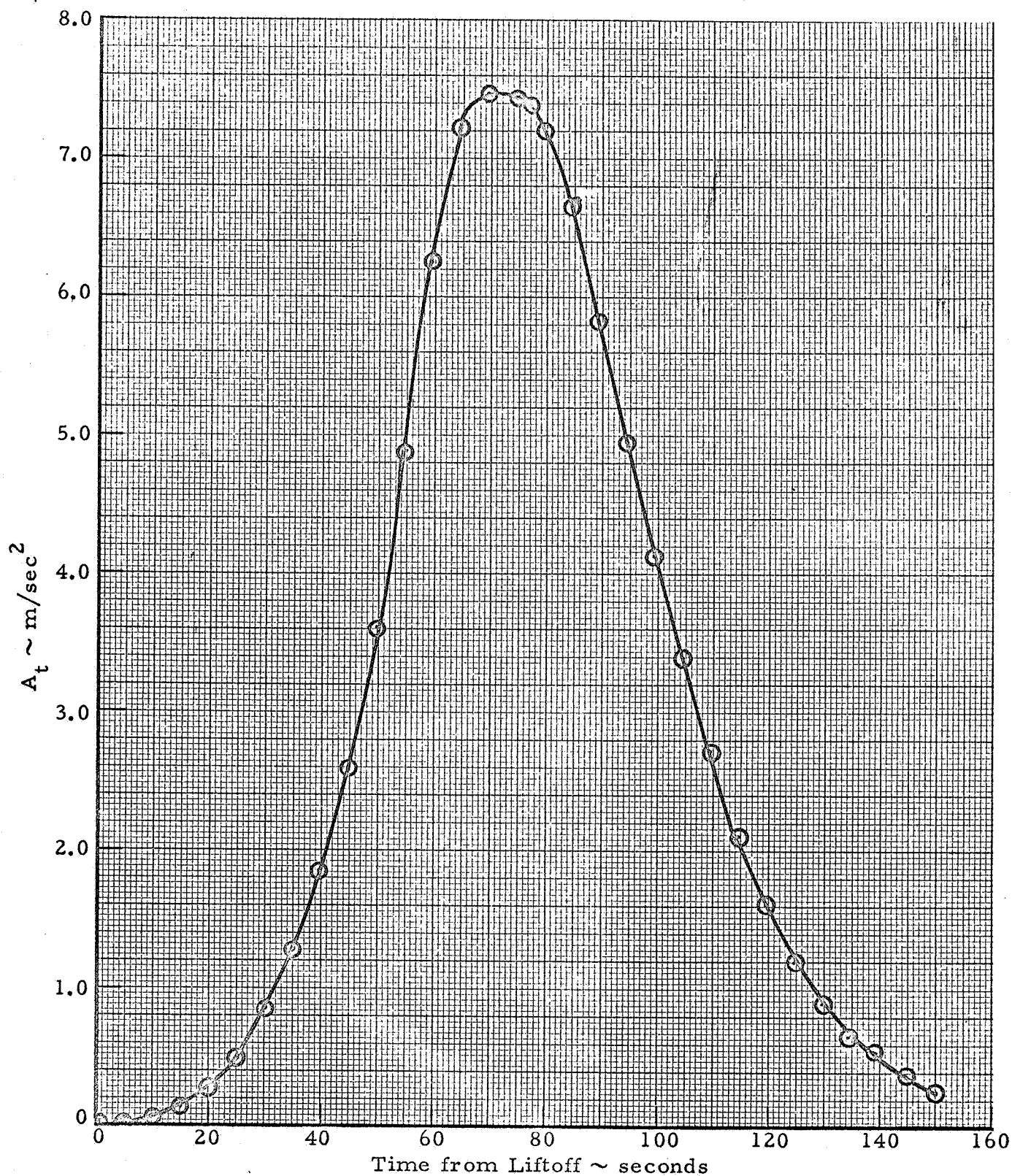
The International System of Units (SI Units) is used throughout (Ref: NASA TT F-8365).

Appendix D
AS-503 INPUT DATA

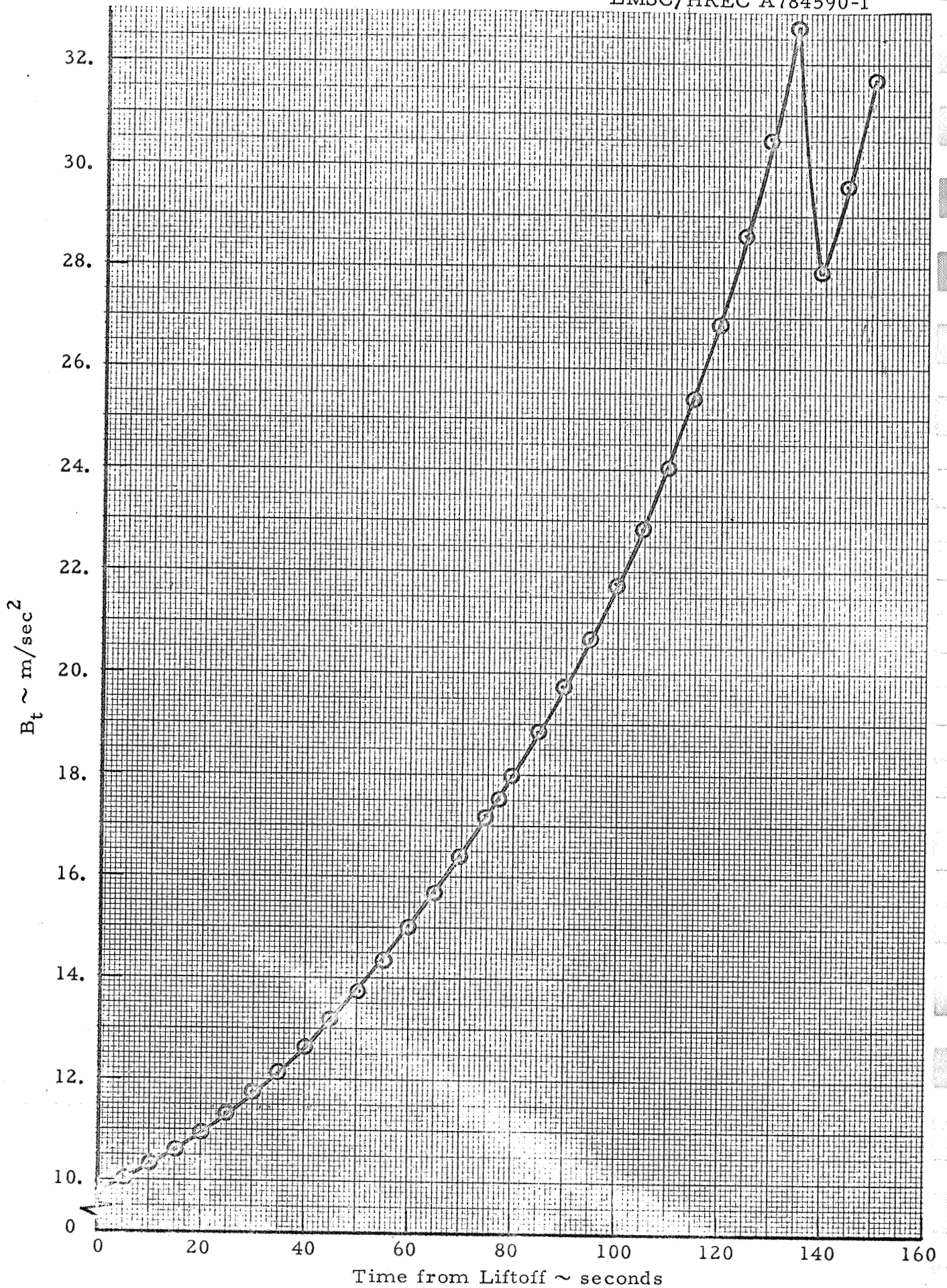
Appendix D
AS-503 INPUT DATA

The time varying parameters used in the simulation of the first stage flight of the Saturn V AS-503 vehicle as required for the model presented in Appendix B are presented for convenience in graphical form. The marks indicate data points used in the table look-up of the digital simulation.

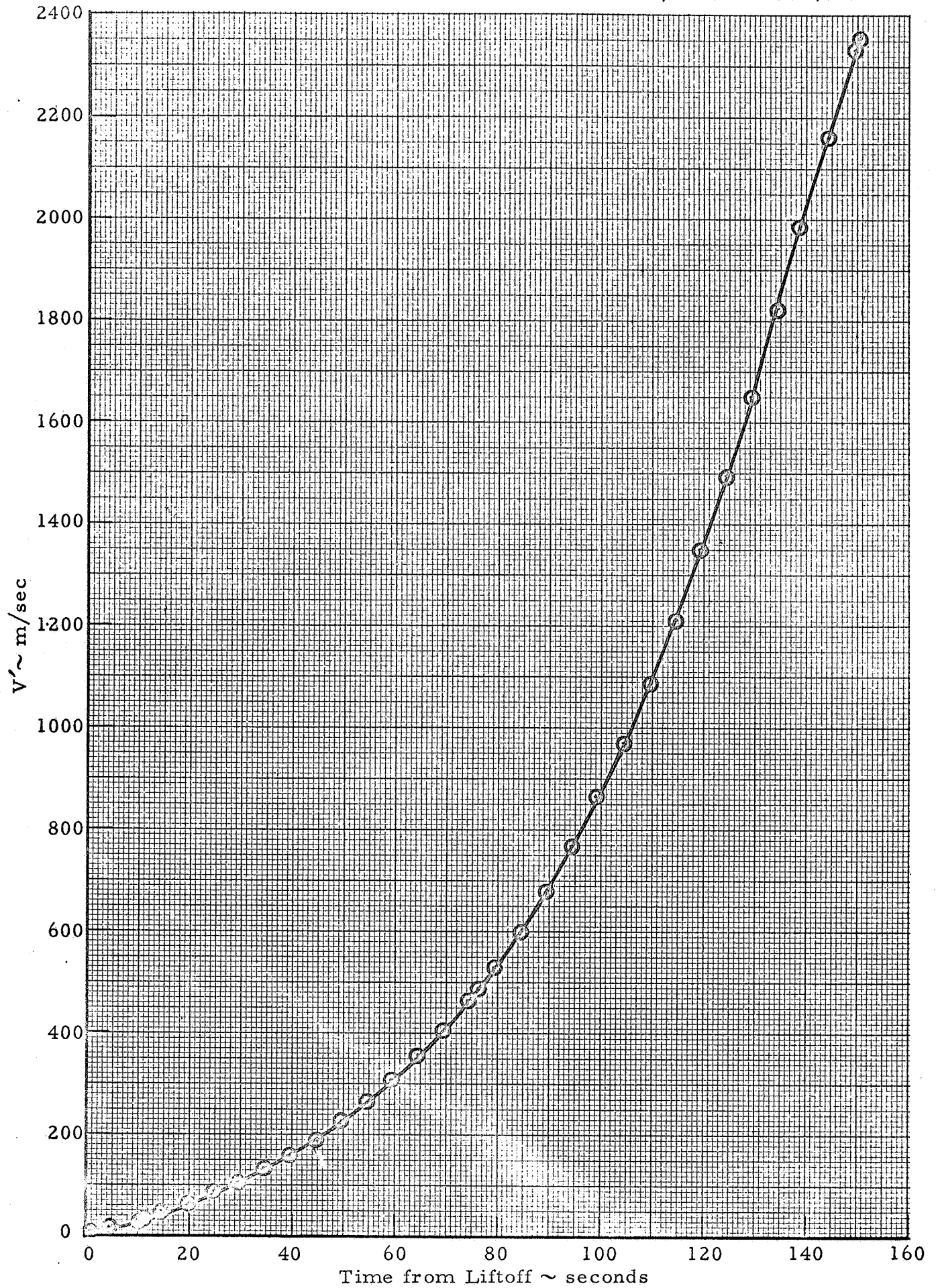




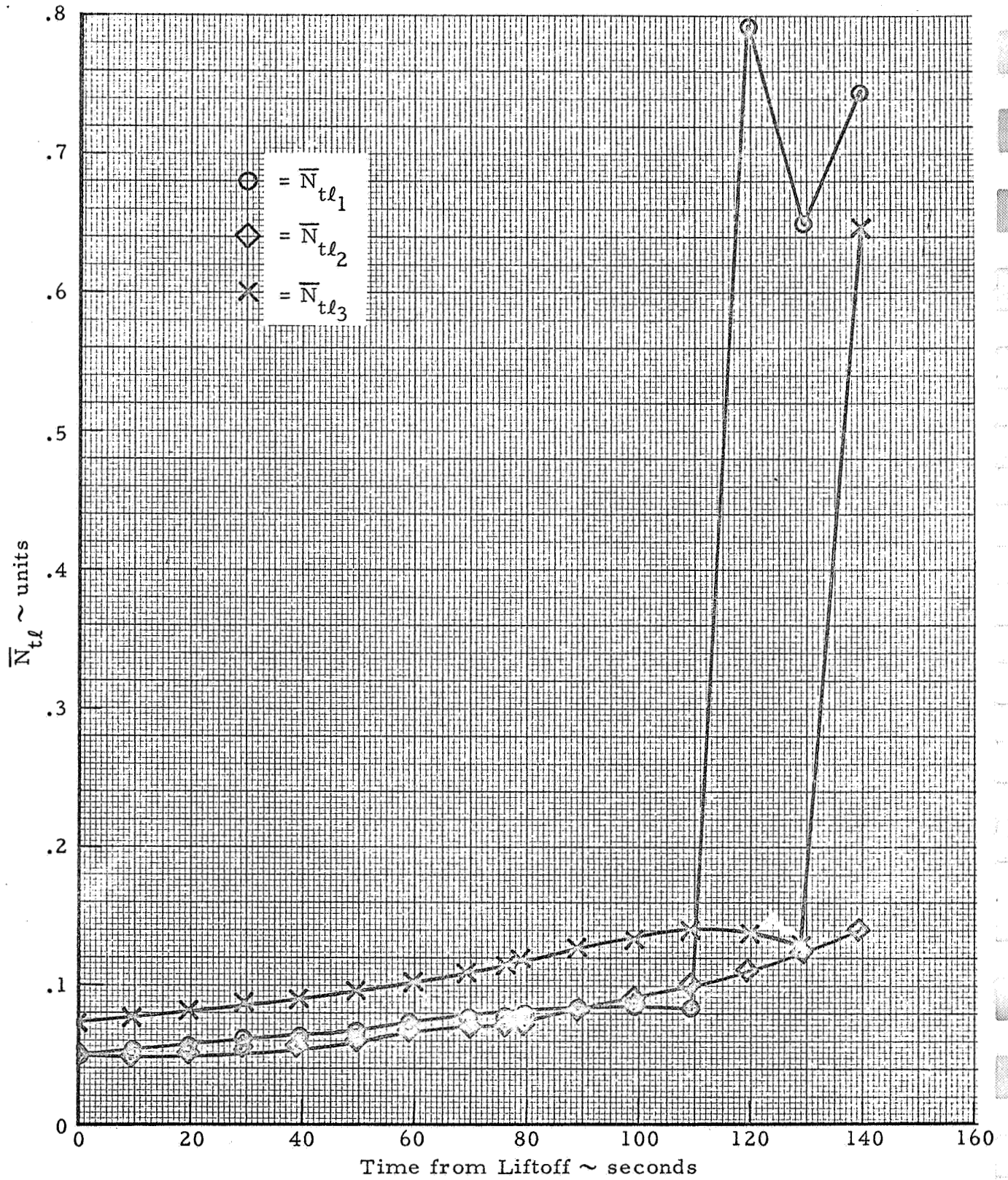
AS-503, S-IC Stage, Time Varying Coefficients



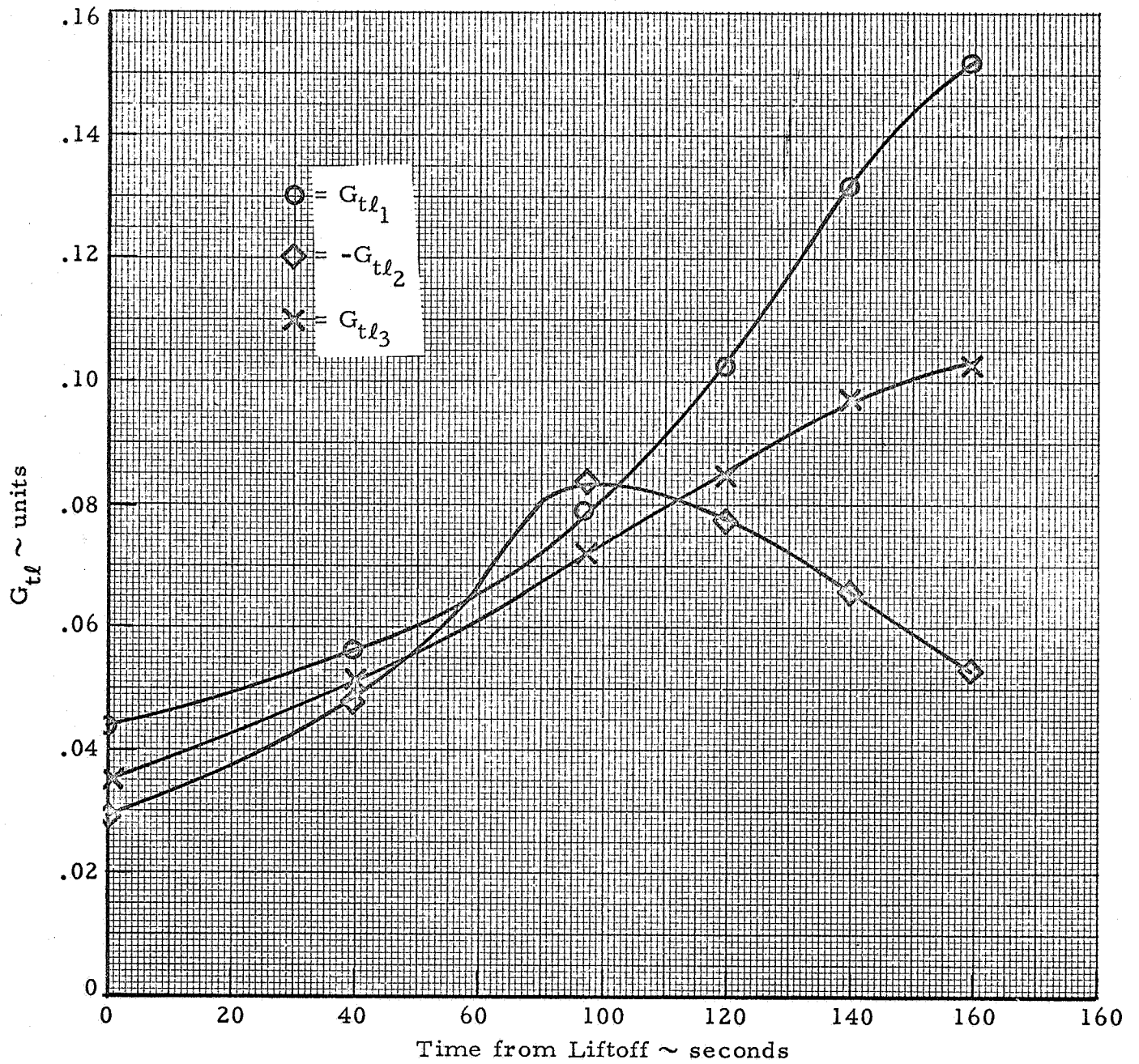
AS-503, S-IC Stage, Time Varying Coefficients
D-4



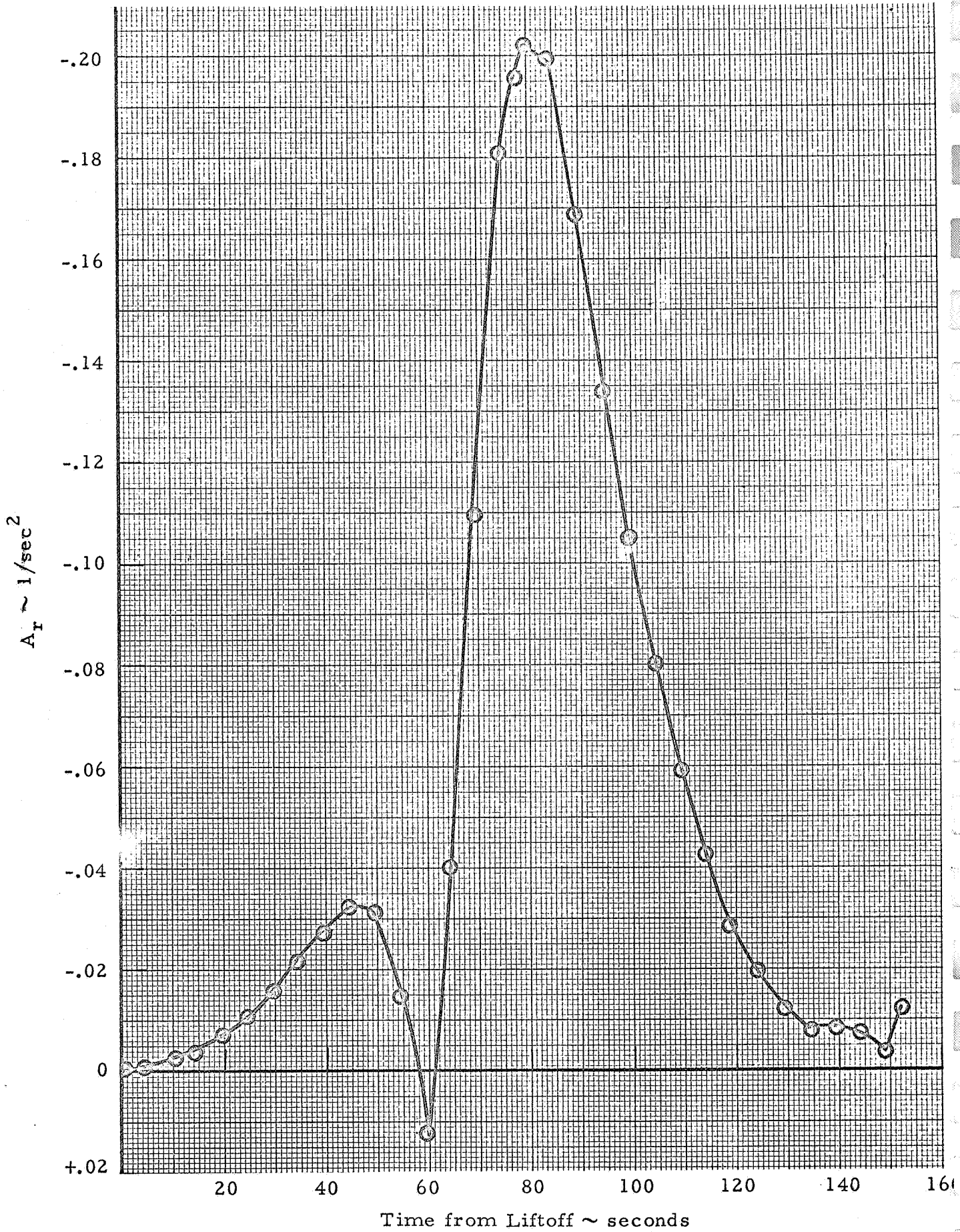
AS-503, S-IC Stage, Time Varying Coefficients
D-5



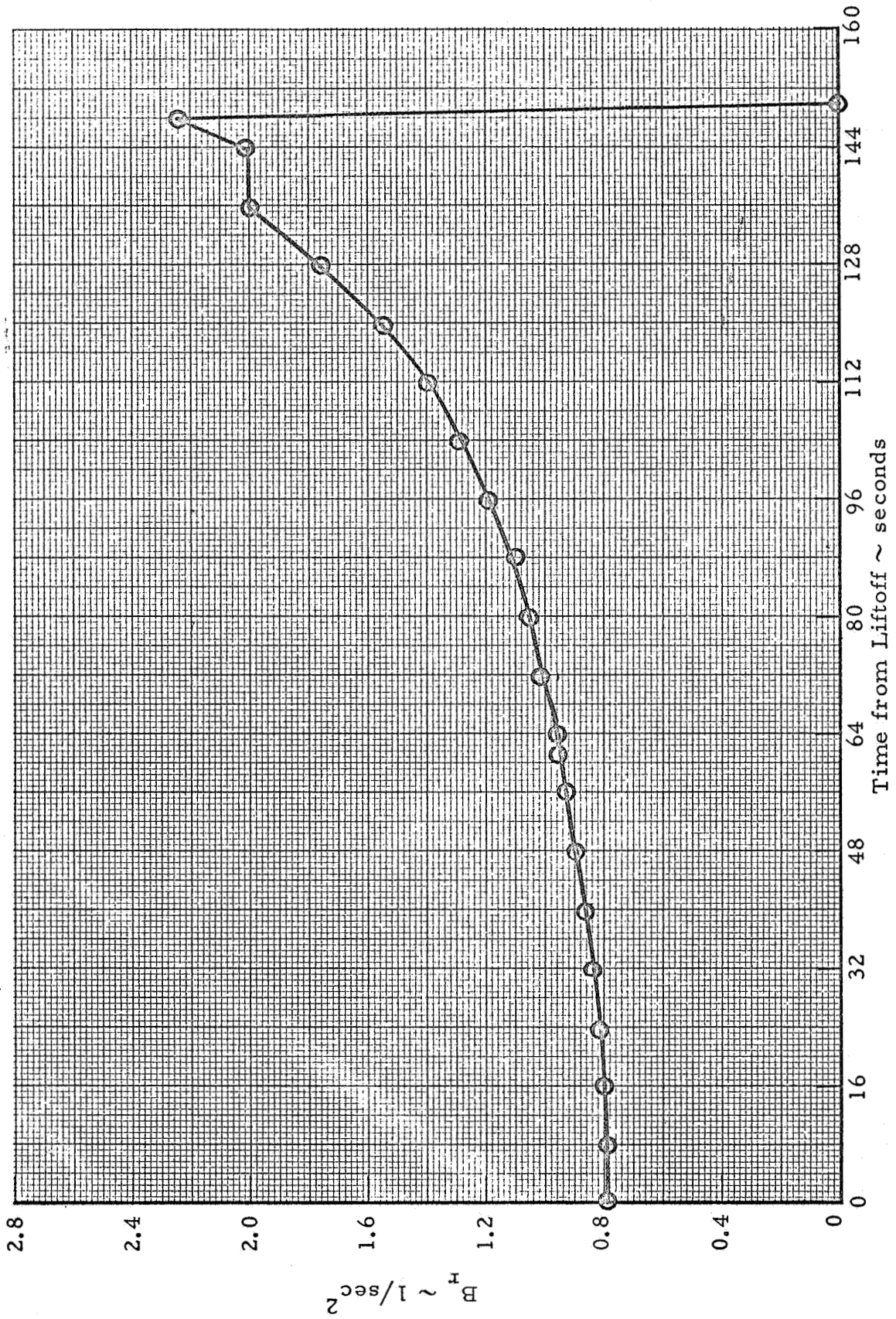
AS-503, S-IC Stage, Time Varying Coefficients



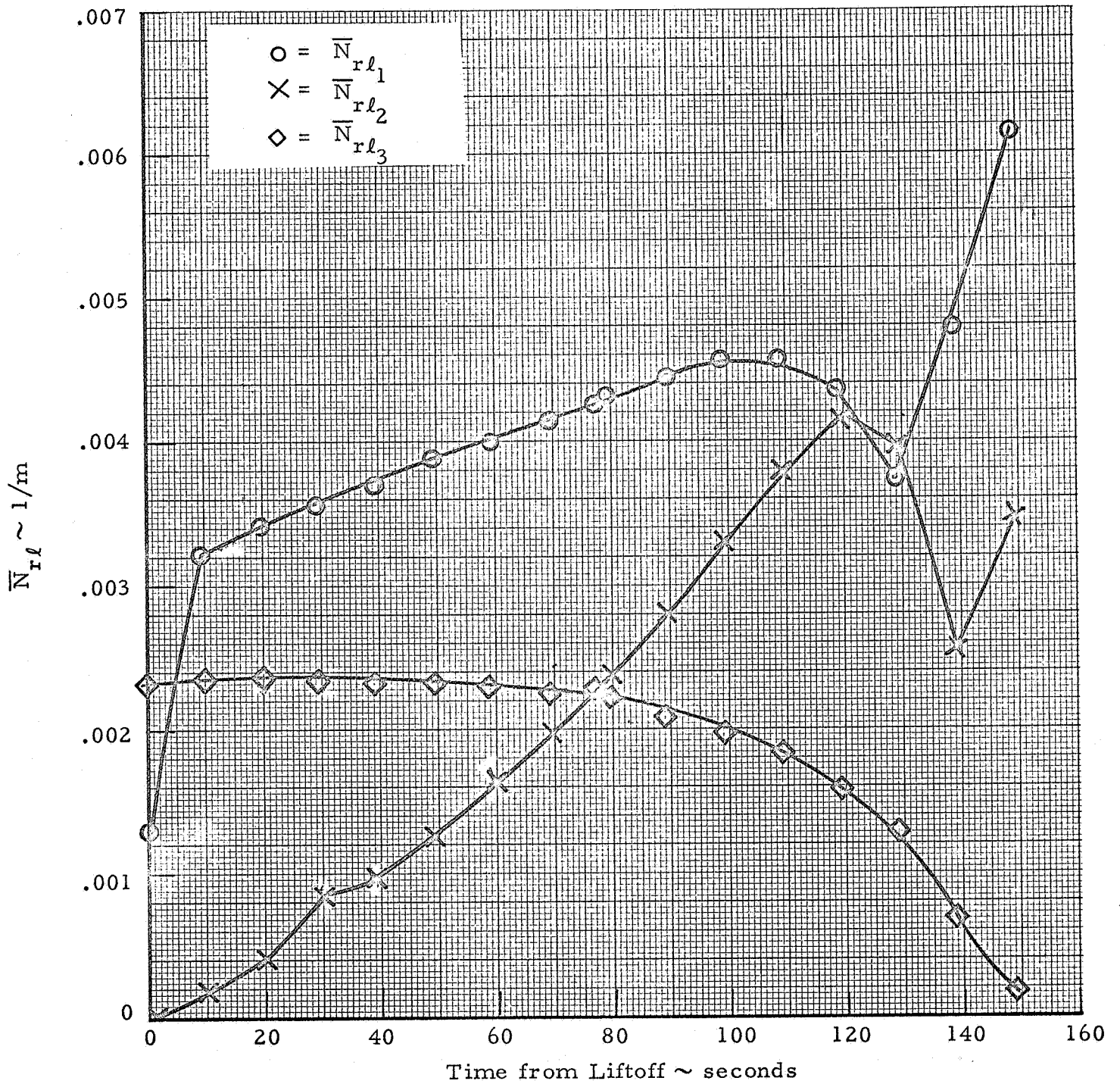
AS-503, S-IC Stage, Time Varying Coefficients



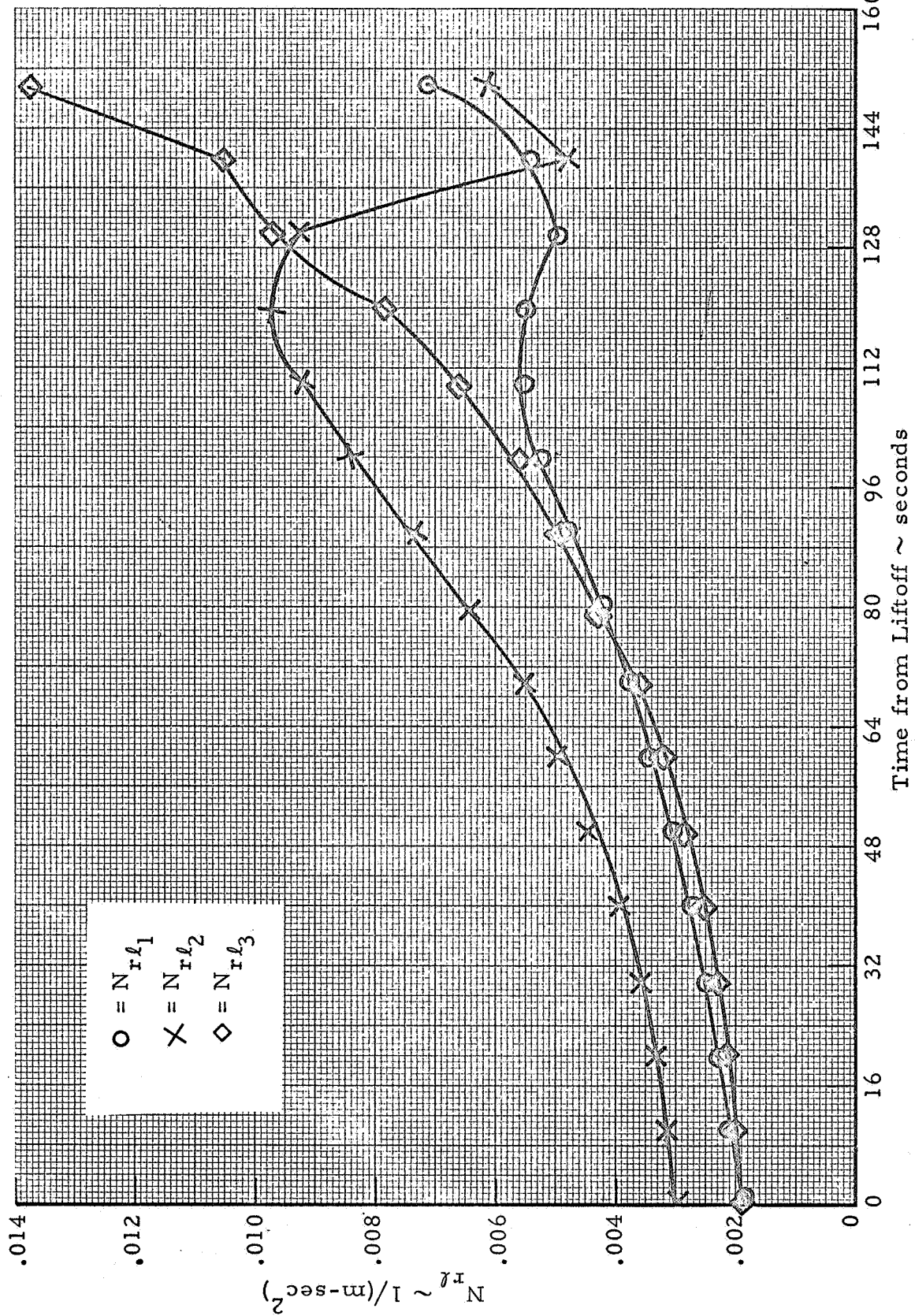
AS-503, S-IC Stage, Time Varying Coefficients
D-8



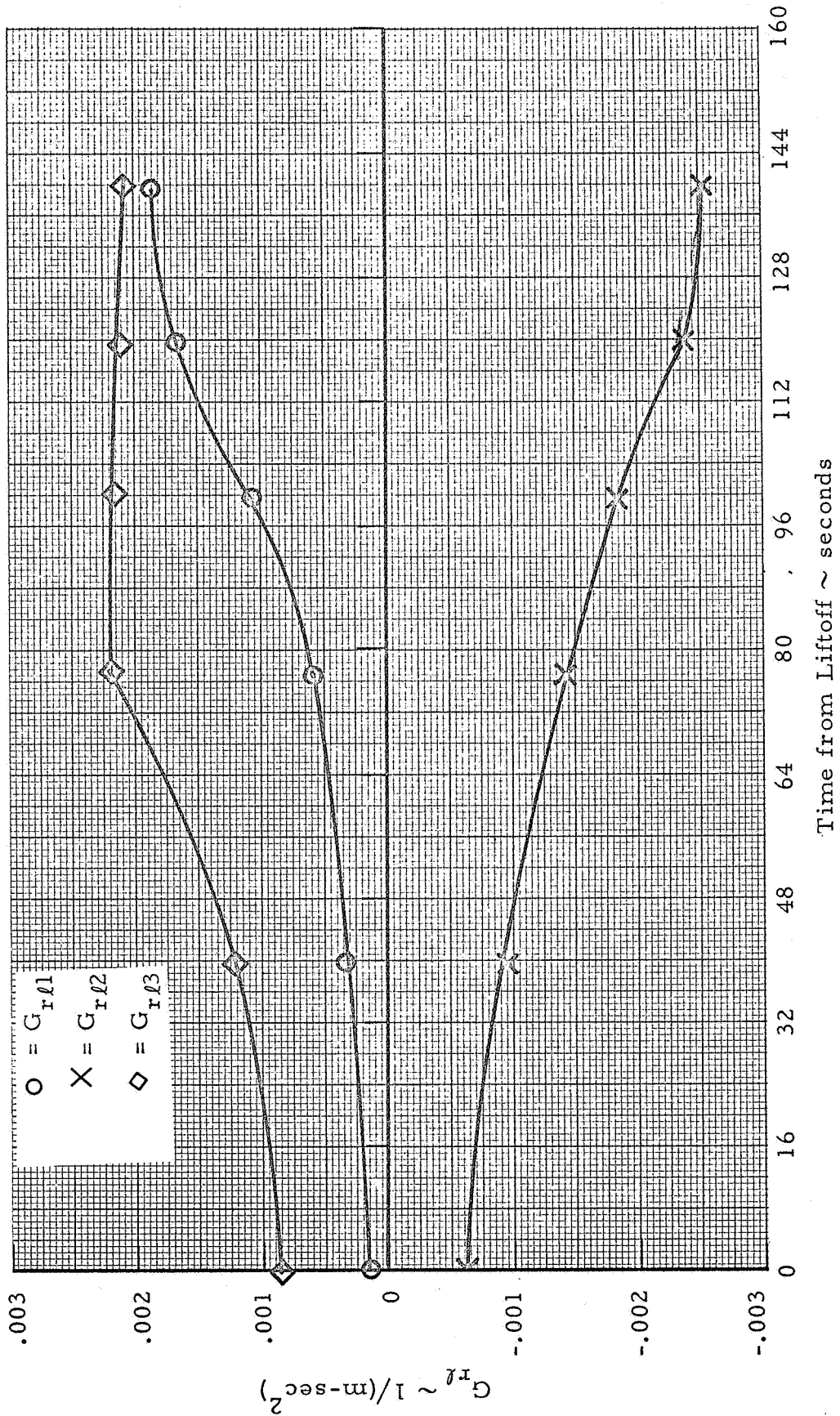
AS-503, S-IC Time Varying Coefficients



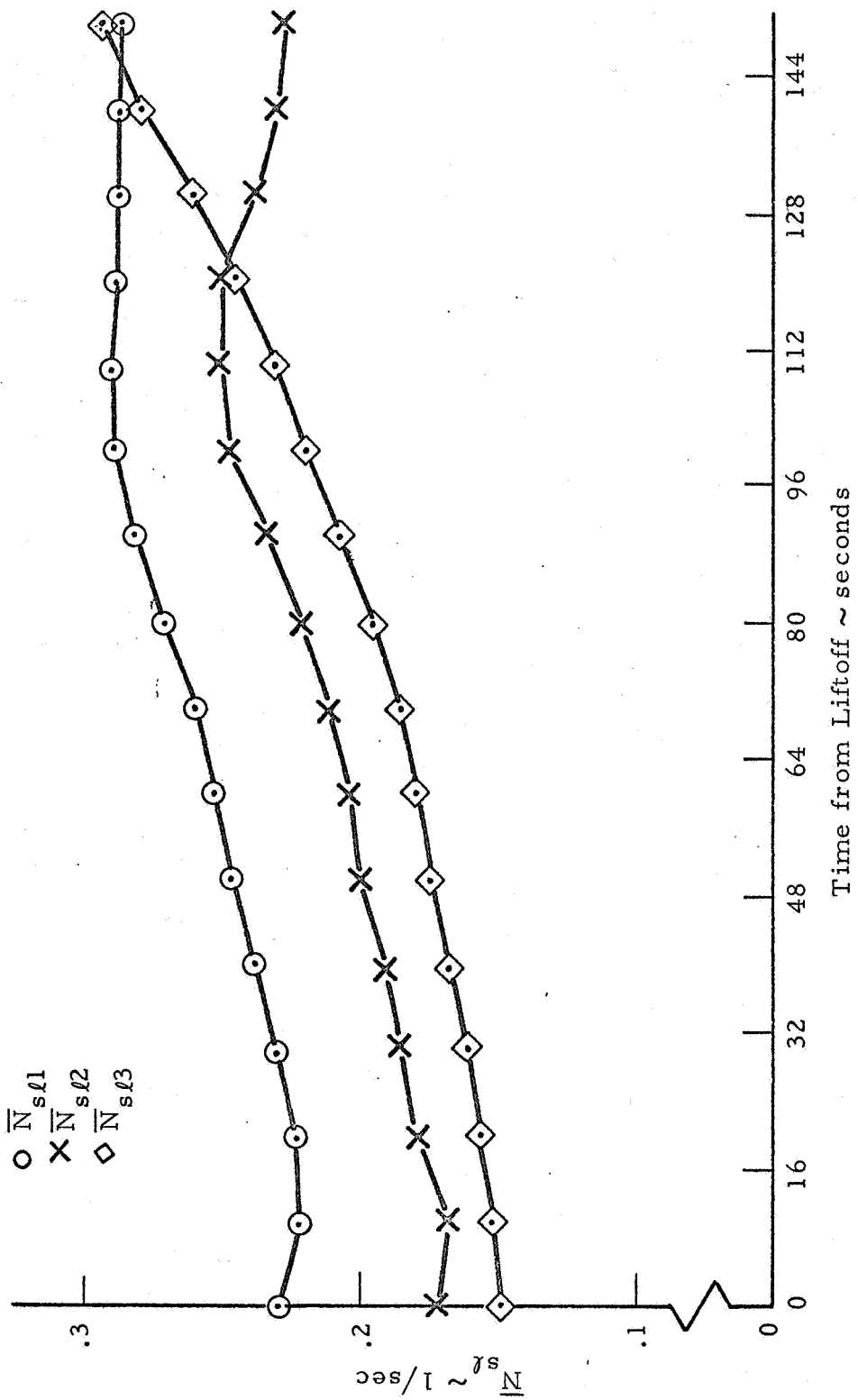
AS-503, S-IC Stage, Time Varying Coefficients



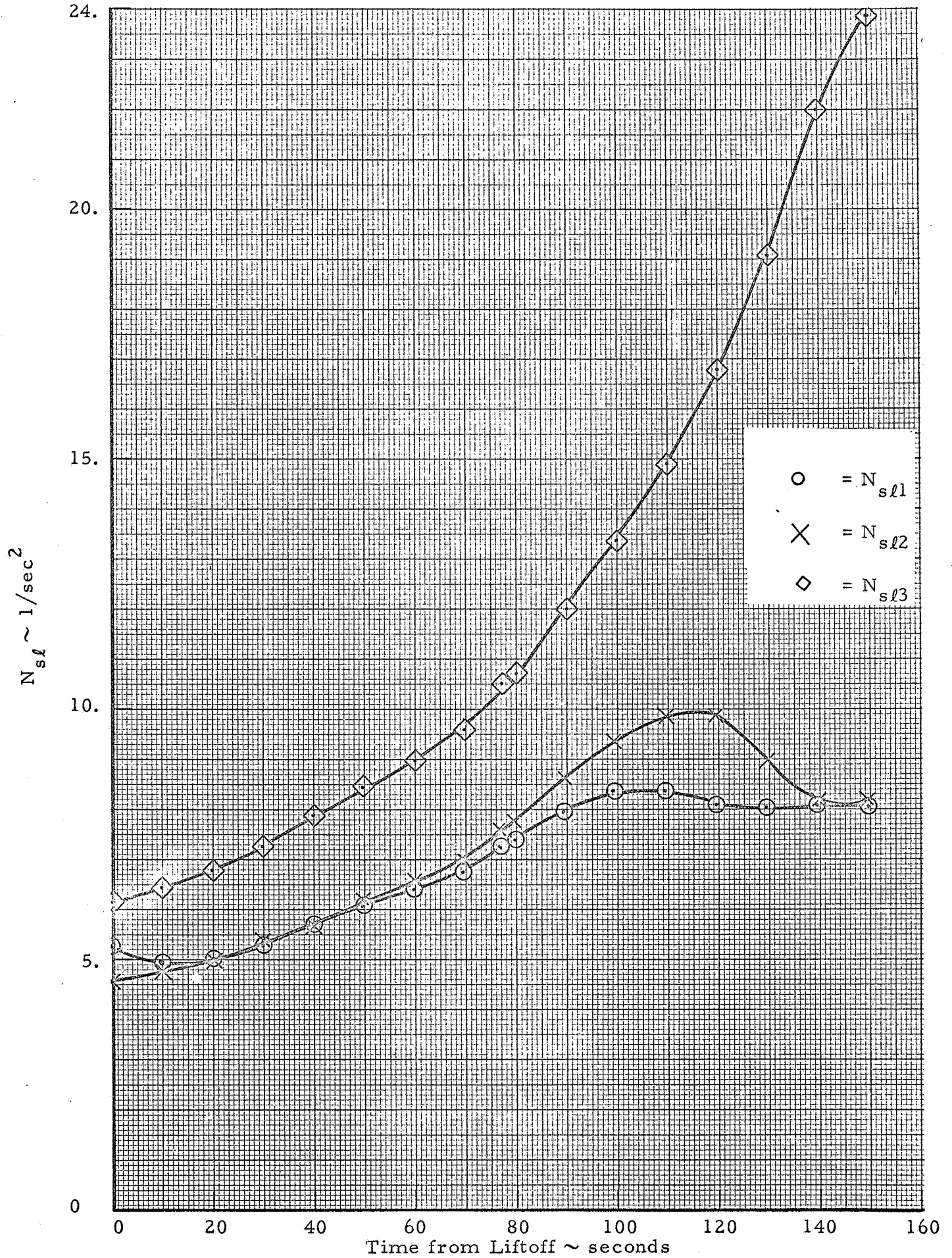
AS-503, S-IC Stage, Time Varying Coefficients



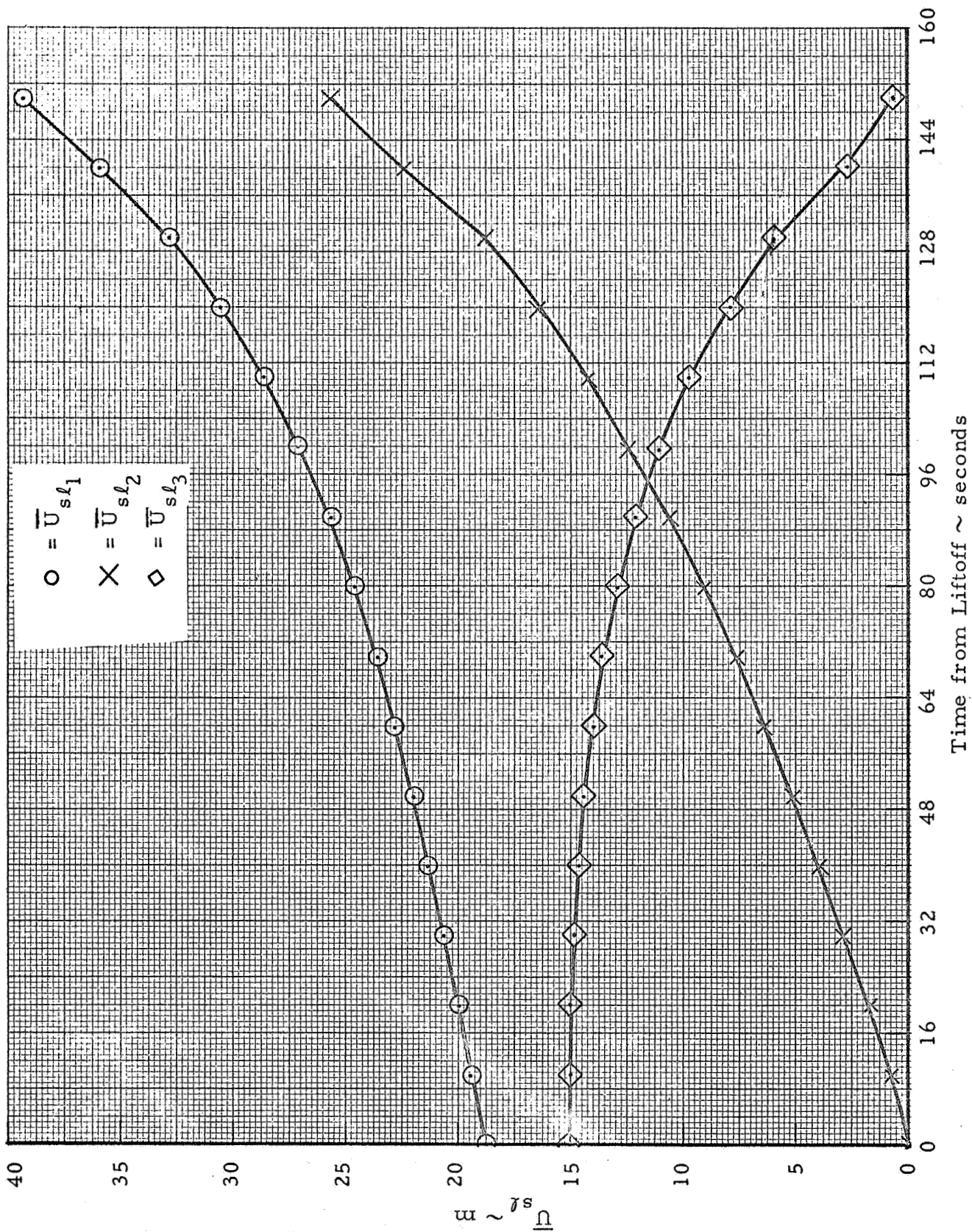
AS-503, S-IC Stage, Time Varying Coefficients



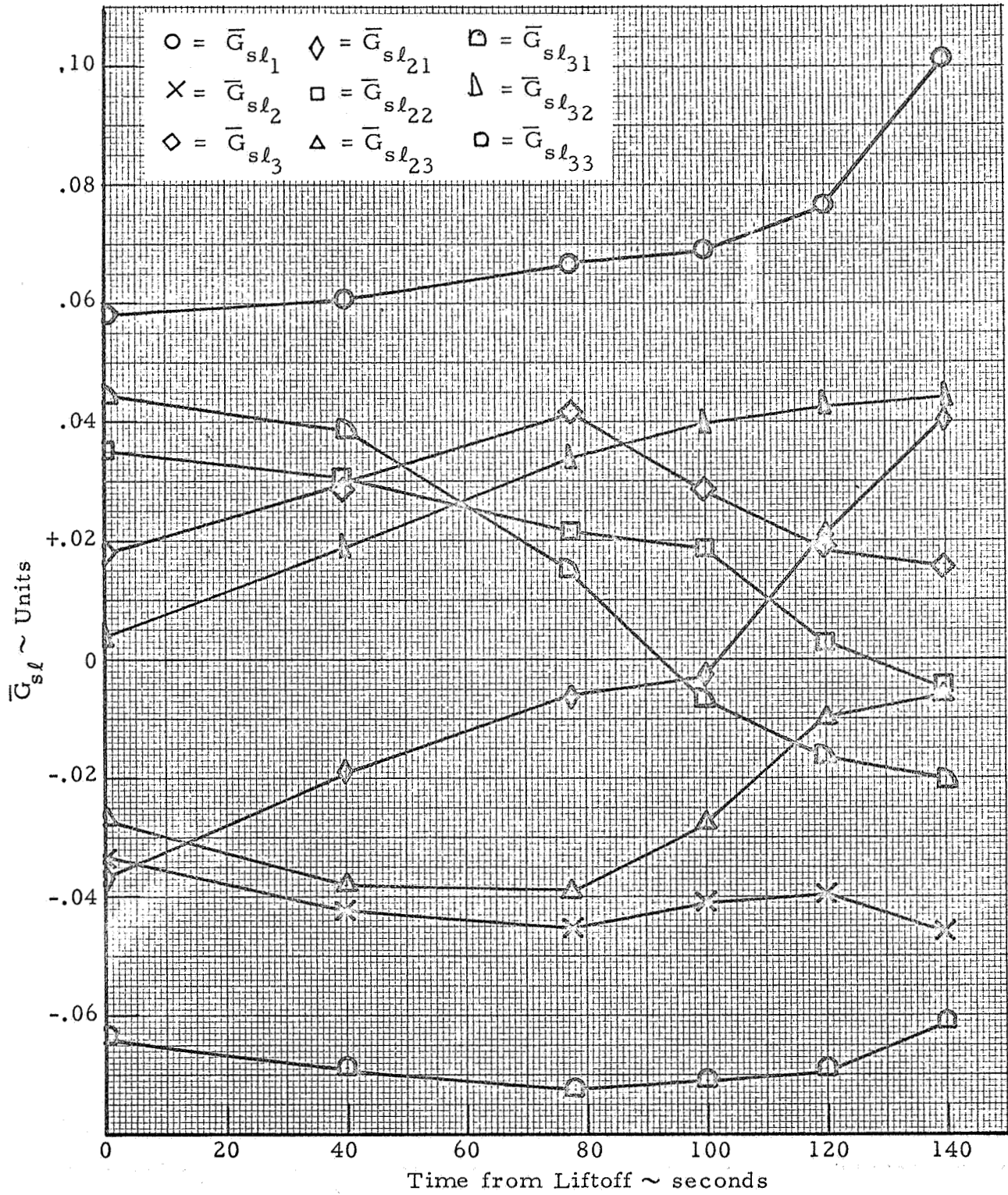
AS-503, S-IC Stage, Time Varying Coefficients



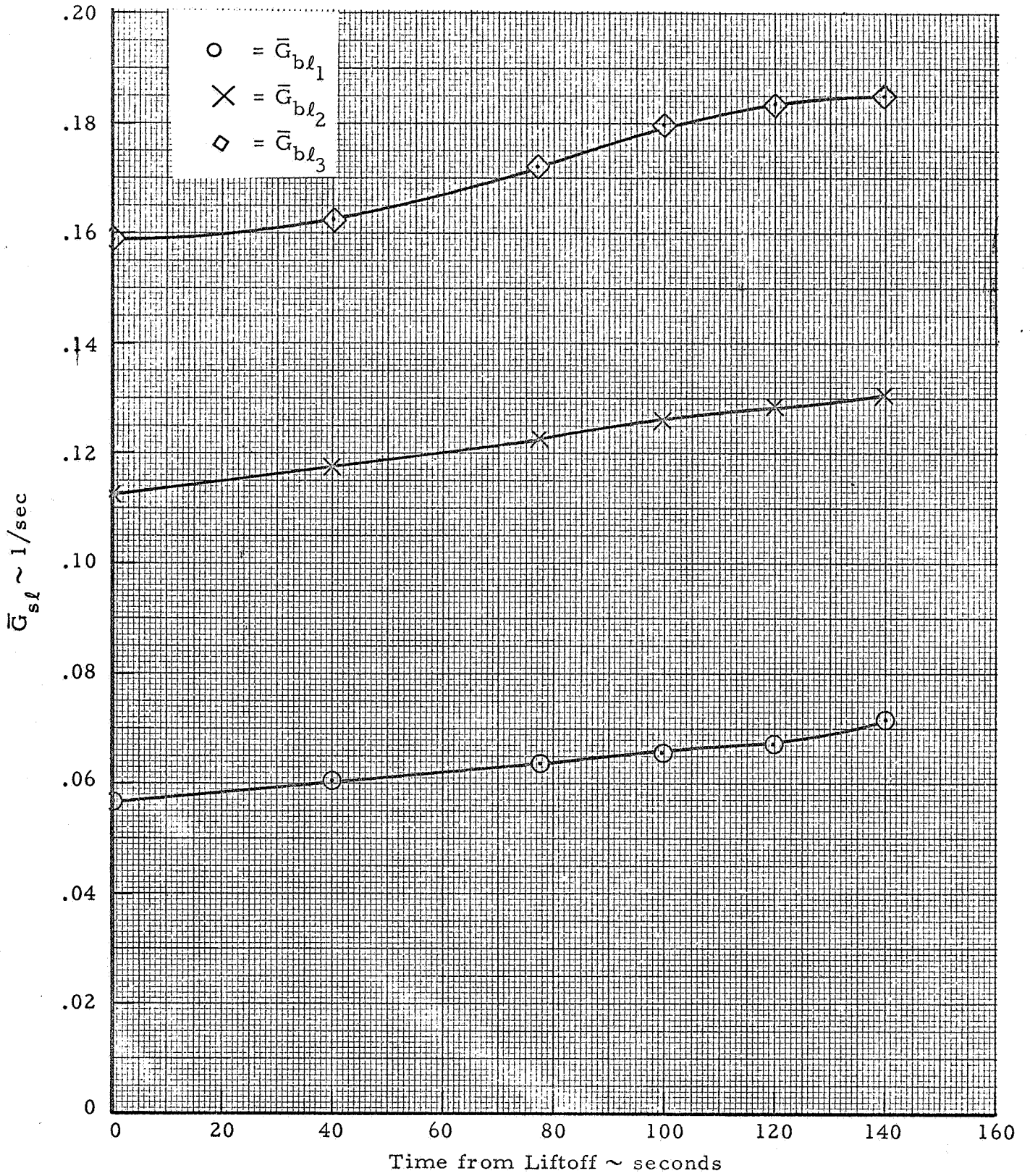
AS-503, S-IC Stage, Time Varying Coefficients



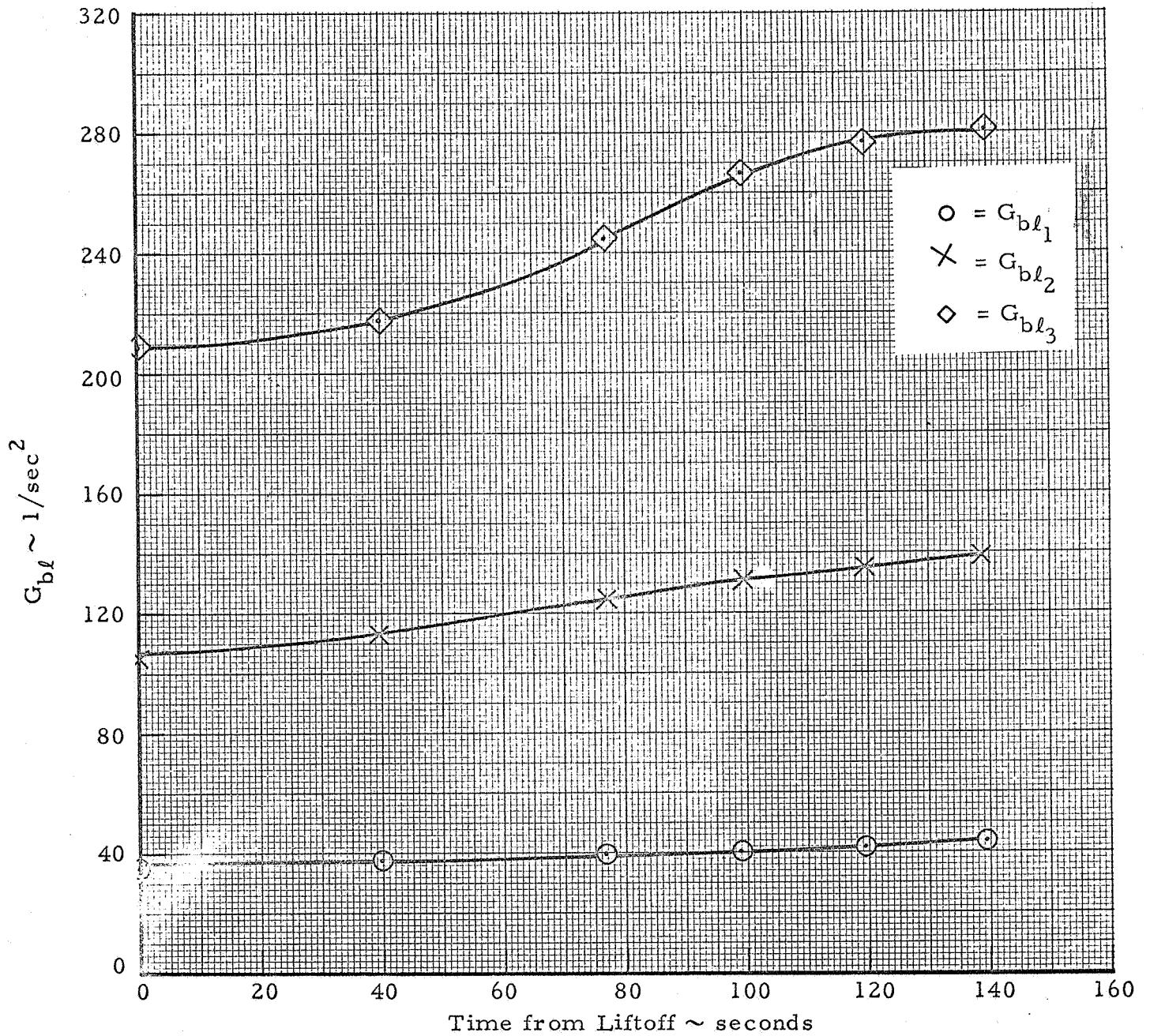
AS-503, S-IC Stage, Time Varying Coefficients



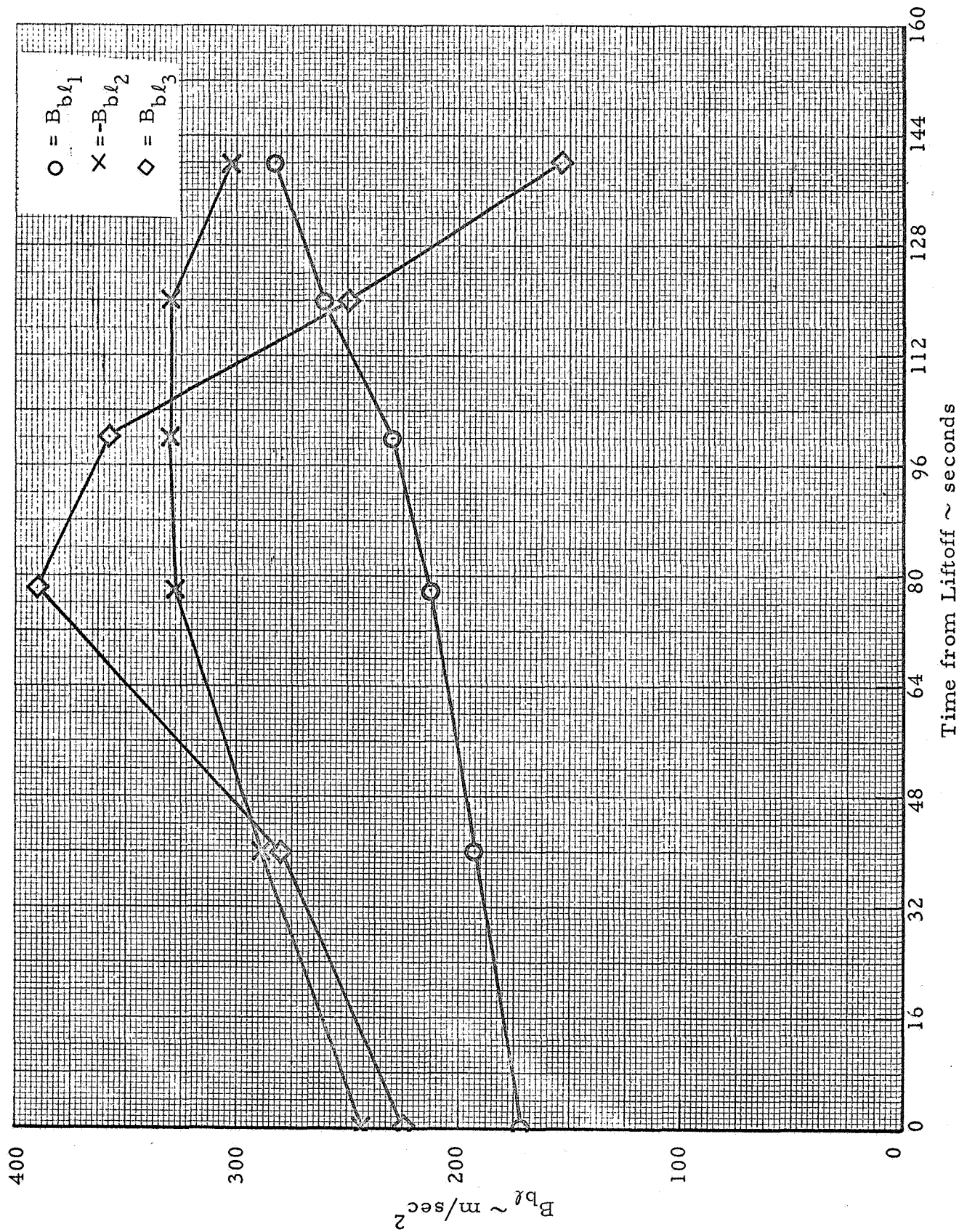
AS-503, S-IC Stage, Time Varying Coefficients



AS-503, S-IC Stage, Time Varying Coefficients

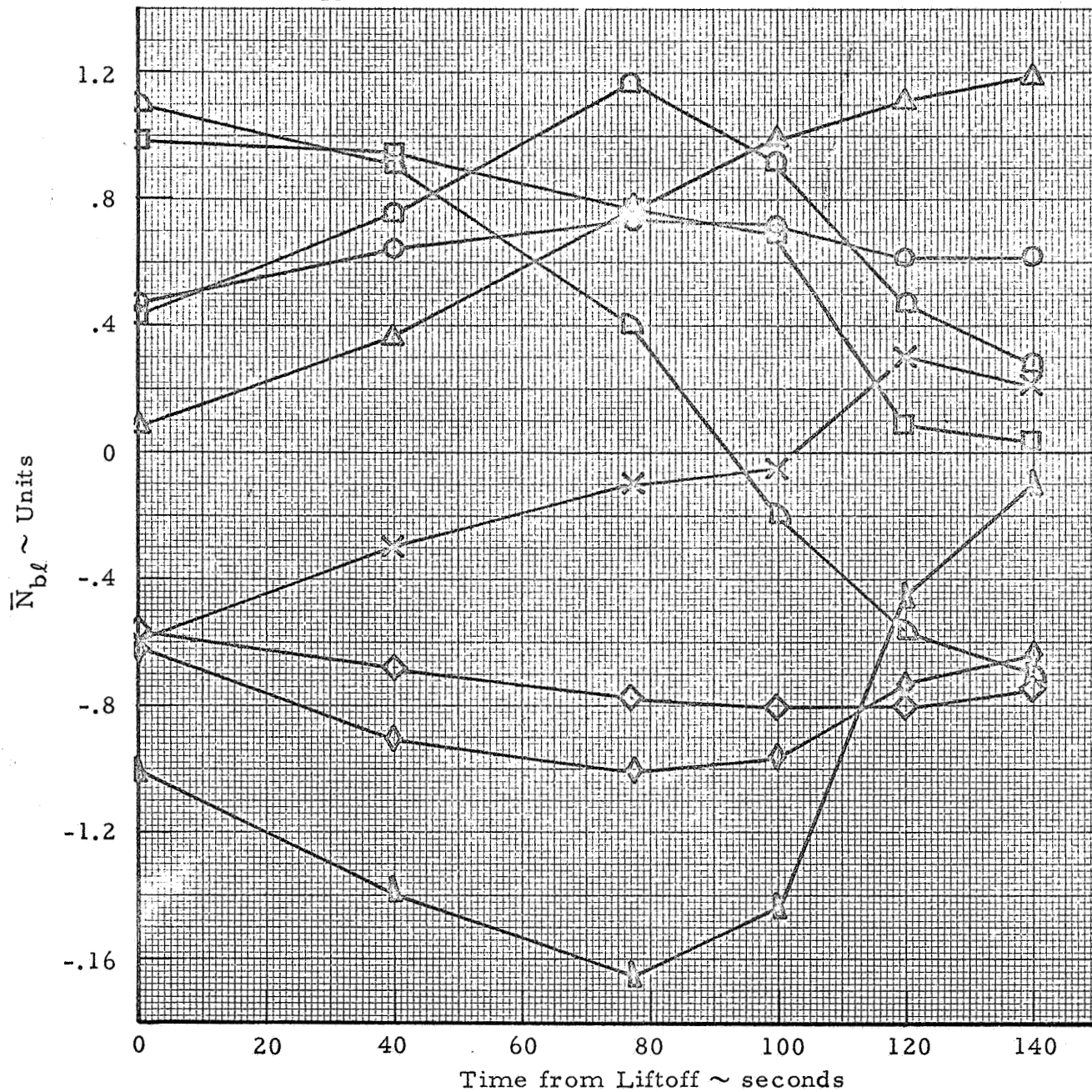


AS-503, S-IC Stage, Time Varying Coefficients

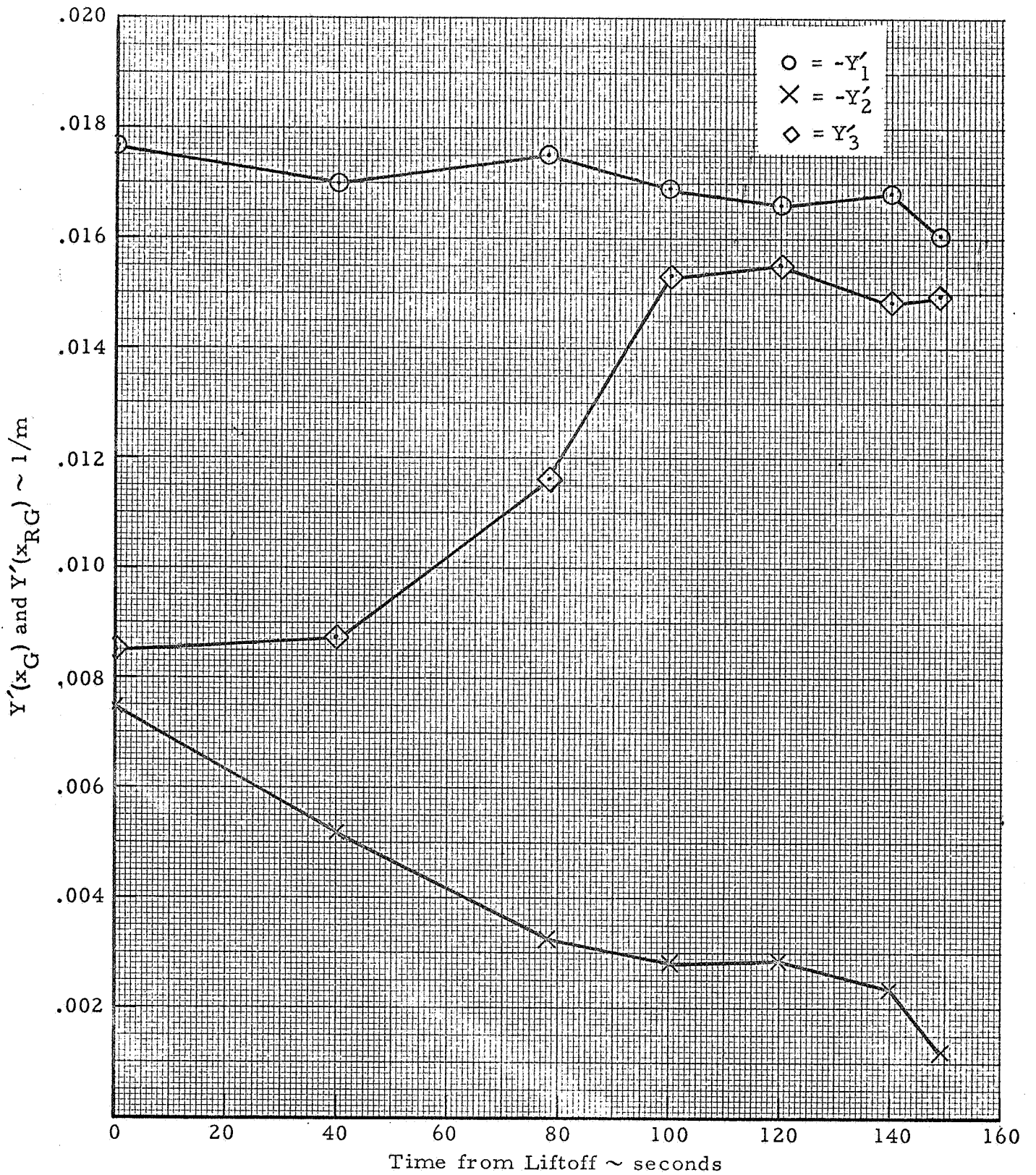


AS-503, S-IC Stage, Time Varying Coefficients

- | | | |
|--------------------------------|---------------------------------|---------------------------------|
| $\circ = \bar{N}_{bl_{11}}$ | $\diamond = \bar{N}_{bl_{21}}$ | $\square = \bar{N}_{bl_{31}}$ |
| $\times = \bar{N}_{bl_{12}}$ | $\square = \bar{N}_{bl_{22}}$ | $\triangle = \bar{N}_{bl_{32}}$ |
| $\diamond = \bar{N}_{bl_{13}}$ | $\triangle = \bar{N}_{bl_{29}}$ | $\square = \bar{N}_{bl_{33}}$ |



AS-503, S-IC Stage, Time Varying Coefficients



AS-503, S-IC Stage, Time Varying Coefficients

Appendix E
REFERENCES

Appendix E
REFERENCES

1. Lockheed Missiles & Space Company, Huntsville Research & Engineering Center, "A Nonlinear Filter for High Frequency Cutoff," TR HREC/0268-1, LMSC/HREC A782442.
2. Lockheed Missiles & Space Company, Huntsville Research & Engineering Center, "The Nonlinear Cutoff Filter in the Saturn V Vehicle with Time Varying Coefficients, TM 54/20-106, LMSC/HREC A783123.
3. Shaw, H., "Discrete Analogs for Continuous Filters," J. Assoc. Comp. Mach., 13, 4, October 1966, pp. 600-604.
4. Boole, G., Calculus of Finite Differences, 4th Ed., Chelsea Pub. Co., New York, 1958.
5. "Official Dynamics Data, Tolerances, Damping and Local Effects Estimates for Saturn V Vehicles," Marshall Memorandum, R-AERO-DD-22-67, 19 April 1967.
6. "Stabilization Networks for S-IC Stage Burn, Pitch and Yaw," Marshall Memorandum, R-ASTR-F-67-83, 22 March 1967.
7. "Static Aerodynamic Characteristics of the Apollo-Saturn V Vehicle," NASA TM S-53517, 16 September 1966.
8. "Control Feedback Stability Analysis," Army Ballistic Missile Agency Report No. DA-TR-2-60, 11 January 1960.
9. "SA-503 Structural Dynamic Characteristics," Boeing Company Document D5-15522-3, 30 December 1966.
10. "Thrust Vector Control (TVC) System Dynamics," Boeing Company Document D5-15381-5, (no date).
11. "AS-503 Launch Vehicle Reference Trajectory," Boeing Company Document D5-15480-1, CONFIDENTIAL (data used are from unclassified pages).
12. "Slosh Damping Values for AS-501 through AS-503 During Powered Flight," Marshall Memorandum, R-AERO-DD-95-65, 17 December 1965.